SPATIO-TEMPORAL COUPLING OF THE ELECTRIC AND HEMODYNAMIC BRAIN RESPONSES IN HUMANS

THÈSE N^{O} 3664 (2006)

PRÉSENTÉE LE 27 OCTOBRE 2006

À LA FACULTÉ SCIENCES ET TECHNIQUES DE L'INGÉNIEUR

Institut de traitement des signaux

SECTION DE GÉNIE ÉLECTRIQUE ET ÉLECTRONIQUE

ÉCOLE POLYTECHNIQUE FÉDÉRALE DE LAUSANNE

POUR L'OBTENTION DU GRADE DE DOCTEUR ÈS SCIENCES

PAR

Roberto MARTUZZI

Laurea in ingegneria elettronica, Politecnico di Torino, Italie
et de nationalité italienne

acceptée sur proposition du jury:

Prof. J.-M. Sallese, président du jury
Prof. J.-Ph. Thiran, Prof. R. Meuli, directeurs de thèse
Prof. O. Blanke, rapporteur
Dr M. M. Murray, rapporteur
Prof. A. C. Nobre, rapporteur

ÉCOLE POLYTECHNIQUE
FÉDÉRALE DE LAUSANNE

Lausanne, EPFL
2006

Contents

Acknowledgements

There are many people I wish to thank, and I apologize if I have forgetten someone.

First of all, I would like to thank my two thesis advisors, Professors Reto Meuli and Jean-Philippe Thiran who gave me the opportunity to complete my Ph.D. project here in Lausanne. Throughout my thesis, they continuously gave me all the technical and scientific support needed to conceive, conduct, and finish all the experiments and results presented in this work. They allowed me to discover fantastic places where I have be able to conduct research, both within the Department of Radiology at the CHUV (Centre Hospitalier Universitaire Vaudois) and within the Signal Processing Institute at the EPFL (École Polytechnique Fédérale de Lausanne). Lausanne has also been an amazing place to live.

Further, a special thanks goes to Dr. Micah M. Murray, for his invaluable contributions that he gave me throughout the period of my thesis. Together, we spent a lot of time chatting about experiments (and other topics too). During these discussions, we often had new ideas for improving our current projects. In addition, I have to give him credit for a big contribution to my improvements in both writing and speaking English.

I would like to acknowledge all the members of the jury, that included, in addition to the two advisors Professors Reto Meuli and Jean-Philippe Thiran and to Dr. Micah M. Murray, the president Dr. Jean-Michel Sallese, and Professors Olaf Blanke and Kia Nobre. I'm very thankful that they accepted to review and evaluate this thesis and we had an interesting and constructive discussion during my dissertation.

I wish also to thank Eleonora Fornari, who really pushed me to come to Lausanne and who gave me technical and linguistic support when I first arrived in Lausanne without knowing a single word in French. Without her contribution this thesis would have probably never begun. Moreover, I have to thank her for being able to put up with me during these past five years spent together sharing our office.

I would also like to thank all the co-authors of the papers and posters we have published or submitted. Among the others, I'd like to mention Stephanie Clarke, Philippe Maeder, Christoph Michel, Rolando Grave de Peralta Menendez, and Sara Gonzalez Andino. Their comments and suggestions played an important role in raising the quality of this work and of our publications.

Last but not least, there is a list of people with whom I shared experiments (reciprocally being subject for each other's experiments), suggestions, and above all a lot of pleasant time

inside and outside the CHUV, which turned into real friendships. Such a list includes Patric Hagmann, Leila Cammoun, Raphaël Meylan, Laura De Santis, Lucas Spierer, Eric Tardif, Carolyn Sacco, Melanie Aeschlimann, Jean-François Knebel, and Ulrike Toepel.

I would really like to thank all these people (and all those that I could have inadvertently forgotten) for having given me important support without which ending this work would have been a much harder task.

Financially, I was supported by the Biomedical Engineering grant Lausanne-Geneva, by the Swiss National Science Foundation (SNSF 3200B0-100606), and by the centre d'imagerie biomedicale (CIBM).

Abstract

Our comprehension of human brain functions and their dynamics has been dramatically improved by recent developments in non-invasive imaging techniques. These methods can be divided into two different categories, according to the nature of the measured signal: hemodynamic techniques, such as functional magnetic resonance imaging (fMRI) and positiron emission tomography (PET), and electromagnetic techniques, such as electroencephalography (EEG) and magnetoencephalography (MEG). These two categories are have complementary characteristics: hemodynamic techniques have a good spatial resolution (on a millimeter spatial scale) but have a poor temporal resolution, which is inherently limited by the rate changes in blood flow and oxygenation. Electromagnetic techniques have sub-millisecond temporal resolution but have a poor spatial resolution, since the analysis of intracranial generators requires the solution of an *underdetermined* inverse problem (i.e. there are infinite solutions that can explain equally well the same scalp-recorded distribution). The complementarity of the characteristics of these two families of methods allowed researchers to suppose that the understanding of spatio-temporal brain dynamics can be drastically improved by their combination (so-called *multimodal imaging*). Unfortunately some caveats hinder such combination. First, the nature of neurovascular coupling is still poorly understood. Second, analytical methods for multimodal imaging are largely in their infancy.

The first part of this thesis focuses on the analysis of the temporal characteristics of the blood oxygenation level dependent (BOLD) signal and on how they are modulated by stimulus conditions. To analyze the BOLD dynamics, a novel method for synchronizing stimulus delivery and volume acquisition was developed. This method allows for estimating the BOLD signal with a high temporal resolution (in this thesis up to 125 ms) and for studying how the temporal characteristics (in this thesis mainly the BOLD peak latency and slope) are modulated by stimulus conditions (with an approach similar to that used in the analysis of the EEG evoked potentials). We applied this novel technique to a simple reaction time task to lateralized visual stimuli (the so-called Poffenberger paradigm) as well as to a multisensory auditory-visual reaction time task. In the first study (the Poffenberger paradigm) the analysis of BOLD dynamics supported the theory of a bilateral visuo-motor pathway even in the case of a visual stimulus ipsilateral to the responding hand. In the second study, (the auditory-visual multisensory reaction-time task), the analysis showed

auditory-visual interactions within both primary auditory and visual cortices that could not be otherwise revealed by traditional fMRI analysis methods since it does not involve changes in signal amplitude.

The second part of this thesis focuses on the comparison of the statistical results obtained by the analyses of fMRI and of the intracranial local field potentials (LFPs), estimated by the ELECTRA inverse solution. We first developed a new method for the analysis of EEG data. This method is based on the statistical comparison of the spectral characteristics of the estimated intracranial LFPs of the pre- and post- stimulus onset periods. Each single trial is analyzed independently, without including an averaging step, so that the information carried by high frequencies is preserved. We also propose a new metric, called resemblance, to investigate the relationship between fMRI and the estimated intracranial LFPs. Single-trial analysis and the resemblance metric were applied in an experiment involving separate EEG and fMRI acquisitions during the same passive visual stimulation protocol. This experiment revealed that only a limited set of LFP frequencies shows a spatial correlation with fMRI. This set of frequencies changes across brain areas, such that progression from lower to higher cortical levels of visual processing incorporates at each step new frequencies.

In conclusion, in this thesis we show that the estimation and the analysis of the BOLD time course can give an important contribution to better understanding brain functions and brain organization. To fully understand the meaning of changes in BOLD dynamics, we need a better knowledge of the neuro-vascular coupling. To do that, we introduced a new method for evaluating the relationship between EEG and fMRI across frequencies and anatomical regions.

Keywords: EEG, fMRI, BOLD dynamics, multi-modal imaging

Version Abrégée

Notre compréhension des fonctions cérébrales s'est fortement améliorée par le développement récent des techniques d'imageries non-invasives. Ces techniques peuvent être divisées en deux différentes familles, selon la nature des signaux enregistrés: les techniques de mesure hémodynamique, comme l'imagerie par résonance magnétique fonctionnelle (IMRf) et la tomographie par émission des positrons (PET), et les techniques électromagnétiques, comme l'électroencéphalographie (EEG) et la magnétoencéphalographie (MEG). Ces deux familles ont des caractéristiques complémentaires: les techniques hémodynamiques ont une excellente résolution spatiale (à une échelle millimétrique) mais, elles ont une très faible résolution temporelle, intrinsèquement limitée par le taux de changement du flux sanguin et de son oxygénation. Les techniques électromagnétiques, par contre, ont une résolution temporelle inférieure à la milliseconde, mais elles ont une très faible résolution spatiale, car l'évaluation des générateurs intracrâniens nécessite la solution d'un problème inverse sous-déterminé (une infinité de solutions peuvent expliquer de manière similaire la distribution du champ électrique enregistré sur le scalp). En raison des caractéristiques complémentaires de ces deux types de techniques, la compréhension des processus spatio-temporels cérébraux peut être améliorée par leur combinaison. Cependant, plusieurs problèmes empêchent une telle combinaison. D'une part, la nature du couplage neuro-vasculaire n'est pas complètement comprise. D'autre part, les méthodes analytiques pour cette combinaison ne sont pas suffisamment développées.

La première partie de cette thèse se focalise sur l'analyse des caractéristiques temporelles du signal BOLD (blood oxygenation level dependant) et sur la façon dont ces paramètres sont modifiés par les conditions expérimentales. Pour analyser le signal BOLD, une nouvelle méthode de synchronisation entre la présentation du stimulus et l'acquisition des volumes fonctionnels a été développée. Cette technique permet d'estimer le signal BOLD avec une plus bonne résolution temporelle (jusqu'à 125ms, dans cette thèse), et d'étudier les modifications des caractéristiques temporelles (la latence des pics et la pente, dans cette thèse) induites par les conditions expérimentales (avec une approche similaire à ce qui est utilisé dans l'analyse des potentiels évoqués dans l'EEG). Nous avons appliqué cette nouvelle technique à une tâche de simple détection du stimulus visuel latéralisé (le paradigme de Poffenberger) et à une tâche de détection de stimuli multisensoriels (audio-visuels). Dans le paradigme de Poffenberger, les résultats de l'analyse du signal BOLD confirment la présence

d'un chemin visio-motor bilatéral, même dans le cas d'un stimulus ipsilateral à la main qui répond. Dans la deuxième étude (la tâche de détection des stimuli audio-visuels), l'analyse montre des interactions audio-visuelles dans les aires primaires auditives et visuelles, qui ne peuvent être révélées par les techniques d'analyses d'IRMf traditionnelles.

Dans la deuxième partie, cette thèse se focalise sur la comparaison des résultats statistiques obtenus par l'analyse IRMf et par le LFP (local field potentials) estimé à l'aide de la solution inverse ELECTRA. Premièrement, nous avons développé une nouvelle méthode d'analyse des données d'EEG. Cette méthode est basée sur la comparaison statistique des caractéristiques spectrales des LFP estimés pendant les périodes précédent et suivant le début de la stimulation. Chaque essai est analysé d'une manière indépendante des autres, sans inclure un moyennage, et donc en préservant toute l'information contenue dans les hautes fréquences. Nous avons aussi proposé une nouvelle métrique, nommé resemblance, pour évaluer la relation entre l'IRMf et les LFP estimés. L'analyse individuelle de chaque essai et la métrique resemblance ont été utilisés dans une expérience visuelle passive, avec l'acquisition de l'IRMf et de l'EEG en deux sessions différentes. Cette étude montre que seul un nombre limité de fréquences des LFP présente une corrélation spatiale avec l'IRMf. La distribution des fréquences change selon les régions cérébrales: en se déplaçant du bas vers les hauts niveaux de la hiérarchie corticale du traitement visuel, cette distribution des fréquences incorpore de nouvelles fréquences.

En conclusion, dans cette thèse, nous montrons que l'estimation et l'analyse de l'évolution temporelle du signal BOLD peuvent contribuer à mieux comprendre le fonctionnement et l'organisation du cerveau. Pour comprendre complètement la signification des changements du signal BOLD, nous avons besoin d'une meilleure connaissance du couplage neurovasculaire. Pour ce faire, nous avons défini une nouvelle méthode pour évaluer la relation entre l'IRMf et l'EEG en fonction des différentes fréquences et des régions anatomiques étudiées.

Mots-clés: EEG, fMRI, signal BOLD, imagerie multi-modale

List of Abbreviations

BA	Broadmann Area
BOLD	Blood oxygenation level dependant
ECD	Equivalent current dipole
EEG	Electroencephalography
ERP	Event-related potential
fMRI	functional magnetic resonance imaging
FoV	Field of view
FWHM	Full width half maximum
GLM	General lineal model
HRF	Hemodynamic response function
ISI	Inter-stimulus interval
LAURA	Local auto-regressive averages
LFP	Local field potential
MEG	Magnetoencephalography
MNI	Montreal neurological institute
MUA	Multi-unit activity
PET	Positron emission tomography
RF	Radiofrequency
RT	Reaction time
SD	Standard deviation
SNR	Signal-to-noise ratio
TE	Echo-time
TR	Repetition time
VHFO	Very high frequency oscillation

1 Introduction

Blood oxygenation level dependent (BOLD) functional magnetic resonance imaging (fMRI) was first introduced in 1992 [3, 77, 113] and has rapidly revealed itself an exquisite tool for localizing *in vivo* neuronal activity, revolutionizing cognitive neuroscience. Based on the coupling between neuronal activity and local brain hemodynamics (blood flow and oxygenation), this technique allows the localization of brain activity with millimeter precision in a completely non-invasive manner. However, the relationship between the fMRI signal and the underlying neuronal activity is not yet clear.

The interpretation of fMRI data rely on the basic idea that the BOLD signal is proportional to the mean local neuronal activity within a volume of several cubic millimeters and within several seconds [9, 44]. The simplest model proposes a linear relation between the BOLD signal and the underlying neuronal activity, the so-called *linear transform model* of the fMRI signal [62]. No assumptions are made about the relationship between the stimulus and neuronal activity, both of which can be arbitrarily complex.

The linear transform model is an approximation of the neuro-vascular coupling, but it incredibly simplifies the analyses and the interpretation of fMRI data. If the model were considerated as a satifactory approximation, the relationship between neuronal activity and BOLD signal could be completely defined by the *hemodynamic response function* (HRF); that is the fMRI signal obtained in response to a brief burst of neuronal activity (ideally an impulse). Once that the HRF is known, under the assumption that the linear transform model is a valid approximation, it is possible to deconvolve the fMRI time signal to estimate the underlying neuronal activity.

To fully understand the capabilities and limitations of fMRI in making inferences on the underlying neuronal activity, the relationship between the BOLD signal and neuronal activity has to be more clearly understood. Neuronal activity, within a certain cortical region and over a certain period of time, can be characterized by many different features, including but not limited to the mean firing rate (of the entire neuronal population or of a

certain subpopulation), the local field potential (LFP), the multi-unit activity (MUA), or the current source density. One important but still unanswered question is what characteristics of neuronal activity are more tightly related to the fMRI signal? Or, in other words, what characteristics of neuronal activity can be better predicted by the fMRI signal? In the last years, researchers have begun conducting experiments to answer this and similar questions.

1.1 Outline

The aims of the present work are twofold. First, we studied the temporal characteristics of the HRF. In particular we analyzed how, within a certain region, BOLD peak latency and slope are modulated by experimental conditions. Traditionally, fMRI analysis is based on the analysis of the peak amplitude, while temporal characteristics are often discarded. We investigated how the temporal aspects of the BOLD signal can reveal some aspects of the underlying neuronal activity that would have been missed if attention were only focussed on the signal amplitude. In Chapter 2, after a brief introduction to the BOLD signal we introduce a novel method for the estimation of the hemodynamic response with high temporal resolution. This analysis of the BOLD dynamics will be used either to further support a theory already hypothesized by the traditional amplitude-based fMRI analysis (Chapter 3) or to show effects that could not be revealed by the traditional fMRI analysis methods since they do not involve changes in signal amplitude (Chapter 4).

The second aim of this thesis is to analyze the relationship between BOLD signal and the brain electrical signals, as recorded by the surface electroencephalography (EEG). Thanks to the ELECTRA inverse solution method [56] we were able to estimate the intracranial LFPs generating the EEG recorded at the surface of the scalp, and we analyzed how the relationship between LFP and BOLD signal varies across different frequencies. In Chapter 5, after a brief introduction to the EEG signal we will show a novel method for the analysis of EEG data, and in particular for the estimated intracranial LFPs. This method is based on the spectral analysis of each single trial individually and allows for evaluating the contribution of all the frequencies, including the very high-frequency oscillations. Moreover, in Chapter 5 we will also show a method for comparing the results of fMRI analysis with those of the abovementioned single-trial analysis. Finally, this method will be employed in a passive visual experiment to evaluate the contribution of high-frequency oscillations and to study how the relationship between fMRI and LFP statistical maps vary across frequency and anatomical regions (Chapter 6).

1.2 Main Contributions

The main contributions of this work can be divided in methodological and neurophysiological results.

- Methodological findings include:

  - Development of a novel technique to estimate the HRF with high temporal resolution (technique first presented in a paper published in Experimental Brain Research [89] and also applied in [88]).
  - Development of a method, the analysis of BOLD dynamics, which provides an essential translational link with electrophysiology as well as animal models (technique first presented in a paper published in Experimental Brain Research [89] and also applied in [88]).
  - Demonstration that the analysis of the temporal characteristics of the BOLD signal can reveal effects that may go undetected using traditional analysis approaches, based on BOLD amplitude (result presented in [88]).
  - Development of a novel EEG single-trial analysis method (technique presented as a poster at the HBM 2006 annual meeting).
  - Development of a method to evaluate the regional relationship between fMRI and EEG single-trial statistical maps (technique presented as a poster at the HBM 2006 annual meeting).

- Neurophysiological findings include:
  - Demonstration of a parallel distributed brain process in response to a simple visuo-motor task (result published in Experimental Brain research [89]).
  - Non-invasive demonstration of auditory-visual multisensory interactions within both primary visual and auditory cortices in humans (result presented in [88]).
  - Non-invasive demonstration of the contribution of very high-frequency oscillations during a passive visual paradigm (result presented as a poster at the HBM 2006 annual meeting).
  - Non-invasive demonstration that the relationship between BOLD and estimated intracranial LFPs varies across frequencies and anatomical regions (result presented as a poster at the HBM 2006 annual meeting).

Part I

Analysis of BOLD dynamics

2 The BOLD signal

Part I focuses on the study of the BOLD signal and on how the analysis of its temporal characteristics can be a useful tool to improve our understanding of human brain functions.

This chapter first provides a brief description of the BOLD signal, its origin, and its salient features. Then, we describe a novel method for estimating the HRF with high temporal resolution. The basic idea underlying this method was first proposed in [71], but this the first demonstration that this technique allows the HRF to be estimated with a temporal resolution much higher than the volume acquisition rate.

2.1 Physiological bases of the BOLD signal

The BOLD fMRI signal is an indirect measure of oxyhemoglobin (hemoglobin carrying an oxygen molecule), and therefore of the oxygen locally present in the blood flow. While oxyhemoglobin has almost no magnetic properties, deoxyhemoglobin (hemoglobin not containing an oxygen molecule) packed in red blood cells is paramagnetic and creates local inhomogeneities in the surrounding magnetic field. The higher the concentration of deoxyhemoglobin, the greater the local inhomogeneity and, therefore, the greater is the decrease in the fMRI signal [62, 93].

The typical model of the hemodynamic response to a brief burst of neuronal activation is made of three different stages [62] (a theoretical example is show in Fig. 2.1). Following the neuronal activation, there is a local increase in the oxygen consumption and, therefore an increase of the relative amount of deoxyhemoglobin. This fact causes a small and not always detectable decrease in the fMRI signal known as the *initial dip* [155]. After this stage, we observe a large increase in the blood supply that overcompensates the oxygen extracted by the neuronal activity. This blood oversupply leads to a decrease of the relative amount of deoxyhemoglobin and consequently to a large increase of the BOLD signal, which reaches its maximum approximately five seconds after the stimulus onset. Finally, the blood flow

starts to return slowly to the baseline level and the fMRI signal decays. In this stage we observe an undershoot of the signal before again reaching a stable level, approximately 24 seconds after the stimulus onset [62].

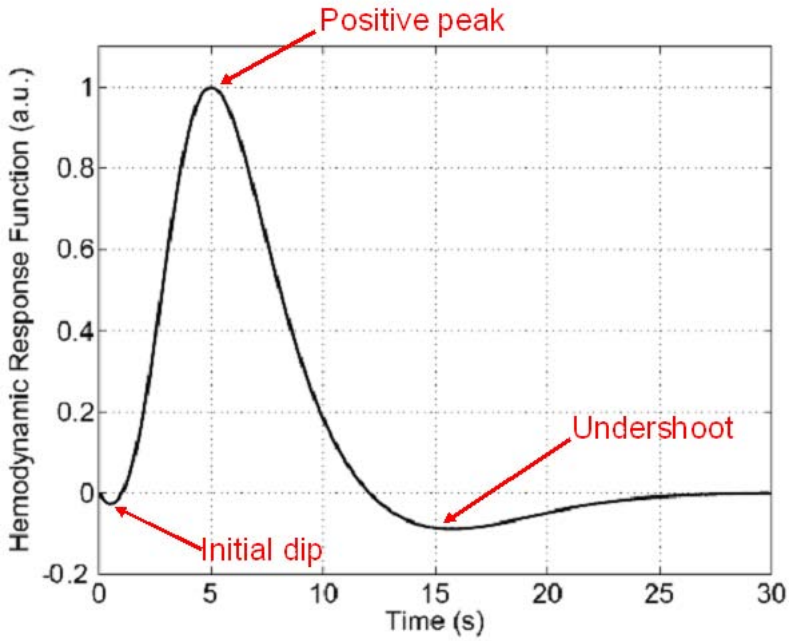

Figure 2.1: Hypotetical response to a brief pulse of neuronal activity (HRF)

There are some important caveats to keep in mind in the interpretation of fMRI results. First of all, fMRI is an indirect measure of the neuronal activity. Therefore, all the hypotheses that can be drawn on the underlying neuronal activity strongly depend on the assumptions made on the neurovascular coupling. Secondly, the fMRI signal reflects the average neuronal activity over a certain volume, containing a large number of neurons [62]. Therefore, we can not ascertain wether an increase in the fMRI signal is related to a high neuronal activity in a small group of neurons or to a small activity in a large group of neurons. Thirdly, the fMRI activation maps can be biased by the larger veins [78, 95, 155]. Changes in the relative level of deoxyhemoglibin are higher in the large than in the small veins. Hence, the maximum of the BOLD signal is more likely localized near such large veins, that can be few millimeters away from the real focus of activation. Moreover, veins drain blood from a volume that is usually larger than the active area [78, 93, 95, 155]. This fact induces an implicit spatial blurring leading to a detection of a wider areas than true neuronal activation. Finally, it is noteworthy that the BOLD signal evolves on a temporal scale much longer than the underlying neuronal activity and, as a first approximation, can be seen as its smoothed version [66]. Due to the temporal characteristics of the BOLD signal, fMRI has a relatively poor temporal resolution, especially if compared with the sub-millisecond temporal resolution of the electromagnetic techniques — i.e. electro- and magneto- encephalography (EEG and MEG, respectively). This reduced temporal resolution is inherent in the BOLD signal and hence can not be improved by innovations in

the acquisition technique. The only way to overcome this limitation would be to obtain a measure that reflects more directly the neuronal activity (pioneering examples can be found in [8] and [161]).

2.2 Temporal analysis of the BOLD signal

Traditional fMRI data processing methods restrict their analyses to the signal amplitude, discarding all the other features. However, there is increasing evidence that the latency of the HRF may be informative on the neuronal activity following brief stimulation (e.g. [63, 75, 97, 100]).

Part of this thesis project concerns the evaluation of the peak latency of the BOLD signal (see section 2.3) and its modulation across different experimental conditions (see Chapters 3 and 4). Although tempting, it should be kept in mind that this analysis cannot be used to compare latencies across different regions (as used in electrophysiology to estimate the temporal order of engagement of different brain areas involved in a certain task), because of the regional variabilities in the HRF time course [58, 100], that can induce changes in the peak latencies that can be larger than those induced by a different pattern of neuronal activity. A difference in the HRF within the same region, instead, can be explained only by a change in the neurovascular coupling or by a change in the neuronal activation pattern. We consider that in absence of other changes in the experimental conditions (e.g. drug injection or blood oxygenation) it is reasonable to assume that the HRF in a certain area does not change markedly across time, therefore changes in its shape can be ascribed to changes in the processing at the neuronal level.

Several methods have been proposed for estimating the latency and other parameters of the HRF time course (e.g. [20, 40, 45, 63, 75, 76, 83, 100, 122, 125, 132]). Using the general linear model to estimate fMRI activation maps, latencies can be estimated by including in the estimation model, not only a model of the expected HRF, but also its temporal derivative [45], or a different shifted version of the expected model [40]. Recently, robust approaches have been proposed to estimate the latency and its standard error of the HRF [63, 83]. Other authors proposed non-linear methods based on HRF iterative fitting procedures [20, 100, 122, 127]. These methods allow for including a bigger number of free parameters and hence they can better take into account the regional and inter-subject variabilities of the HRF. On the other hand, however, the increased complexity of these methods leads to a higher computational load, and in noisy data they might not converge to a final solution. Even if these methods can be blindly applied throughout the entire brain, they are usually used during post-hoc analyses over some previously selected regions of interest [40, 127].

All the abovementioned methods rely on a predefined model of the HRF and their sensibility is tightly linked to how well that model fits the acquired data. The shape of the HRF is not precisely known and can vary between regions and individuals due to either (or both) anatomical (e.g. different vascularization) and neuronal coupling (e.g. different neuronal recruitment strategies). Even if these methods include some free parameters to

deal with this variability, the goodness of fit of the model, and therefore the sensibility of the method, can vary across brain regions. To avoid this problem some authors estimated the HRF with methods that are 'blind' to *a priori* assumptions, such as 'independent component analysis' (ICA) [94], an approach that decomposes the data into maximally statistically independent components, without relying on any *a priori* assumption on the shape of the HRF. This technique has been used to evaluate single trial variability [35] or to analyze HRFs with unexpected time courses [144].

2.3 Estimation technique

In this work, we propose an alternative technique to estimate the HRF without employing any particular model. The only assumption made is that within a certain region the HRF in response to a particular sort of stimulus remains constant for the entire duration of the experiment. This method is simple and computationally easy, and does not require any *a priori* hypothesis on the waveform of the BOLD signal. The drawback is that, if we do not want to include any assumption on the summation of the BOLD responses, this method requires a rather long inter-trial interval to minimize overlap between fMRI responses elicited by adjacent stimuli in time.

2.3.1 High temporal sampling

There are technical limitations in the temporal sampling of the BOLD signal. The first limit is the acquisition time. This value changes dramatically with the the number of slices acquired, the in-plane resolution, and the particular MR scanner used. At present, it is difficult to acquire faster than 100 ms per single slice. Another limitation is related to the fact that when exciting the same slice rapidly, the nuclei of that slice do not have time to come back to the original condition before the new radiofrequency (RF) pulse arrives (the so-called T1 saturation). This fact produces a reduction of the signal, but not of the noise and, therefore, in a reduction of the signal-to-noise ratio (SNR). The shorter the time between two successive RF pulses (TR), the lower is the SNR. This means that it is possible to track precisely the hemodynamic response in a particular region, acquiring rapidly one single slice, but this comes at the cost of a reduced SNR.

We propose a technique that, under the hypothesis that the HRF in response to a particular stimulus remains constant during the entire duration of the experiment, allows us to estimate the HRF with a temporal resolution finer than the TR. The basic idea is that since it remains constant during the experiment, the HRF can be sampled at different time points across trials by varying the temporal relationship between volume acquisition and stimulus presentation. A schematic representation of this technique is shown in Figure 2.2.

We introduce a pseudo-random, variable delay between stimulus onset time and volume acquisition. By varying the temporal relationship between volume acquisition and stimulus presentation, the hemodynamic response is sampled at different time points after the stimulus onset. For example, if the stimulus onset is synchronous with the image acquisition, we

sample the HRF at 0 s, after 1 TR, after 2 TRs, etc. When the stimulus onset precedes the image acquisition of Δ s, we sample the HRF at Δ s, 1 TR+Δ s, 2 TR+Δ s, etc. At the end of the acquisition, if the different delays (Δ) are evenly distributed in the interval [0 TR], we can reorder all the samples acquired according to their temporal distance with the stimulus onset. In this way, it is possible to effectively sample the HRF with a temporal resolution finer than the TR. This method is a variant of that proposed by Josephs et al. [71], but in this work we highly increased the temporal resolution of the estimates.

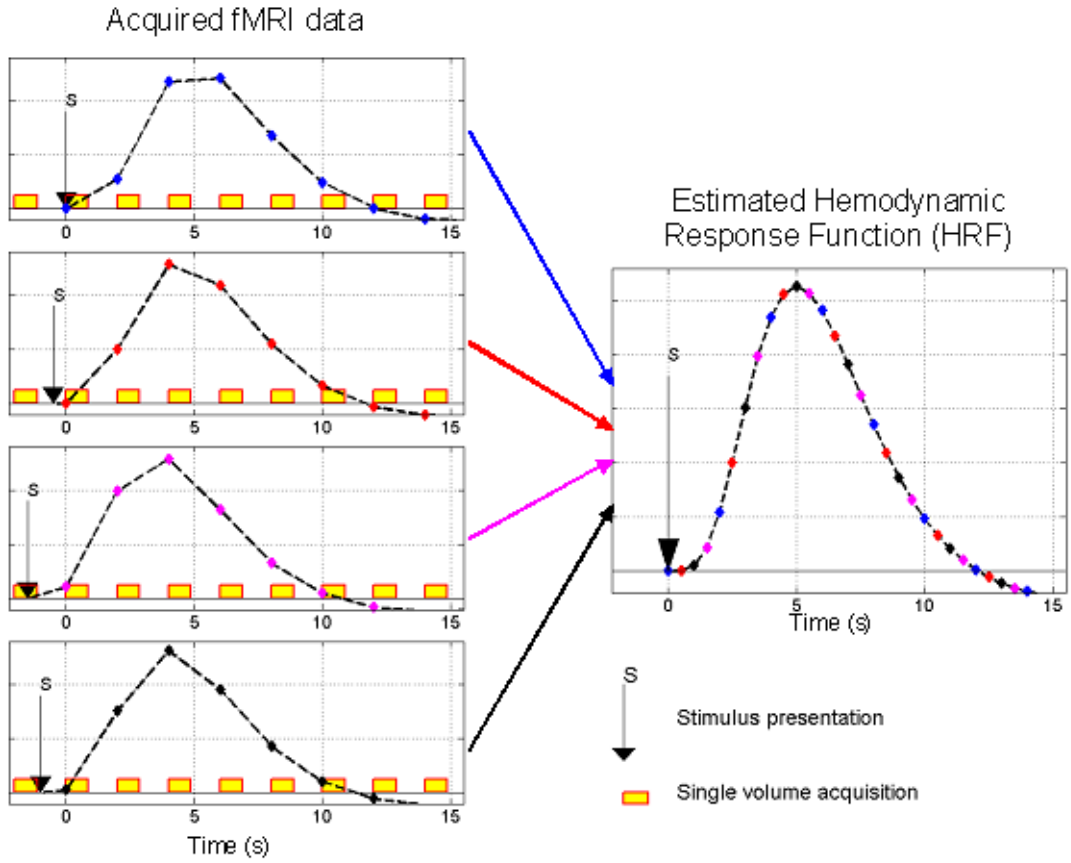

Figure 2.2: Schematic representation of stimulus presentation and fMRI signal acquisition.

2.3.2 Analytical method

To avoid any other assumption on the characteristics of the HRF (except the temporal reproducibility), we decided to widely space the stimulus presentations to allow the BOLD signal to return to baseline before a new stimulus. Using inter-trial intervals larger than 15 s, it is reasonable to assume minimal interaction between responses to successive stimuli meaning that each sample acquired contains information on the response to the preceding stimulus [17, 96]. Therefore, the HRF can be estimated by simply averaging the samples collected per each time point. Signal values are finally recomputed in terms of percent signal

change referred to the baseline value, estimated as the mean value of the signal during the two seconds preceding the stimulus onset.

To reduce the high-frequency noise still present in the signal, data are low-pass filtered. The filter employed is a 4^{th} order elliptic filter with a cut-off frequency of 0.28 Hz. To prevent phase distortion in the filtered signal, the filter was applied according to the *zero-phase forward and reverse filtering technique* [92].

In this work, the analysis of the signal peak latencies is conducted as a *post-hoc* analysis restricted to active regions, as defined by classical fMRI data analysis tools based on signal amplitude. This choice has been done to restrict the analysis of delays to the regions denoting a effective response to the stimulus. To better estimate BOLD peak latency, the signal around the peak (approximately 1.2 s before and after the peak) is fitted with a cubic curve, and the latency is estimated as the peak of this cubic fit.

2.4 Summary

In this chapter we described a new technique for estimating the HRF with high temporal resolution. The basic idea of this method is that by changing the synchronization between stimulus delivery and volume acquisition it is possible to sample the HRF with a temporal resolution much finer then the volume acquisition rate. The only underlying hypothesis is that the BOLD signal in response to a particular stimulus remains constant during the entire experiment.

While the idea of improving the temporal resolution of the estimate by jittering stimulus delivery and volume acquisition [71], this is the first demonstration that this method permits sampling the HRF with a temporal resolution fine enough to study the temporal characteristics of the signal. In particular, this technique makes it possible to evaluate how the temporal parameters of the BOLD signal are modulated by experimental conditions, giving an additional tool to improve our understanding of human brain functions. Two examples of the application of this method are reported in Chapters 3 and 4.

Visuo-motor pathways revealed by event-related fMRI

3

In Chapter 2 we described a method that, with minimal *a priori* hypotheses, allows for estimating the HRF with a temporal resolution much higher than the volume acquisition rate. In this chapter, we apply this technique to a simple reaction time task in response to lateralized visual stimuli (the so-called Poffenberger paradigm) to test whether the brain shows either topographically or temporarily different responses after stimulations of the visual hemifield ipsi- or contra- lateral to the responding hand. This will be useful in evaluating parallel vs. serial models of visuo-motor routing.

3.1 Introduction

Anatomical studies of the visual system have demonstrated how cortical areas are highly interconnected and organized in parallel, distributed networks both in animals (e.g. [37, 156, 163]) as well as humans (e.g. [19, 28, 30, 34, 164]). Moreover, neurophysiological evidence indicates that responses to sensory stimuli can rapidly propagate through these networks and that several regions can be simultaneously active (e.g. [7, 41, 87, 98, 103, 107, 109, 112, 133, 134, 136, 138, 141, 151–153]). Of increasing interest, therefore, are the questions of both how and when information is routed through such interconnected networks, as well as which pathways play a critical role in mediating behavior.

One particular case is that of visuo-motor routing, as in a simple reaction time paradigm wherein the subject performs a motor response to the detection of a visual stimulus. The initially divided representations of the visual fields as well as the lateralized motor representations make it possible to generate experimental conditions that, in principle, would result in distinct routes of visuo-motor interaction. Specifically, visual stimuli presented laterally to either the same or opposite side of space as the hand mediating the motor response produce the so-called "uncrossed" and "crossed" conditions, respectively. Poffenberger [120]

used these conditions as a putative means of measuring interhemispheric transmission time. The underlying premise is that the "uncrossed" condition does not require visuo-motor information transfer to the other hemisphere, since the hemisphere mediating the motor response is the same as that initially receiving the sensory input. By contrast, in the "crossed" condition information must be transferred between the hemispheres. The typical behavioral consequence with this paradigm is that reaction times are slower for the crossed versus uncrossed condition (the so-called crossed-uncrossed difference or CUD). Relatively consistent CUD estimates on the order of 4 ms have been obtained from healthy individuals [67, 90], which have been interpreted as reflecting the engagement of a longer/slower visuo-motor pathway in the crossed condition than in its uncrossed counterpart. That is, these conditions would either (1) utilize distinct brain networks for visuo-motor routing and/or (2) engage the same networks but with different temporal/functional dynamics.

The robustness of this behavioral measure raises the question of its neurophysiological basis. The predominant hypothesis is that the CUD reflects transmission time across the corpus callosum, or at least the additional collective transmission time in the case of the crossed conditions. A critical role of callosal fibers is supported by the repeated observation of substantially larger CUD measures in acallosal and callosotomized patients than in healthy subjects (reviewed in [90]). Despite this clear demonstration of the importance of the corpus callosum in normal brain functions and behavior, direct generalization is problematic due to likely plasticity in these patients (e.g. [15]). In fact, recent functional imaging studies of such patients would indicate that these individuals might use an altogether different brain network than healthy controls [91]. While such data provide important insights on the possibility of multiple interhemispheric anatomic channels, it cannot be concluded from the study of such patients whether these channels are regularly used in the intact brain or rather become functionally relevant only after injury and/or agenesis. Thus, the precise functional importance of the corpus callosum and other, subcortical interhemispheric pathways requires investigations of the intact brain.

Recently, several groups have used hemodynamic brain imaging methods in healthy individuals to determine the neurophysiological basis of the CUD. Three such fMRI studies provide evidence for increased activity in the white matter tracks of the corpus callosum [115, 150, 160]. However, the neurophysiologic credibility of BOLD activation within the white matter remains debated, leading many authors, who do observe activations within the corpus callosum, to suggest caution in over-interpreting their findings (e.g. [150]). Two other groups provide evidence for a predominant role of parietal areas in mediating the CUD [69, 91]. In addition to different spatial patterns of activations, methodological variations hinder consensus across these studies. For example, some applied a blocked design, increasing the likelihood of attentional biases [91, 150, 160]. Others observed CUD in BOLD activity only after applying a relaxed statistical criterion [115], or had tested a limited number of participants with very few trials per condition [69]. Consequently, the results of each of these studies await replication, and the identification of regions differentially activated under crossed and uncrossed conditions remains largely unresolved.

There are additional difficulties in interpreting the CUD behavioral measure. One

source stems from the fact that some groups have either failed to observe such reaction time differences or have observed differences opposite to anatomical predictions — i.e. the crossed condition resulted in faster reaction times than the uncrossed condition (see e.g. [11, 82, 133–135, 151]). By contrast, others have observed stable CUD measures across a wide distribution of reaction times [67]. Likewise, and as mentioned above, there is abundant anatomical data concerning the interconnectivity of the cerebral hemispheres as well as functional data concerning neural response propagation. Anatomical tracing studies indicate that even lower levels of the visual anatomical hierarchy are interconnected with the opposite hemisphere (e.g. [29, 30, 34] see also [23] for recent diffusion tensor tractography results). fMRI has extended upon these anatomical results to show activity within the occipital and parietal cortices of the ipsilateral hemisphere in response to passively viewed unilateral stimuli [10, 38, 154]. This activation pattern further varied as a function of the stimuli's physical properties, with moving gratings yielding both a dorsal and ventral extension within the ipsilateral hemisphere and naturalistic images yielding predominantly the latter [154]. Corroborating results are also available from electroencephalographic studies that observed early ipsilateral responses over posterior as well as frontal scalp sites (e.g. [26, 107, 130, 133, 134, 136]; see also [7] for human intracranial evidence). Other studies using hemodynamic methods and blocked designs, however, report little or no evidence of such bilateral responses to unilaterally presented stimuli (e.g. [91, 150]). Thus, the extent to which unilateral stimuli lead to bilateral responses remains unresolved. However they were critical for determining whether the CUD comparison might be better interpreted as reflecting a relative functional difference in visuo-motor pathways, rather than an absolute measure of interhemispheric versus intrahemispheric transmission (see also [134]).

A similarly controversial aspect of visuo-motor routing is concerned with the functional level at which interhemispheric interactions occur (e.g. [24]). The application of electrophysiological and hemodynamic measures to the Poffenberger paradigm has yielded conflicting interpretations. Interhemispheric transfer of visuo-motor information in the "crossed" condition has been proposed to occur first at a pre-motor/motor level (e.g. [68, 69, 150, 151]), or already at a visual level (e.g. [14, 70, 107] see also [32] for supporting evidence from patients with partial callosal lesions/sections). Others, applying a case-study approach to the analysis of electrophysiological data, report how visuo-motor routing varies both between individuals and also as a function of reaction time [133, 134]. One possibility, for which these authors provide preliminary data, is that trials leading to fast reaction times within a subject's own reaction time distribution may rely on a predominantly motor-level of interhemispheric interaction, whereas trials leading to slow reaction times might rely on a predominantly visual-level transfer [133, 134] (see also [27]). This proposition would appear to run counter to that put forward by Iacoboni and Zaidel [67], which suggests that the CUD across the reaction time distribution reflects hard-wired, functionally invariant mechanisms. The question whether there are distinct and behaviorally defined networks of visuo-motor routing for the crossed and uncrossed conditions as a function of subjects' reaction times, therefore, remains unresolved.

To examine the pathways of visuo-motor routing fMRI was used. Specifically, to de-

termine whether the so-called "crossed" and "uncrossed" conditions rely on distinct brain networks for visuo-motor integration, an event-related fMRI paradigm was used as subjects completed a simple RT task with a 2 hemifield × 2 hand of response design. Recent developments in the analysis of event-related fMRI data indicate that latency analyses can be performed on the directly measured hemodynamic response function (HRF) by means of rapid sampling of the BOLD signal (e.g. [6, 39, 63, 97, 128, 131]). As such, both the spatial as well as the temporal pattern of responses during visuo-motor integration were analyzed.

3.2 Materials and methods

3.2.1 Subjects

Ten subjects (aged $25 - 51$ years, mean $\pm$ SD $= 33.1 \pm 8.8$ years; 4 male and 6 female) participated after providing written informed consent. All subjects were right-handed [114], had no history of neurological or psychiatric disease, and had normal or corrected-to-normal vision. The Ethical Committee of the Centre Hospitalier Universitaire Vaudois approved all procedures. This research was in agreement with the Code of Ethics of the World Medical Association (Declaration of Helsinki).

3.2.2 Magnetic resonance imaging

Functional MRI data were acquired using an event-related design on a 1.5 T Siemens Magnetom Vision system equipped for echoplanar imaging. To reduce head motion, subjects' heads were fixed in the coil by a vacuum beanbag. The BOLD signals were obtained with a single shot gradient-echo EPI sequence (TR = 2 s, TE = 60 ms, FoV = 240 mm, flip angle = 90°, matrix size 64×64). Each volume was comprised of 16 slices (slice thickness 5 mm, gap 1 mm) parallel to the bicommissural plane and covering the entire cerebral hemispheres. Slices were acquired in descending order (i.e. first slice at the top of the head). To provide precise structural and anatomical localization of brain activity, a sagittal T1-weighted 3D gradient-echo sequence (MPRAGE) was acquired for each subject (128 contiguous sagittal slices, slice thickness 1.25 mm, matrix size 256×256, TR = 9.7 ms, TE = 4 ms, FoV = 256 mm, flip angle = 12°).

3.2.3 Experimental procedure

Subjects performed a simple reaction time task to laterally presented black-and-white checkerboard stimuli (3° wide × 4° high; the middle of which appeared 9.5° from central fixation) projected onto a screen affixed to the end of the head coil. Subjects viewed this screen from an inclined mirror positioned above their eyes, as they lay supine within the magnet's bore. Approximately every 16 s (see below for precise intervals), a checkerboard appeared in either the right or left visual field (RVF or LVF, respectively) for a duration of 100 ms. The visual field stimulated was randomly intermixed across trials. Subjects were asked to respond to stimulus detection by pressing keys on a MRI-compatible device

(Photon Control Inc., Burnaby, BC, Canada) in a manner similar to rolling keys on a piano (i.e. by pressing four keys, one per finger, in one swift and continuous movement like tapping one's finger's on a table). Reaction times were recorded as the latency at which the first of the keys was pressed. This type of response was selected to optimize motor activations in fMRI images. Response hand was maintained throughout a block of trials, and subjects completed two blocks — the first with the right hand (RH) and the second with the left (LH). This 2 (response hand) $\times$ 2 (visual field) design yielded the following four experimental conditions for each subject: RH-RVF, RH-LVF, LH-RVF, and LH-LVF.

The inter-stimulus interval (ISI) varied pseudo-randomly from 14.125 to 17.875 s in steps of 125 ms. This range of long ISIs was chosen to allow the BOLD signal to return to baseline between stimulus presentations. There was a pseudo-random, variable delay between stimulus onset time and volume acquisition of 0 to 1.875 s at steps of 125 ms, yielding a total of 16 different delays. This variable temporal relationship between volume acquisition and stimulus presentation allowed the BOLD signal to be effectively sampled with a temporal resolution of 125 ms (see details in section 2.3.1). Each of the four experimental conditions included 32 trials, allowing for two volume acquisitions at each of the 16 delays used. 514 volumes were acquired during each session, and the first two volumes were discarded to allow for T1 equilibration effects.

3.2.4 Data analyses

Two types of analyses were conducted in order to investigate whether the "crossed" and "uncrossed" combinations of visual field stimulated and response hand engage distinct networks for visuo-motor routing. The first determined whether distinct spatial patterns of activated brain regions were present. The second determined whether the temporal dynamics within activated brain regions varied across experimental conditions. This was done by measuring the peak latency of the estimated HRF (details are described below).

Spatial Domain: activation maps

Activation maps were obtained using SPM99 software (Wellcome Department of Cognitive Neurology, London, UK) running on a Silicon Graphics Octane computer. Volumes were first spatially realigned to the first volume acquired in the session to reduce the effect of head movement during the acquisition. Each volume was then temporarily realigned to the first slice acquired (the one at the top) to correct the effect that slices in the same volume were acquired sequentially during a period of 1.7 s and therefore have a different delay relative to stimulus onset. Volumes were then normalized to a standard brain, based on the Montreal Neurological Institute (MNI) template, re-sampled to a voxel size of $3 \times 3 \times 3\,\mathrm{mm}^3$ using a bilinear interpolation, and smoothed with an isotropic Gaussian kernel (FWHM = 9 mm).

For each subject, a high-pass filter was applied on the time series to minimize possible effects of baseline drift, and the statistical analysis was performed with the General Linear Model (GLM), using the canonical HRF and its temporal derivative as a basis function, as defined in SPM99. An F-test was then performed to obtain the statistical parametric maps,

which were thresholded ($p < 1 \times 10^{-5}$ uncorrected) to identify active voxels in the data of each individual subject. Structural and functional volumes were co-registered within the same coordinate system by normalizing structural images to the MNI template brain and re-sampling voxels to a $1 \times 1 \times 1\,\mathrm{mm}^3$ size. Inference on the population (group analysis) was obtained by means of a second level of statistics, according to the random effects theory [65].

Several spatial analyses were conducted. The first determined active regions in each condition (voxel-level threshold at $p < 0.001$; 20 voxel spatial extent threshold). This addressed the question of whether or not each condition resulted in bilateral responses, even though functionally unnecessary in the uncrossed conditions. The second set of analyses tested for main effects of each visual field and each response hand, as well as of crossed versus uncrossed conditions (see [150] for a similar analysis). Effects of LVF were identified by contrasting conditions involving the LVF with those involving the RVF, independently of response hand [i.e. (LH-LVF + RH-LVF) versus (LH-RVF + RH-RVF)]. The inverse contrast tested for a main effect of RVF stimulation. The main effect of left response hand was assessed with the contrast of (LH-LVF + LH-RVF) versus (RH-LVF + RH-RVF), and the main effect of right response hand was assessed with the inverse contrast. Global crossed versus uncrossed differences in BOLD activation patterns were assessed with the contrast of (LH-RVF + RH-LVF) versus (LH-LVF + RH-RVF). More focused contrasts then examined the effect of stimulated visual field while holding response hand constant, as well as the effect of response hand while holding the stimulated visual field constant. In all cases, only those activations significant at $p < 0.001$ (voxel-level) and with a spatial extent of at least 20 contiguous voxels were considered. A third set of analyses tested for differences in the BOLD activation patterns as a function of reaction time. Those trials yielding the fastest, the middle, and the slowest third of reaction times were analyzed separately ($N = 11$ trials per condition and subject for the fastest and the slowest reaction time portion, $N = 10$ for the middle portion). In both cases, crossed versus uncrossed conditions were compared [i.e. (RH-LVF + LH-RVF) versus (RH-RVF + LH-LVF)].

Temporal domain: estimated hemodynamic responses

Areas were selected according to the SPM activation maps obtained from the group study and from each individual subject, in the four conditions (i.e. the first spatial analysis described above). For each experimental condition, only those areas showing activity for all subjects were retained for temporal analysis. Anatomical localization was defined on cortical structural basis and MNI coordinates (see e.g. [79, 162]). Inside each of those regions, the hemodynamic time course was extracted at the location of the statistically most activated voxel. Analysis was restricted to only this most activated voxel (instead of a group of voxels) because the denoising effect provided by such a spatial averaging was already performed effectively by the Gaussian spatial filter, applied during the pre-processing steps described above (this filter itself is a spatial averager, since it weights the response at one voxel by its neighbors, thereby reducing the variability across space).

Given the rather long ISI used, it was reasonable to assume minimal interaction be-

tween responses to successive stimuli [17, 96]. Therefore, it was possible to reconstruct the hemodynamic response by simply averaging the two samples collected at each time point relative to stimulus onset, applying the method described in section 2.3.2. To do this, a customized toolbox for Matlab was developed (The Mathworks Inc., Natick, MA, USA). Baseline value was estimated as the mean value of the signal during the 2 s preceding the stimulus onset.

Delays in the hemodynamic signals were estimated as the latency of the peak of the reconstructed response. As described in section 2.3.2, the signal around the peak (e.g. 1.25 s, equal to ten data points before and after the peak) was fitted with a cubic curve and the latency was estimated as the peak of this cubic fit. Estimation of the delay in the hemodynamic signal based on the latency of the peak was preferred to analyses using HRF fitting because this simple method does not require a priori hypotheses on the shape of the response. Note that it was not feasible to perform this analysis as a function of reaction time, since there was no means of assuring that reaction times were evenly distributed throughout the ISI range of the study, which is necessary to estimate the hemodynamic signal. A further comment worth mentioning is that in the present study only two samples were collected at each time point relative to stimulus onset. While increasing this number would have the benefit of improving the estimation of the timecourse of the BOLD response, it would come at the cost of extending an already long experiment for the subject and therefore possibility introducing effects of arousal and fatigue.

3.3 Results

3.3.1 Behavioral results

In the four conditions, mean (±SD) reaction times were 473 ± 81 ms for RH-RVF, 472 ± 86 ms for RH-LVF, 496 ± 87 ms for LH-RVF, and 487 ± 85 ms for LH-LVF. These values were submitted to a 2×2 repeated measures ANOVA with the within subjects factors of response hand and visual field stimulated. Neither main effect nor their interaction reached our significance criterion of $p \leq 0.05$, providing no statistical evidence of a robust CUD. However, comparison of the group mean reaction times from the "crossed" conditions (484 ms) with those from the "uncrossed" conditions (480 ms) yielded an absolute CUD of ~ 4 ms (note: this is not the result of a statistical test, but rather a quantification measure), consistent with the findings of previous research (e.g.[67, 90, 150]). A Page test [64] evaluated the relative reaction time speed across the four experimental conditions, and the following rank order was observed: RH-LVF < RH-RVF < LH-LVF < LH-RVF ($p = 0.031$). This pattern is largely consistent with that observed in a previous meta-analysis, where the LH-RVF condition consistently had the slowest reaction time [90]. This general consistency with previous studies provide one indication that our paradigm indeed emulates a prototypical Poffenberger experiment, despite the lengthy ISI used and the non-standard motor response required. We would also note at this point that other studies that obtained a similar pattern of behavioral results used a blocked design as well as more

simple light flashes, suggesting that the Poffenberger paradigm withstands such variations (as already noted by Marzi et al. [90]). It likewise is worth mentioning that our RTs are substantially slower than what has been obtained in several prior fMRI/PET studies (e.g. [91, 150, 160]). One possibility is that this follows from the different motor response required of subjects*. Another is that such differences follow from blocked versus event-related paradigms and potential influences on attention/arousal. Further experiments will be required to fully resolve this issue.

In order to examine the stability/variability of the CUD across the reaction time distribution of individual subjects, the fastest third, middle third, and slowest third of the reaction times for each subject and experimental condition were separated (hereafter "fast", "middle", and "slow", respectively; $N = 11$, 10, and 11 trials for each subject and condition, respectively). For the fast trials, mean reaction times for the four conditions were 385 ± 72 ms for RH-RVF, 381 ± 71 ms for RH-LVF, 414 ± 79 ms for LH-RVF, and 409 ± 76 ms for LH-LVF. Comparison of the group mean reaction times from the crossed conditions (397 ms) with those from the uncrossed conditions (397 ms) yielded an *absolute* CUD of < 1 ms. For the middle trials, mean reaction times for the four conditions were 471 ± 83 ms for RH-RVF, 472 ± 93 ms for RH-LVF, 490 ± 91 ms for LH-RVF, and 486 ± 83 ms for LH-LVF. Comparison of the group mean reaction times from the crossed conditions (481 ms) with those from the uncrossed conditions (479 ms) yielded an *absolute* CUD of ~ 2 ms. For the slow trials, mean reaction times for the four conditions were 568 ± 105 ms for RH-RVF, 569 ± 109 ms for RH-LVF, 593 ± 103 ms for LH-RVF, and 577 ± 98 ms for LH-LVF. This case yielded an *absolute* CUD of ~ 9 ms (581 versus 572 ms). Thus, the CUD appears to be essentially absent over the fastest and middle thirds of reaction times, but robust over the slowest third. We return to this point below in terms of variation in crossed versus uncrossed differential activation patterns as a function of reaction time. We further submitted mean reaction times to a $2 \times 2 \times 3$ repeated measures ANOVA with the within subjects factors of response hand, visual field stimulated, and portion of reaction time distribution. Not surprisingly, there was a significant main effect of portion of the reaction time distribution ($F_{(2,8)} = 92.18$; $p < 0.001$). No other main effect or interaction reached the $p < 0.05$ significance criterion.

3.3.2 Spatial domain: activated areas versus 'rest'

Group results are shown in Figure 3.1, which shows the activated areas in each of the four experimental conditions from a sample of slices with the left side of the figure corresponding to the left hemisphere, and listed in Table 3.1, which provides the anatomical location, MNI coordinates, and Z scores of the statistically most active voxels for those areas consistently

*We have partially addressed this issue in a separate pilot study examining simple reaction times to visual, auditory, or simultaneous auditory-visual multisensory pairs. The same subjects first responded with a single finger and several weeks later were re-tested using the piano roll movement used in the present study (both the experiments were conducted within the MR scanner environment). The same pattern of reaction times was observed for both types of motor response, except that the reaction time distribution was simply shifted later in the case of the piano roll.

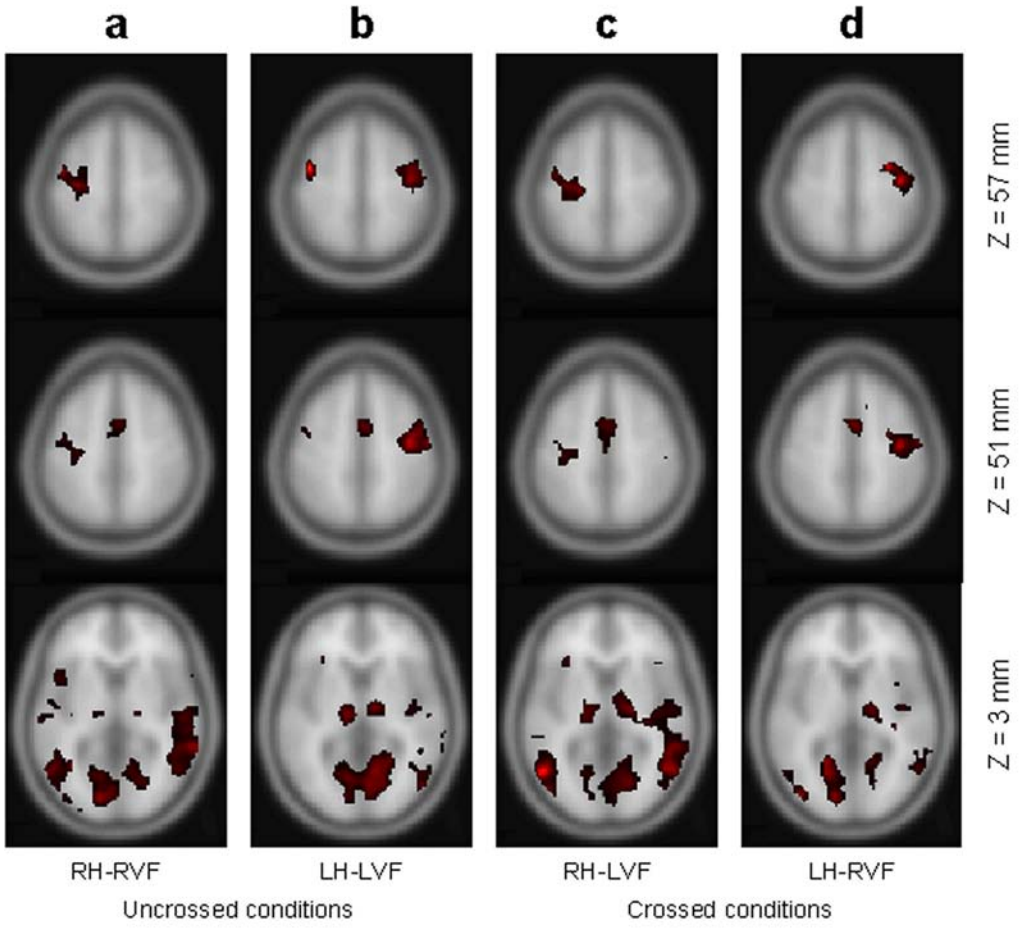

Figure 3.1: Group results showing activated areas in each of the four experimental conditions. a) RH response to RVF stimulation; b) LH response to LVF stimulation; c) RH response to LVF stimulation; d) LH response to RVF stimulation. Slices are parallel to the bicommissural plane at levels z = 3, 51, and 57 mm and are displayed in neurological convention (left hemisphere on left)

activated across subjects. In general across the four conditions, we observed large activations of the medial and lateral occipital lobe contralateral to the hemifield stimulated, as well as a smaller activation of the medial and lateral occipital lobe ipsilateral to the hemifield stimulated. In the right hemisphere such activity often extended into the temporal lobe. Activations of the precentral gyrus were strongly lateralized to the hemisphere contralateral to the response hand with minimal ipsilateral activation. Similar frontal midline activations were observed in all four conditions. However, because of the spatial resolution and filtering of the fMRI data, we are hesitant to classify activity within this region as specifically originating in either the left or right hemisphere. Variable thalamic activations were also present in all conditions.

The coordinates of these regions, when transformed into Talairach space, correspond

Anatomical location	Functional area	Mean MNI coordinates			Mean±SD distance from mean coordinates (mm)	Z-score[a]			
		x	y	z		RH-RVF	RH-LVF	LH-RVF	LH-LVF
Right cuneus (BA 17)	V1 (right)	11	-79	5	6.5±2.8	4.18	4.17	3.10	4.00
Left cuneus (BA 17)	V1 (left)	-10	-82	5	5.6±3.3	4.25	3.42	4.16	3.78
Right posterior middle temporal gyrus (BA 37)	V5 (right)	50	-67	3	9.4±5.6	3.77	4.28	3.70	3.74
Left posterior middle temporal gyrus (BA 37)	V5 (left)	-49	-69	2	8.5±3.5	3.96	4.78	3.43	3.31
Medial frontal gyrus (BA 32)	SMA	0	4	50	8.1±2.9	4.07	3.92	4.22	4.43
Right precentral gyrus (BA 4 and 6)	M1 (right)	41	-12	59	9.3±3.3	3.45	3.63	4.64	4.45
Left precentral gyrus (BA 4 and 6)	M1 (left)	-39	-15	58	10.4±3.9	4.07	4.13	N/A	4.78

[a] Z-score refers to the local maximum in the group statistics nearest to the mean point (listed here in the third column)

Table 3.1: Anatomical location, corresponding functional area, mean MNI coordinates, and Z scores a of the statistically most active voxels across subjects and conditions

to the anatomical location of visual areas V1 and V5 in the occipital lobe and to areas M1 and SMA in the frontal lobe [79, 162]. The mean distance between the most activated voxel in each area of each individual and the mean MNI coordinate was always smaller than 10 mm (maximal standard deviation < 5.3 mm, see Table 3.1). That is, this subset of regions was consistently and reliability activated in all subjects. We return to these regions in our analysis of the time course of BOLD responses, below.

Specifically, the RH-RVF condition (Fig. 3.1a) activated in the left hemisphere (i.e. that contralateral to the stimulus) large regions of the medial and lateral occipital lobe that extended into the temporo-parieto-occipital junction, a large region of the precentral gyrus, and voxels within the posterior thalamus. In the right hemisphere (i.e. that ipsilateral to the stimulus), this condition activated smaller regions of the medial and lateral occipital lobe that extended into the temporo-parieto-occipital junction and superior temporal plane, voxels within the posterior thalamus, and sparse voxels in the precentral gyrus. In addition, there was a large region of the medial frontal gyrus activated.

The RH-LVF condition (Fig. 3.1b) activated in the right hemisphere (i.e. that contralateral to the stimulus) large regions of the medial and lateral occipital lobe that extended into the temporo-parieto-occipital junction, a small region of the precentral gyrus, as well as voxels within the posterior thalamus. In the left hemisphere (i.e. that ipsilateral to the stimulus), this condition activated smaller regions of the medial occipital lobe, a large region of the lateral occipital lobe, a large region of the precentral gyrus, and voxels within the posterior thalamus. A large region within the medial frontal gyrus was also activated.

The LH-RVF condition (Fig. 3.1c) activated in the left hemisphere (i.e. that contralateral to the stimulus) large regions of the medial and lateral occipital lobe, and a large region of the medial frontal cortex. No activation was observed in the left precentral gyrus. In the right hemisphere (i.e. that ipsilateral to the stimulus) this condition activated smaller regions of the medial and lateral occipital lobe, voxels within the posterior thalamus and insula, as well as a large region of the precentral gyrus.

The LH-LVF condition (Fig. 3.1d) activated in the right hemisphere (i.e. that contralateral to the visual stimulus) large regions of the medial and lateral occipital lobe that

included extension into the temporo-parieto-occipital junction, a large region of the precentral gyrus, voxels within the posterior thalamus and insula, and a large region of the medial frontal cortex. In the left hemisphere (i.e. that ipsilateral to the visual stimulus) this condition activated smaller regions of the medial occipital lobe and only a few voxels in the lateral occipital lobe and precentral gyrus.

Thus, robust bilateral responses were obtained for each of the four experimental conditions. A Page test evaluated the relative magnitude of global activity (i.e. the total number of active voxels irrespective of hemisphere and without the application of the 20-voxel spatial criterion) across the four experimental conditions, and the following rank order was observed: RH-LVF > RH-RVF > LH-LVF > LH-RVF ($p < 0.01$). This pattern mirrors that observed with reaction times, such that conditions leading to faster responses activated a larger number of voxels. Conditions involving the right hand or left visual field consistently activated a larger number of voxels. To test whether the combination of response hand and stimulated visual field influenced the extent of bilateral activation, we calculated the total number of activated voxels for each condition and hemisphere (Table 3.2) and submitted these values to a three-way repeated measures ANOVA with the within subjects factors of response hand, visual field stimulated, and cerebral hemisphere. Only those effects yielding p-values ≤ 0.05 were considered statistically significant. There was a main effect of response hand ($F_{(1,9)} = 6.94$; $p = 0.027$), with conditions requiring right-hand responses yielding more activated voxels than conditions requiring left-hand responses. Both the main effect of visual field stimulated ($F_{(1,9)} = 3.35$; $p = 0.100$) and of hemisphere ($F_{(1,9)} = 3.94$; $p = 0.078$) approached our significance criterion. The interaction between these factors of visual field and hemisphere was significant ($F_{(1,9)} = 21.61$; $p = 0.001$), indicating that the number of activated voxels observed in each hemisphere varied with the visual field stimulated. Despite this interaction, we would emphasize that unilateral visual stimulation always led to a bilateral response. Moreover, follow-up comparisons revealed that LVF presentations led to a preponderance of activity within the right versus left hemisphere ($t_{(9)} = 3.75$; $p = 0.005$), and RVF presentations led to a statistically indistinguishable number of activated voxels in each hemisphere ($t_{(9)} = 0.02$; $p = 0.98$). All other interactions in the ANOVA failed to reach the 0.05 significance criterion.

To this point, these analyses indicate that brain responses to the "uncrossed" condition were bilateral and not restricted to a single cerebral hemisphere. Rather, the "uncrossed"

Experimental condition	Left hemisphere[a]	Right hemisphere[a]	Total
RH-RVF	3577 (50.3%)	3530 (49.7%)	7107
RH-LVF	4180 (48.4%)	4462 (51.6%)	8642
LH-RVF	2350 (49.5%)	2393 (50.5%)	4743
LH-LVF	2497 (43.0%)	3305 (57.0%)	5802

[a] The percentage of the total across hemispheres is given in parentheses

Table 3.2: Average number of active voxels (i.e. in the absence of spatial extent criterion) in each experimental condition

conditions led to robust activity (predominantly) within the medial and lateral occipital lobe of the hemisphere ipsilateral to the visual stimulus. This constitutes demonstration of interhemispheric transfer under unilateral viewing conditions, in contrast to the conclusions of previous hemodynamic brain imaging studies reporting activity restricted to the contralateral hemisphere [91]. In addition, the present results run counter to the observation of a rostral versus caudal asymmetry between uncrossed and crossed conditions, respectively, in a PET study using a blocked design [91]. It is important to note, however, that this previous study [91] as well as the subsequent fMRI study by this group [150] never analyzed experimental conditions versus 'rest', which is necessary for determining the extent of bilateral activity elicited by unilateral stimuli. Another, non-exclusive possibility is that the blocked design of these studies (and the attentional set assumed by subjects) significantly contributed to the observed activation patterns. Instead, our data support the activity of a common spatial network across all conditions. We next address whether and how responses within this network differed with visual field, response hand, as well as crossed versus uncrossed conditions.

3.3.3 Spatial domain: main effects of visual field and response hand

Figure 3.2 and Table 3.3 show the main effects of visual field and response hand. The contrast of conditions involving stimulation of the RVF versus those involving the LVF revealed activation within the left occipital lobe. The inverse contrast revealed a similar, though larger, activation in the right occipital lobe. The contrast of conditions involving manual responses with the right hand versus those involving the left hand revealed activation within the left precentral gyrus. The inverse contrast similarly revealed activation in the right precentral gyrus. This pattern largely replicated that observed by Tettamanti et al. [150], who used a blocked design, indicating the sensitivity of the present event-related fMRI paradigm. Likewise, it provides one indication of subjects' adequate fixation and cooperation with the motor task.

3.3.4 Spatial domain: crossed versus uncrossed activation patterns

The global comparison of crossed versus uncrossed conditions failed to reveal any differentially active regions. To more focally test for differences in the activation patterns between the "crossed" and "uncrossed" conditions, we first contrasted RVF and LVF stimulus presentations when the same response hand was used (Fig. 3.3a). This contrast yielded activated voxels in the occipital lobe contralateral to the visual hemifield where the stimulus was presented, irrespective of whether or not the motor response was ipsilateral to the visual stimulation. Details on activated areas revealed by this contrast are provided in Table 3.4. We next contrasted RH and LH motor responses when the same visual field was stimulated (Fig. 3.3b). This contrast activated voxels in the motor representation contralateral to the hand mediating the response (see Table 3.4 for details). That is, our analyses provide no evidence of an alteration in the spatial activation pattern at either a global or focal level between the "crossed" and "uncrossed" conditions. No distinct regions were selectively

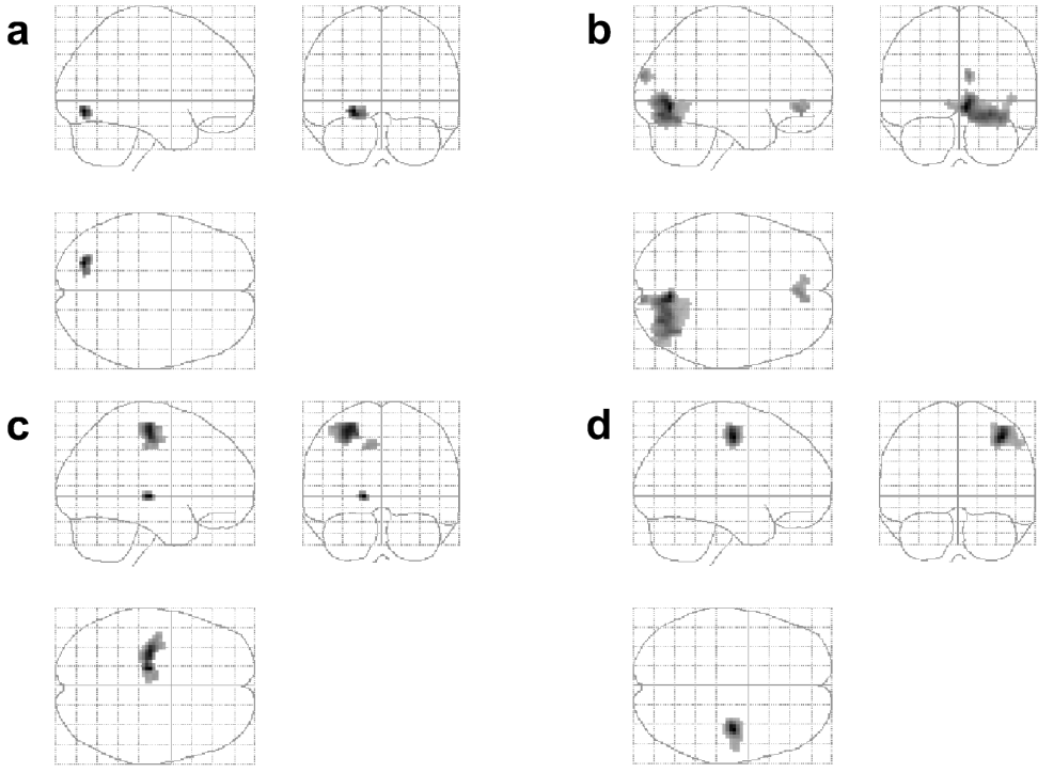

Figure 3.2: Group results showing activated areas for the main effects of each visual field and each response hand. These activations are schematized on a glass brain. a) Main effect of stimulation to the right visual field; b) main effect of stimulation to the left visual field; c) main effect of responding with the right hand; and d) main effect of responding with the left hand. See section 3.2 for details on these contrasts

observed for either the "crossed" or "uncrossed" conditions.

Given that our behavioral data would suggest that the CUD varies across different thirds of the reaction time distribution (< 1 ms, ~ 2 ms, and 9 ms for the fastest, middle, and slowest thirds, respectively), we repeated the comparison of crossed versus uncrossed spatial patterns of BOLD activations separately for each of these portions of the reaction time distribution (Fig. 3.4 and Table 3.5). This comparison with fastest trials as well as the middle trials failed to reveal any statistically significant activation. By contrast, this comparison with slow trials revealed several clusters of differential activation within the right occipital gyrus (BA 19) and right fusiform gyrus, extending into the right middle temporal gyrus (BA 37/39). These results suggest that the speed of reaction time may contribute to whether or not differential activation strengths are observed for the crossed versus uncrossed comparison. Likewise, visual cortical areas appear to play a critical role in interhemispheric interactions during slow trials. To further assess this possibility, we correlated CUD magnitude with the crossed versus uncrossed difference in BOLD responses for each of the three portions of the reaction time distribution, separately. Clusters where

	MNI coordinates			Z Score
	x	y	z	
Effect of right visual field stimulation				
(RH-RVF + LH-RVF) – (RH-LVF + LH-LVF)				
Left lingual gyrus (BA 19)	-24	-75	-9	3.89
Effect of left visual field stimulation				
(RH-LVF + LH-LVF) – (RH-RVF + LH-RVF)				
Right lingual gyrus (BA 18)	6	-69	-6	4.67
Right cuneus (BA 19)	9	-93	21	3.83
Right medial frontal gyrus (BA 10 and 11)	3	45	-9	3.74
Effect of right hand response				
(RH-RVF + RH-LVF) – (LH-RVF + LH-LVF)				
Left thalamus	-15	-18	0	4.43
Left precentral gyrus (BA 4)	-30	-18	57	4.29
Left cingulate gyrus (BA 24)	-12	-21	42	3.52
Effect of left hand response				
(LH-RVF + LH-LVF) – (RH-RVF + RH-LVF)				
Right precentral gyrus (BA 4 and 6)	39	-12	51	4.91

Table 3.3: Anatomical location, MNI coordinates, and Z scores of the statistically most active voxels for main effects of visual field stimulated and response hand

this correlation was conducted were defined by the above results for slow trials. A significant correlation between CUD magnitude and BOLD response difference was observed within BA37 for slow trials ($r = 0.764$; $p = 0.01$), but not for middle trials ($r = -0.470$; $p = 0.17$) or fast trials ($r = 0.173$; $p = 0.63$). No significant correlations were observed in any of the other tested clusters. Lastly, the comparison of the uncrossed versus crossed spatial patterns of BOLD activations separately for each of these portions of the reaction time distribution failed to reveal any significant voxels.

3.3.5 Temporal domain: time course of BOLD responses

The estimated BOLD signal time courses (displayed as the percent signal change) and their mean peak latencies are shown in Figure 3.5 and Table 3.6, as measured at the locations listed in Table 3.1. The BOLD responses for these voxels were averaged across subjects for each of the four experimental conditions, separately. Signal amplitudes are consistent with previous event-related fMRI experiments (e.g. [39, 63]). Time delays of the signals were measured as the latencies of the positive-going peaks in BOLD responses from stimulus onset (see section 3.2 for details). Since the signal from M1 ipsilateral to the responding hand consistently yielded a negative BOLD signal (see Fig. 3.5), this region was excluded from this temporal analysis.

Peak latencies as measured from each of the remaining brain regions were submitted

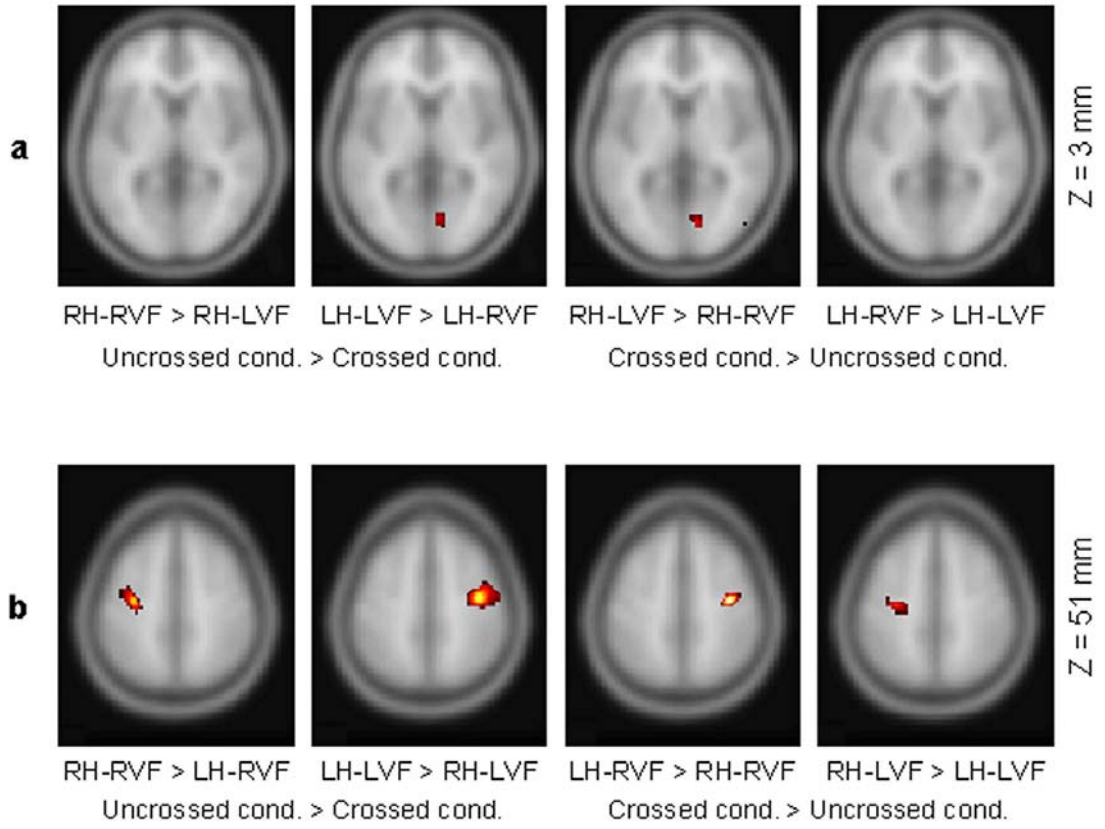

Figure 3.3: Group results of focal contrasts to examine effects of visual field and response hand. a) V1 and surrounding areas (z = 3 mm) that present higher activation during the stimulation of one visual field, keeping fixed the motor response and b) SMA and M1 areas (z = 51 mm) that present higher activation during the response of one hand, keeping fixed the visual stimulation. Slices are in the same convention as in Figure 3.1

to a 2×2 repeated measures ANOVA with within-subjects factors of visual field and response hand. This was done for each functional area separately. For area V1 of the right hemisphere, there was a significant main effect of stimulated visual field ($F_{(1,6)} = 8.773$; $p = 0.025$) with stimulation of the LVF yielding earlier peak latencies. For area V1 of the left hemisphere, the main effect of stimulated visual field approached our significance criterion ($F_{(1,6)} = 4.101$; $p = 0.089$), with stimulation of the RVF demonstrating earlier peak latencies. There was also a significant interaction between stimulated visual field and response hand ($F_{(1,6)} = 9.621$; $p = 0.021$) that followed from a larger LVF versus RVF difference for left-handed versus right-handed responses (mirroring the patterns of reaction times). This indicates that the responding hand plays a role in modulating the peak of the BOLD response in V1. This may reflect an effect of task set (responding hand was blocked) similar to effects of attention recently described by Weber et al. [160]. Lastly, neither main effect nor their interaction reached our significance criterion for area V5 of

	MNI coordinates			Z Score
	x	y	z	
Effect of stimulated visual field (holding response hand constant)				
RH-RVF – RH-LVF				
No suprathreshold clusters				
LH-LVF – LH-RVF				
Right lingual gyrus (BA 18)	9	-75	3	3.76
Right lingual gyrus (BA 18)	21	-72	-15	3.68
RH-LVF – RH-RVF				
Right fusiform gyrus (BA 19)	39	-75	-15	4.72
Right lingual gyrus (BA 18)	12	-78	-3	4.29
LH-RVF – LH-LVF				
No suprathreshold clusters				
Effect of response hand (holding stimulated visual field constant)				
RH-RVF – LH-RVF				
Right precentral gyrus (BA 4 and 6)	-30	-18	57	4.55
LH-LVF - RH-LVF				
Left cingulate gyrus (BA 31)	-9	-24	42	4.72
Right thalamus	9	-3	9	4.03
Left precentral gyrus (BA 4 and 6)	-30	-18	51	3.98
LH-RVF – RH-RVF				
Left precentral gyrus (BA 4 and 6)	39	-15	60	5.12
RH-LVF – LH-LVF				
Left precentral gyrus (BA 4 and 6)	39	-12	51	4.61

Table 3.4: Anatomical location, MNI coordinates, and Z scores of the statistically most active voxels for focal contrasts of visual field stimulated and response hand

either hemisphere or SMA.

It is important to note that peak latency of the BOLD response need not correspond with neural response latencies. However, demonstration of a change in BOLD dynamics across stimulus conditions (all of which have the same presentation duration) does suggest that functional anatomy plays a role in peak BOLD response latencies within a given voxel. Whether or not these shifts in BOLD dynamics are directly related to the shifts in neural activity (as observed with other methods including event-related potentials) is beyond the scope of the present study and must instead await further experimentation and methodological advances that enable the precise localization of ERP sources.

3.4 Discussion

The main finding of the present study is that highly similar spatial patterns of brain activation were observed for all experimental conditions of a simple visual reaction time paradigm,

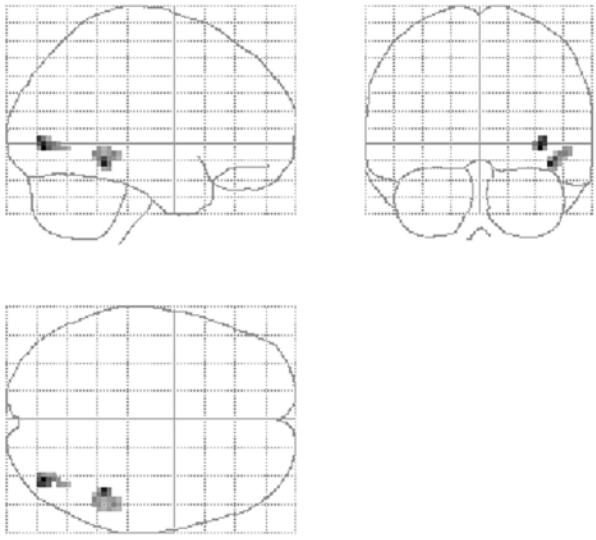

Figure 3.4: Group results showing activated areas for the global crossed versus uncrossed conditions contrast for the slowest third of reaction times (see section 3.2 for details). These activations are schematized on a glass brain

	MNI coordinates			Z Score
	x	y	z	
Crossed vs. Uncrossed Difference (RH-LVF + LH-RVF) – (RH-RVF + LH-LVF)				
Fast trials: No suprathreshold clusters				
Middle trials: No suprathreshold clusters				
Slow trials:				
Right inferior occipital gyrus (BA 19)	36	-78	-3	3.71
Right middle temporal gyrus (BA 37)	42	-42	-12	3.68

Table 3.5: Anatomical location, MNI coordinates, and Z scores of the statistically most active voxels in the global crossed versus uncrossed comparison for trials leading to the fastest third or slowest third of reaction times

wherein the visual field of stimulation and/or hand of motor response were varied. Additional results indicate that the global comparison of crossed conditions against their uncrossed counterparts failed to reveal differentially activated areas. However, such differential activity was observed within visual cortical areas when distinct portions of the reaction time distribution were separately analyzed, indicating that visuo-motor pathways may vary with processing speed. This suggests that visuo-motor pathways can vary functionally. In support of this suggestion, we found a significant correlation between the strength of the CUD measured from the BOLD response and the magnitude of the CUD measured from reaction times within BA37 for the slowest third of the reaction time distribution. This was not observed for the middle or fastest thirds. These results have implications for our understanding of visuo-motor routing and response propagation. First, these results are

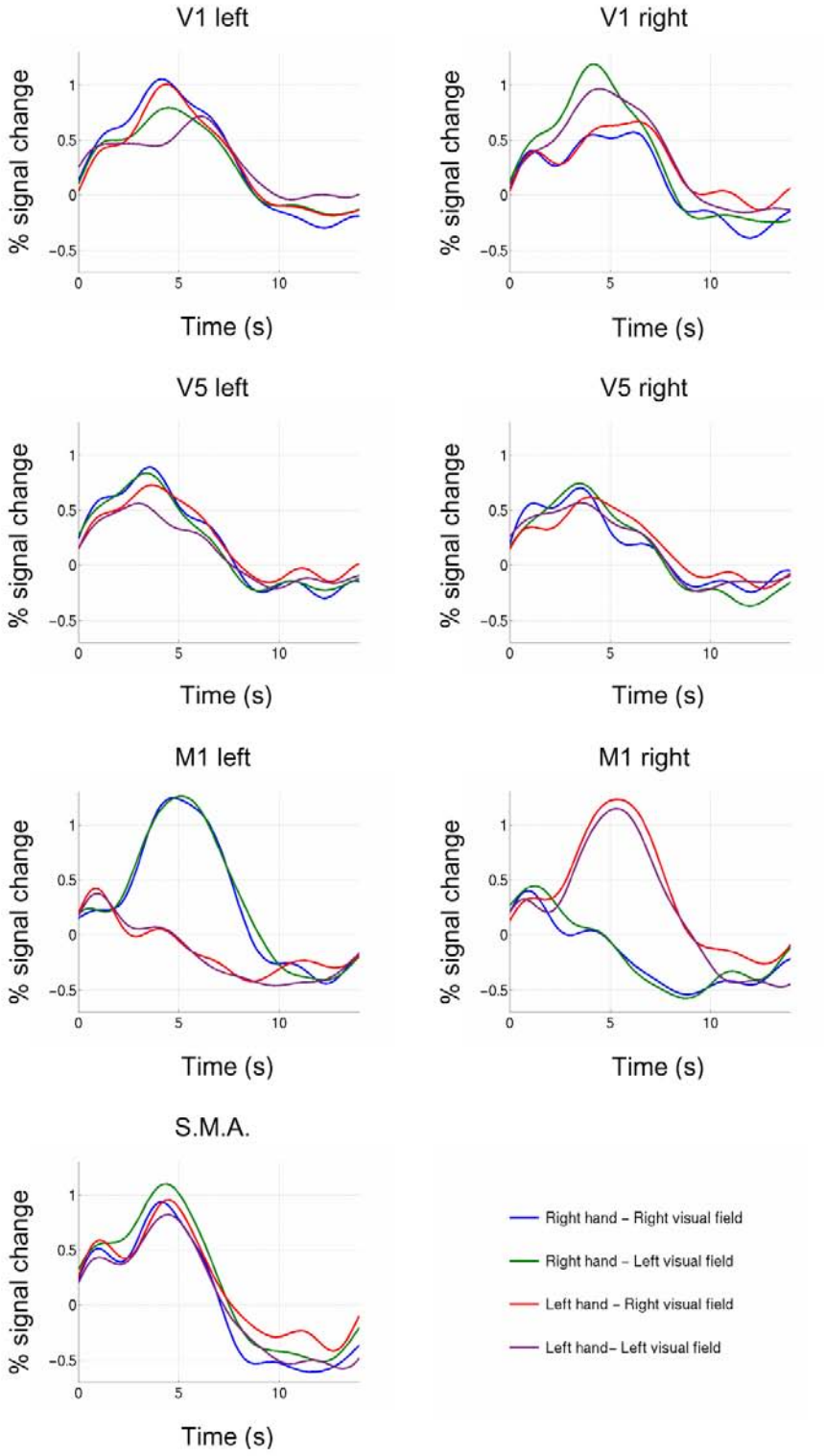

Figure 3.5: Time course of the mean BOLD signal in the areas of interest, listed in Table 3.1, during the four experimental conditions

	V1 right	V1 left	V5 right	V5 left	SMA	M1 right	M1 left
RH-RVF	5.11 ± 1.47	3.83 ± 1.17	3.46 ± 1.05	3.60 ± 1.11	4.32 ± 0.62	N/A	5.03 ± 0.73
RH-LVF	3.97 ± 0.80	4.43 ± 1.19	3.86 ± 1.26	3.52 ± 0.89	4.41 ± 0.50	N/A	5.05 ± 0.54
LH-RVF	5.05 ± 1.73	4.36 ± 0.48	4.14 ± 1.42	4.47 ± 1.20	4.59 ± 0.63	5.50 ± 0.83	N/A
LH-LVF	4.40 ± 0.83	5.80 ± 1.54	3.80 ± 0.98	3.21 ± 1.11	4.51 ± 0.51	5.43 ± 0.66	N/A

Table 3.6: Average peak latencies (in seconds ± SD) of BOLD signals in the regions of interest

consistent with the parallel and distributed responses observed using electrophysiological methods. Second, the collective data support the view that interhemispheric interactions occur in response to unilaterally presented visual stimuli irrespective of response hand, and that these interactions occur predominantly at the level of visual cortices. Finally, the results of this study indicate that simple models of visuo-motor pathways are insufficient. Rather, a common network of brain areas appears to be active under all conditions, varying instead in its strength as a function of reaction time and crossed and uncrossed conditions.

The present results provide functional evidence that the CUD is likely not the simple result of the selective activation of areas for the crossed conditions, but rather likely follows from a change in the strength and/or dynamics of responses in already active structures (see Fig. 3.1). This notion is predicated on our observation of highly similar spatial patterns of activity for each condition. As such, this conclusion runs counter to those of some previous studies applying hemodynamic methods to the Poffenberger paradigm [91, 150]. Likewise, the comparison between the different activation maps from specific conditions revealed no significant differences in ipsilateral visual or motor areas related to the crossed versus uncrossed comparison (see Fig. 3.3). Moreover, this comparison did not yield any regions selectively activated by the crossed condition. Rather, we consistently observed an enhanced response to LVF stimulation, irrespective of the response hand, in visual areas of the right hemisphere. However, we would note that we cannot exclude the possibility that this stronger activity masked some small differences in the activation pattern related to interhemispheric interactions specific to the "crossed" conditions.

In terms of variation in the strength of responses in already active structures as an explanation of the CUD, our analyses did reveal differences when trials were separately analyzed according to their reaction times. Specifically, the fastest third of trials yielded a CUD of < 1 ms, the middle third a CUD of ~ 2 ms, and the slowest third a CUD of ~ 9 ms. In terms of CUD effects on the BOLD response, only slow trials resulted in significant activation differences (i.e. stronger responses to the crossed than uncross conditions), which were located within right extrastriate visual areas (BA 19 and 37). This pattern is in keeping with the proposition put forward by Saron and colleagues, based on a case-study analysis of event-related potentials of healthy individuals [134], that cortical activation patterns are influenced by reaction times. Specifically, slower reaction times were proposed to rely on more posterior cerebral interhemispheric pathways, a notion supported by our results. In addition, the significant correlation between behavioral and BOLD indices of CUD within BA 37 for the slowest third of trials further suggests that differential responses within this

area are linked to behavioral outcome. A further implication of this finding is that visual cortices play a critical role in visuo-motor interhemispheric interactions. We return to these points below.

We found no evidence for activations in the corpus callosum, even when more relaxed statistical thresholding was applied. This contrasts with previous studies [150, 160]. In addition to the general debate concerning whether BOLD responses within the white matter are physiologically reasonable (c.f. [150]), one of the possible explanations for this discrepancy can be found in the different methodologies employed in these studies. Tettamanti et al. [150], as well as Weber et al. [160], used a block-designed paradigm that is known to be more sensitive than event-related protocols, and activations in the white matter are considerably smaller than those in the gray matter [121]. On the other hand, event-related protocols are not biased by the shift of attention implicit in a block-designed paradigm, which has been shown to play an important role in the recruitment of cortical brain areas [160]. It is further possible that this difference between event-related and blocked designs and/or the type of motor response required are the bases for the discrepancy between RT distributions between our study and those of Marzi's group. Another possibility is that the long ISI of the present study does not adequately tax the brain systems underlying signal changes within the corpus callosum. Despite the absence of differential activity within the corpus callosum, we would emphasize that a role for callosal fibers in interhemispheric interactions is supported by our data demonstrating a predominant role of visuo-visuo interhemispheric interactions (see below).

Further investigation will be required to replicate and detail these findings. For example, one possibility is that differential activations were observed for slow trials simply because the CUD in reaction times was sufficiently large, whereas such was effectively absent for fast and middle trials. Nonetheless, the present findings highlight the importance of considering the impact of intra-subject performance variations on patterns of brain activation. As such, our findings (albeit with a limited number of trials) also suggest that both reaction time indices of CUD and also interhemispheric activations may not be constant across an individual's reaction time distribution (see [67] for evidence to the contrary).

In terms of the dynamics of responses in already active structures, the event-related design and high temporal sampling of the BOLD response allowed us to examine this possibility (albeit with substantially less temporal resolution than other — most notably electromagnetic — techniques). Here, we formulate some speculative comments on the dynamics of brain responses across multiple functional areas (see Table 3.6). As mentioned briefly above, it was only in V1 where peak latencies of the BOLD signal were statistically different across conditions. This is in keeping with the current understanding of contralateral representations of the visual hemifields and the lack of direct ipsilateral projections (either via naso-temporal overlap or callosal fibers beyond the representation of the vertical meridian) within V1 (e.g. [15, 30, 154]). Moreover, each experimental condition exhibited a homologous ordinal sequence of peak latencies across these functional brain regions. Although the precise coupling between hemodynamic measures and neural activity remains to be fully resolved, previous studies have demonstrated the interpretability of temporal in-

formation in the BOLD signal in terms of relative latency differences between brain regions (e.g. [39, 63, 97, 128]), despite the unresolved question concerning the variability of the BOLD response across different brain areas. In the present study, the observed sequence across areas is consistent with observations of rapid visual response propagation using electrophysiological methods (e.g. [16, 38, 41, 98, 103, 112, 141]). Interestingly, while we found nearly homologous BOLD responses for V5 bilaterally (both in terms of magnitude and peak latency), those from V1 differed between the contra- and ipsi- lateral hemispheres. One implication, which is supported by both anatomical (e.g. [30]) and functional data (e.g. [70, 154]), is that there exist distinct interhemispheric channels even within the visual system. Visual areas, including some bilaterally, and SMA may thus work in a continuous stream that need not be directly linked with the timing of responses in M1 and by extension, reaction time. In support, electrophysiological investigations in both humans (e.g. [7, 41, 136, 151]) and non-human primates (e.g. [18, 141]) indicate that premotor regions, including SMA and frontal eye field (FEF), are active nearly simultaneously with visual regions.

The present data likewise provide evidence regarding the likely functional level of interhemispheric interactions. On the one hand, the activation maps from each condition versus 'rest' revealed bilateral occipital activation in response to a briefly and laterally presented visual stimulus both in the "crossed" and in the "uncrossed" conditions. Conjointly, responses within motor cortex were consistently lateralized to the hemisphere contralateral to the responding hand, even in the case of "crossed" conditions. A strong implication of these results is that the predominant interhemispheric interactions occur between visual brain areas, in agreement with previous studies [10, 12, 91, 104, 107], rather than motor areas (e.g. [68, 150, 151]). Further supporting this conclusion is our observation of differential activation within visual areas following the crossed versus uncrossed comparison with trials leading to slow reaction times. However, as we observed this pattern with a relatively low number of trials, we cannot unequivocally rule out the possibility of other interhemispheric pathways that may further vary between individuals and/or as a function of finer reaction time subdivisions. Nonetheless, these data provide support for the proposition of Saron and colleagues (that posterior interhemispheric pathways predominate trials leading to slower reaction times [134]). We would note that additional transfer mechanisms involving the SMA cannot be excluded based on the present results, since we were unable to resolve hemispheric differences within the SMA. However, peak responses in SMA were consistently delayed relative to those in visual areas, and putative interhemispheric interactions involving the SMA may play a secondary role in visuo-motor routing. Further experiments that continue to capitalize on the event-related design of the present experiment will be required to more fully resolve this question.

The collective results permit some comments on models of visuo-motor interactions. First, the spatial activation patterns support the hypothesis that interhemispheric interactions take place in response to unilateral visual stimuli for both crossed and also uncrossed conditions to the same degree; to the extent that the intensity of the BOLD response accurately reflects neural response intensity. This pattern is in solid agreement with notions of

parallel distributed processing within the visual system (e.g. [37, 41, 141]) and extends these findings to suggest that brief unilateral visual stimulation produces volleys of responses in both cerebral hemispheres. Second, the spatial pattern of activations included lateralized responses within motor cortex and bilateral responses within visual cortices. This pattern provides additional evidence that interhemispheric interactions are predominantly between visual cortical regions and that visuo-motor integration likely occurs within a hemisphere (though we cannot unequivocally exclude the possibility of heterotopic interhemispheric interactions or such mediation via the SMA). Moreover, since crossed-uncrossed differences in peak BOLD responses were observed only within V1 (among those areas tested; see Fig. 3.5 and Table 3.6), a model of interhemispheric interactions occurring predominantly at a functionally extrastriate visual level is again supported. An additional speculative possibility is that this interhemispheric signal not only triggers visuo-motor integration, but also top-down modulation within ipsilateral V1. Third, our data would indicate that CUD differences in BOLD response that are apparent for different portions of the RT distribution reflect modulations in the strength of responses of the same brain network, rather than the selective activation of brain regions when reaction times are delayed. These data do not provide evidence of functionally distinct interhemispheric pathways that vary with reaction time. Rather, reaction time appears to modulate the relative strength of responses within a subset of brain regions — i.e. within visual extrastriate regions of the right hemisphere. One possibility is that activation accumulates and triggers enhanced activity within BA37 when motor responses are not initiated quickly. However, as we mentioned above, we cannot exclude the possibility that the CUD difference observed here is related instead to the (on average) larger CUD, rather than being linked to slower RT trials.

In summary, the collective results favor a parallel, distributed model of brain activation. Visuo-motor processing during a simple reaction time paradigm consistently resulted in bilateral brain responses (particularly within visual cortices) not only for the "crossed" but also the "uncrossed" conditions, providing evidence that a simple model of visuo-motor pathways is insufficient. The presence of interhemiphseric interactions and its consequent bilateral activity is not determined by the crossed anatomic projections of the primary visual and motor pathways. Distinct visuo-motor networks need not be engaged to mediate behavioral responses for the crossed visual field/response hand condition. While anatomical connectivity heavily influences the spatial pattern of activated visuo-motor pathways, behavioral and functional parameters appear to also affect the strength and dynamics of responses within these pathways. While the present study examined the case of visuo-motor routing, future experiments that similarly capitalize on the spatial as well as temporal information within the BOLD response, as well as single-subject analyses, will undoubtedly shed further light on the full breadth of brain function and processing pathways.

3.5 Summary

In this chapter we applied the analysis of BOLD dynamics in conjunction with traditional fMRI data analysis (based on BOLD amplitude) to investigate visuo-motor pathways in

humans. Both activation maps and time curve analysis support the hypothesis of a parallel, distributed brain process in response to a simple visuo-motor task. Bilateral activations were obtained even in the case of visual stimulation ipsilateral to the responding hand. Results also suggest that RTs modulate the amplitude of the BOLD signal of the processing network. Unfortunately, we were not able to study whether or not RTs similarly modulate the temporal features of the BOLD response because we could not assure that the different ISI used were evenly distributed across RT portions.

In this study, the analysis of BOLD dynamics gave an additional support to a hypothesis already drawn from the analysis of activation maps. This method can also reveals interactions that modulate solely some temporal features (e.g. BOLD peak latency) but not the amplitude, and therefore may go undetected by the traditional analyses. An example of such is reported in Chapter 4. Unfortunately, it is still not clear how changes in BOLD dynamics reflect changes in the underlying neuronal activity, since the neurovascular coupling is not completely understood. We will address to this topic in Part II.

Multisensory interactions within human primary cortices revealed by BOLD dynamics

4

Building upon the results described in Chapter 3, the study described here applies the methods developed in section 2.3 in addition to the traditional fMRI analysis methods. In this chapter, such a method is used to investigate multisensory interactions. This is an important topic that not only addresses basic models of brain organization, but also challenges the traditional fMRI methods to identify such interactions. The analysis of BOLD temporal characteristics is an alternative method that bypasses the interpretational concerns associated with traditional fMRI analyses [4, 21, 81] and provides help in linking fMRI and electrophysiological findings as well as human and animal models.

4.1 Introduction

Sensory inputs converge and interact, influencing perception and behavior (e.g. [147]). Neurophysiological bases for these multisensory effects are increasingly being investigated. Anatomical studies in animals have identified direct, monosynaptic projections between primary and immediately adjacent auditory cortices and primary visual cortices [31, 36, 129]. Electrophysiological recordings showed multisensory effects within primary and adjacent auditory regions of monkeys (e.g. [48, 140]) and non-linear response interactions within the initial 100 ms post-stimulus onset in humans (e.g. [42, 49, 52, 102, 110]). The earliest temporal stages of cortical processing and brain areas traditionally held to be unisensory in their function thus exhibit multisensory interactions.

Regarding interactions between the auditory and visual systems, several questions remain unresolved. For example, it is unknown whether monosynaptic projections between primary cortices in monkeys also exist in humans and, if so, whether they produce mul-

tisensory interactions that are measurable non-invasively. While the former is currently not feasible with existing tracing methods, the latter can be assessed using brain imaging techniques. Convergence and interaction effects have been obtained for speech/faces (e.g. [21, 116]), letters/vocalizations (e.g. [157]), and environmental objects (e.g. [5]).

However, the use of fMRI to identify multisensory effects is debated [4, 21, 81]. In particular, it is unclear whether criteria that have been applied in electrophysiological studies at the single neuron level are valid for fMRI analyses. For example, criteria for convergence (i.e. responding to multiple senses), multisensory enhancement (i.e. responding more to multisensory than to both unisensory stimuli), supra-additivity (i.e. responding more to multisensory than to the summed unisensory responses), and sensitivity to congruent stimulus features (e.g. spatial position, temporal coincidence, or object-related/semantic attributes) have been argued as prone to reporting falsely positive results [81]. Despite these considerations, some studies have reported multisensory effects within primary and adjacent auditory cortices in response to somatosensory [43] or visual stimuli (e.g. [116]). To date, none have observed effects within primary visual cortex or examined whether multisensory effects in low-level cortical regions can similarly be elicited by meaningless, rudimentary stimuli. Instead, investigations have thus far been limited to meaningful stimuli, and it remains unknown whether effects in low-level cortices are mediated by higher-order processes. Resolving such questions is critical for determining whether interaction mechanisms between sensory systems are a general, perhaps automatic, property or are instead regulated by stimulus-specific processes.

Interpretational caveats of standard fMRI were bypassed by analyzing dynamics of the BOLD signal. Recent developments in event-related fMRI indicate that latency analyses can be performed on the directly measured BOLD signal (e.g. [6, 63, 71, 89]). As such, we analyzed both the spatial as well as the temporal pattern of responses during auditory-visual integration.

4.2 Materials and Methods

4.2.1 Subjects

Twelve healthy subjects (mean $\pm$ SD age = 29.4 ± 7.1 years; 6 female) with normal hearing, normal or corrected-to-normal vision, and no history of neurological or psychiatric disease participated. Each provided written informed consent to procedures approved by the Ethics Committee of the Faculty of Biology and Medicine at the University of Lausanne.

4.2.2 Stimuli and Task

Subjects performed a simple reaction time task to visual (a non-alternating yellow on black centrally presented checkerboard, measuring $24^\circ \times 32^\circ$ in total size and each square covering $0.8^\circ \times 0.8^\circ$ degrees of visual angle), auditory (a binaural noise burst), or simultaneous auditory-visual stimuli (each 150 ms duration). Stimulus conditions were pseudo-randomly intermixed across trials. Subjects were instructed to respond as fast as possible with their

right hand upon detection of any stimulus by pressing keys. Behavioral data were acquired using button presses on a MRI-compatible device (Photon Control Inc., Burnaby, BC, Canada). Subjects pressed four keys, one per finger, in one swift and continuous movement like tapping one's fingers on a table, and reaction times were recorded as the latency at which the first of the keys was pressed. Stimulus delivery and the acquisition of behavioral data were controlled by E-prime (Psychology Software Tools, Inc., Pittsburgh, PA, USA). Behavioral data from two of the twelve subjects were lost due to technical failures.

The inter-stimulus interval (ISI) varied pseudo-randomly from 14.2 to 17.8 s in steps of 200 ms, allowing the BOLD signal to return to baseline between stimulus presentations (e.g. [71]). There was a pseudo-random, variable delay between stimulus onset time and volume acquisition of 0 to 1.8 s at steps of 200 ms, yielding a total of 10 different delays. Jittering stimulus presentation relative to volume acquisition permitted the BOLD response to be effectively sampled with a temporal resolution of 200 ms (see section 2.3 and [89] for additional details). The experiment consisted of 4 sessions, each including 10 repetitions per experimental condition. Therefore, each of the 3 experimental conditions collectively included 4 volume acquisitions at each of the 10 delays used.

4.2.3 Magnetic Resonance Imaging

Functional MRI data were acquired using an event-related design on a 3.0 T Philips Intera system equipped with an 8-channel head coil. BOLD signals were obtained with a single shot gradient-echo EPI sequence (TR = 2 s, TE = 30 ms, FoV = 224 mm, flip angle = 90°, matrix size 64 × 64). Each volume was comprised of 16 slices (slice thickness 5 mm, gap 1 mm) covering the entire cerebral hemispheres and acquired in ascending order (i.e. first slice at the bottom of the head). To provide precise structural and anatomical localization of brain activity, a sagittal T1-weighted 3D gradient-echo sequence was acquired for each subject (160 contiguous sagittal slices, slice thickness 1 mm, matrix size 256 × 256, TR = 9.9 ms, TE = 4.6 ms, FoV = 256 mm, flip angle = 8°).

4.2.4 Spatial fMRI Analyses

Two types of fMRI analyses were conducted in order to investigate multisensory interactions: the first in terms of the spatial pattern of activated brain regions, the second in terms of changes in temporal dynamics within activated brain regions. The latter analysis was done by measuring the shift in peak latency of the estimated hemodynamic response function within a given area across stimulus conditions (detailed below).

Activation maps were obtained using SPM2 software (Wellcome Department of Cognitive Neurology, London, UK). Functional volumes were first spatially realigned to the first volume acquired and temporarily realigned to the first slice acquired. Volumes were then normalized to the Montreal Neurological Institute (MNI) template, re-sampled to a voxel size of $3 \times 3 \times 3\,\mathrm{mm}^3$, and smoothed with an isotropic Gaussian kernel (FWHM = 6 mm). For each subject a high-pass filter was applied on the time series to minimize possible effects of baseline drift. The statistical analysis was performed with the General Linear

Model, using as a basis function the canonical hemodynamic response function and its temporal derivative, as defined in SPM2. Structural and functional volumes were co-registered within the same coordinate system by normalizing structural images to the MNI template brain and re-sampling voxels to a $1 \times 1 \times 1\,\mathrm{mm}^3$ size. Inference on the population (group analysis) was obtained by means of second-level statistics, according to the random effects theory. Analyses were conducted to determine the active regions in each condition, separately (voxel-level threshold at $p < 0.001$, uncorrected; 15 voxel spatial-extent threshold) both on a single subject basis and on the group results.

4.2.5 Temporal fMRI Analyses

The hemodynamic response was reconstructed by averaging the four samples collected at each time point relative to stimulus onset and then filtering to remove high frequency noise, as described in section 2.3.2. Peak latency and intensity of the hemodynamic signals were measured after fitting the signal around the peak ($\pm 0.8\,\mathrm{s}$, equal to 4 data points before and after the peak) with a cubic curve. We would emphasize that cubic fitting was solely applied to these data points encompassing the peak of the acquired time course response, and that time courses shown always display the filtered raw data.

For each experimental condition, peak latencies were derived for each voxel within the brain. To ensure a valid measure of peak latency, analyses were spatially restricted to the regions identified as responsive to auditory and visual stimuli. For each subject, visual-responsive regions (VRRs) were defined according to the overlap between activation maps from the visual and multisensory conditions and auditory-responsive regions (ARRs) by the overlap between activation maps from the auditory and multisensory conditions (see [4] for a similar approach in analyses of BOLD amplitude). This overlap criterion also minimizes the likelihood of falsely considering a voxel as responsive to either visual or auditory stimulation. Within VRRs we statistically tested (paired t-test) the difference between BOLD peak latencies from the visual and multisensory conditions, while within ARRs this analysis was between auditory and multisensory conditions. It should be noted that these tests were conducted on a voxel-wise level and that not all subjects necessarily exhibited the same VRRs and ARRs. In such instances no peak latency would be measured for a particular subject at a specific voxel. This would result in an empty cell in the analysis matrix and thus increases the propensity for falsely negative results. This constituted the group-level analysis of shifts in BOLD peak latency. We considered only those clusters meeting both a $p < 0.05$ alpha criterion (uncorrected) and also a 15-voxel spatial-extent criterion.

Although the above approach can identify modulation in BOLD peak latency throughout the entire brain, it does not account for inter-subject variability in cortical functional geometry. To partially overcome this limitation without restricting our analyses to particular anatomical subdivisions (i.e. to conduct analyses throughout the entire brain volume), for each subject we identified voxels within individual VRRs and ARRs that were also within the regions defined by the aforementioned group-level analysis of shifts in BOLD peak latency. This analysis yielded a subset of four regions — primary visual and audito-

ry cortices, bilaterally (see section 4.3). Within each of these four individually identified regions, we calculated the mean BOLD response so as to obtain a single time curve per condition and per subject. The peaks of these time curves, within each region separately, were then statistically analyzed (multivariate test and post-hoc paired t-tests) across stimulus conditions. One subject did not show a reliable response (i.e. exceeding the noise level) to auditory stimulation within primary visual areas bilaterally and was therefore excluded from analyses including this condition in these regions. Peak intensity values of these time curves were similarly analyzed. Lastly, we also analyzed the slope of these curves as a post-hoc supplement to our analyses of peak latency. For each curve, the slope was defined in the following manner. First, we defined the positions and intensities of the peak and the immediately-preceding minimum. From these two points, we then fit a line within the acquired data points lying between the 20% and 90% intensity values of this range. The slope of this line was then analyzed, as above, with a multivariate test and follow-up t-tests.

4.3 Results

Behavioral data confirmed that multisensory interactions occurred. Mean reaction times were faster for the multisensory than either visual or auditory condition (mean $\pm$ s.e.m. $= 355 \pm 28$ ms, 379 ± 25 ms, and 400 ± 30 ms, respectively; $F_{(2,8)} = 36.38$; $p < 0.001$; see Figure 4.1a), replicating prior demonstrations of a redundant signals effect between audition and vision (e.g. [101, 102, 123, 139]). Additionally, this facilitation exceeded predictions from probability summation [101, 110], which is a psychometric benchmark of integrative processing. Over the fastest third of the reaction time distribution, there was a higher likelihood of a reaction time following a multisensory stimulus than would be expected if auditory and visual stimuli competed independently to elicit a motor response (i.e. the so-called race model; see [101] for details; Fig. 4.1b and 4.1c).

Our behavioral results are suggestive of an "asymmetry" in the mean reaction time data, such that the difference between the multisensory and visual conditions are approximately the same magnitude as the difference between the visual and auditory conditions. It is important to note, however, that while the difference between the multisensory and each unisensory condition is significant, the difference between the visual and auditory conditions is not (please see caption to Fig. 4.1). This pattern replicates previously published studies [102, 139]. Even if mean reaction times to the visual condition were faster than those to the auditory condition, it would be difficult to draw many direct conclusions. One reason is that we did not attempt to equilibrate the intensity of the visual and auditory stimuli, as this was not pertinent to the experimental aims. Second, as this is the first study to conduct an auditory-visual simple detection paradigm within an fMRI environment, there were no predictions as to how the scanner noise would affect performance. Third, previous research has shown that some subjects are faster with auditory stimuli and others faster with visual stimuli [49]. To date and to the best of our knowledge, there has been no subsequent study that would provide a solid explanation as to why this is the case (though this would certainly be an interesting avenue for future research).

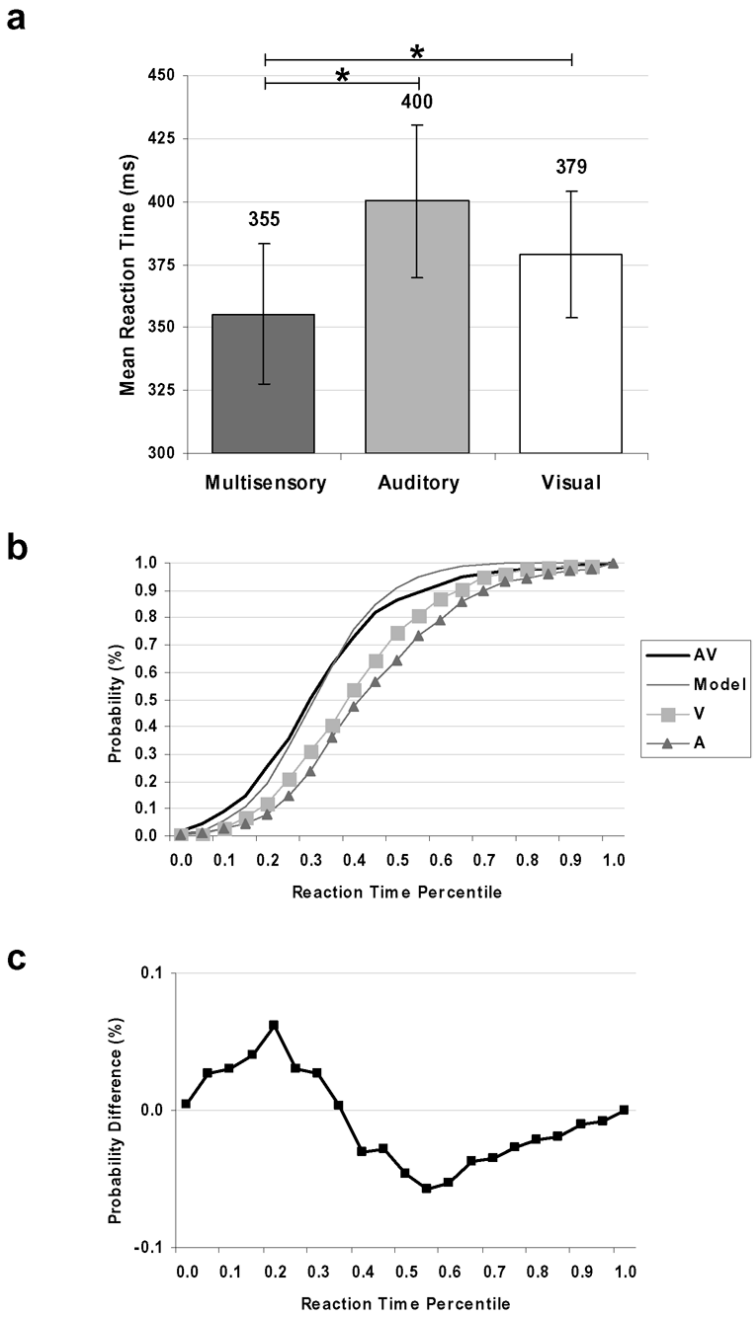

Figure 4.1: Mean reaction times. a. Subjects responded faster to the multisensory than to either visual ($t_{(9)} = 3.4$; $p = 0.008$) or auditory ($t_{(9)} = 6.4$; $p < 0.001$) condition, and reaction times to unisensory stimuli did not significantly differ ($t_{(9)} = 1.8$; $p > 0.10$). Asterisk indicates significant difference ($p < 0.05$; 2-tailed paired t-test). b. Group-average cumulative probability distributions for each stimulus condition as well as the modeled data based on Miller's inequality [101]. c. Reaction times to multisensory stimuli exceeded predictions of probability summation over the fastest third of the distribution (indicated by positive values).

Two series of event-related fMRI data analyses were conducted — one in terms of spatial activation maps, following standard procedures and another in terms of BOLD response peak latencies (see section 4.2). Activation maps (Fig. 4.2) and BOLD times series (Fig. 4.3) show that primary cortices of each sensory modality (i.e. calcarine cortex and Heschl's gyrus) responded to both visual and auditory stimulation, indicative of multisensory convergence. In addition, the activation maps also show robust responses within the left primary motor cortex, left somatosensory areas, the supplementary motor area (SMA), and thalamic regions. Since subjects performed a button-press to each stimulus presentation, irrespective of sensory modality, the tactile input likely elicited responses within somatosensory regions. This notion is in part supported by the left-lateralized activations in somatosensory and motor regions (see Fig. 4.2). Consequently, it would be difficult to disambiguate any multisensory convergence (i.e. responses to the auditory and/or visual stimuli themselves) in these areas.

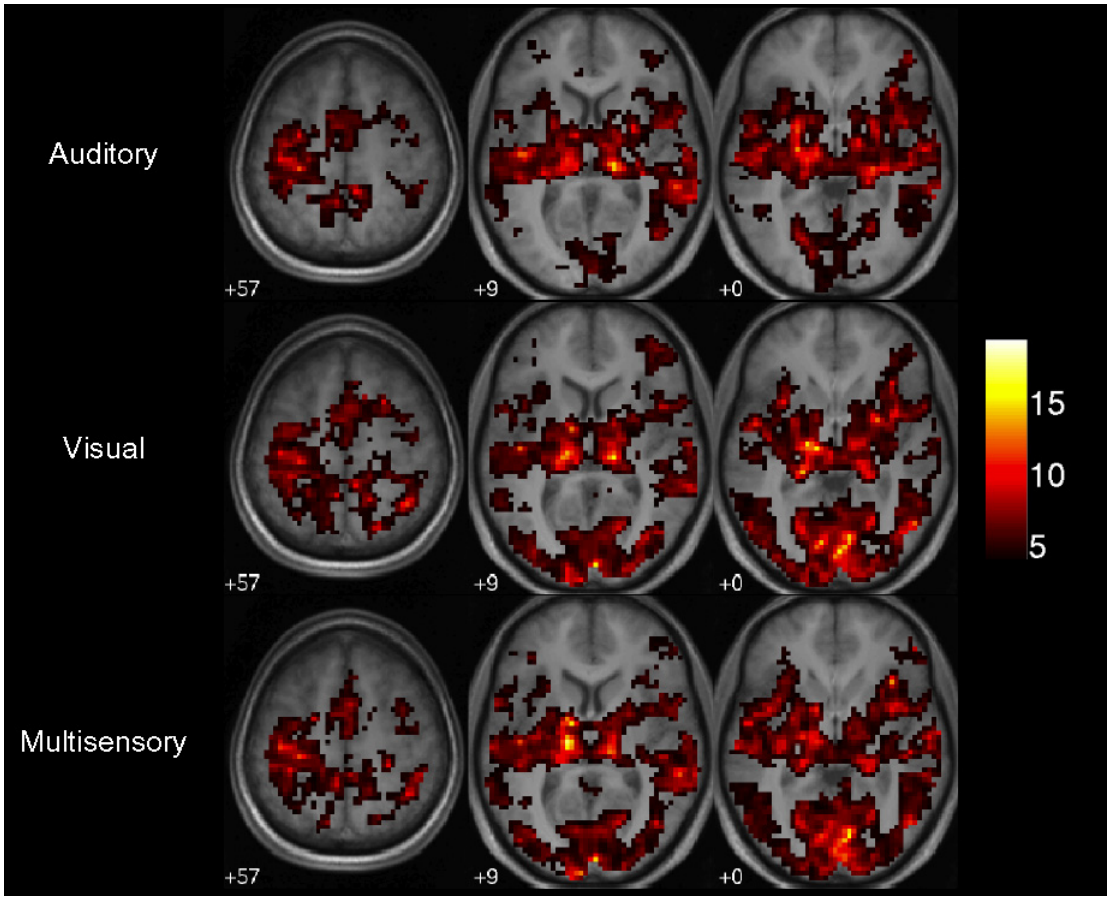

Figure 4.2: Activation maps ($p < 0.001$, cluster-size > 15 voxels; color scale represents t-values) for each stimulus condition show that all conditions led to responses within primary auditory and visual cortices, the left primary motor cortex, the SMA, and thalamic regions. Axial slices are shown at three z-coordinates (indicated in insets), using the MNI system. The left hemisphere is displayed on the left side of the image.

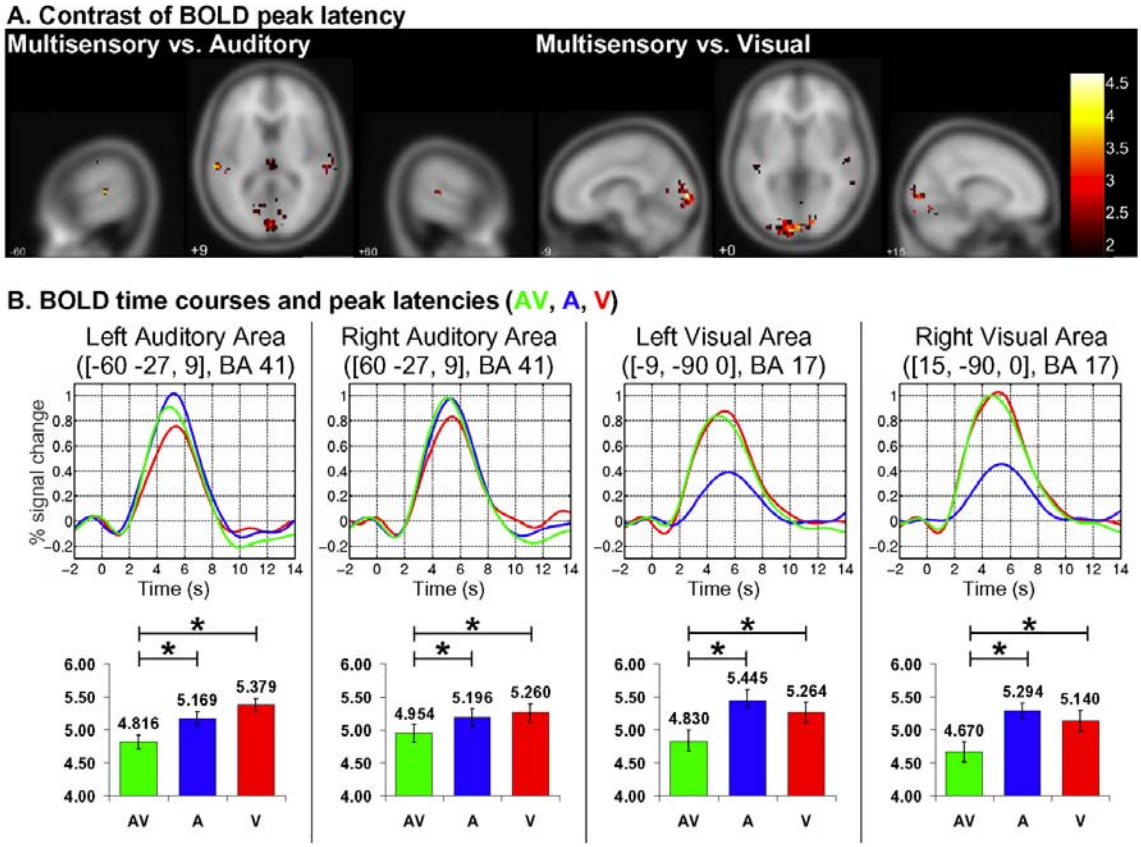

Figure 4.3: Facilitation in BOLD peak latencies in response to auditory (A), visual (V), and auditory-visual (AV) multisensory stimulation (blue, red, and green traces, respectively). a. Contrast of BOLD peak latency (paired t-test, 1-tailed, t-value indicated) at each voxel within VRRs and ARRs (see 4.2 for details). b. Dynamic shifts in BOLD peak latencies within primary cortices. MNI coordinates and Brodmann Area (BA) of the center of the cluster are indicated. Bar graphs show mean peak latencies (s.e.m. indicated). Asterisk indicates significant difference ($p < 0.05$, paired t-test, 2-tailed)

In order to assess multisensory interactions (i.e. where these convergent inputs alter responses to simultaneous auditory-visual stimulation) while also minimizing issues in fMRI investigations of multisensory interactions that stem, in part, from analyses of BOLD signal amplitude [4, 21, 81], we derived peak latencies for each brain voxel, stimulus condition, and subject, separately. These values were measured from the raw BOLD responses sampled every 200 ms. We ensured that latency measures originated from active voxels by spatially restricted temporal analyses to visual-responsive and auditory-responsive regions (VRRs and ARRs, respectively; see secition 4.2 for details). Each of these paired contrasts (i.e. multisensory vs. visual and multisensory vs. auditory) revealed significant ($p < 0.05$) multisensory facilitation in terms of earlier peak BOLD response latencies principally within primary and/or near-primary visual and auditory cortices (Fig. 4.3a), the coordinates of which accord with ranges based on probabilistic mapping [1, 124]. While both VRRs

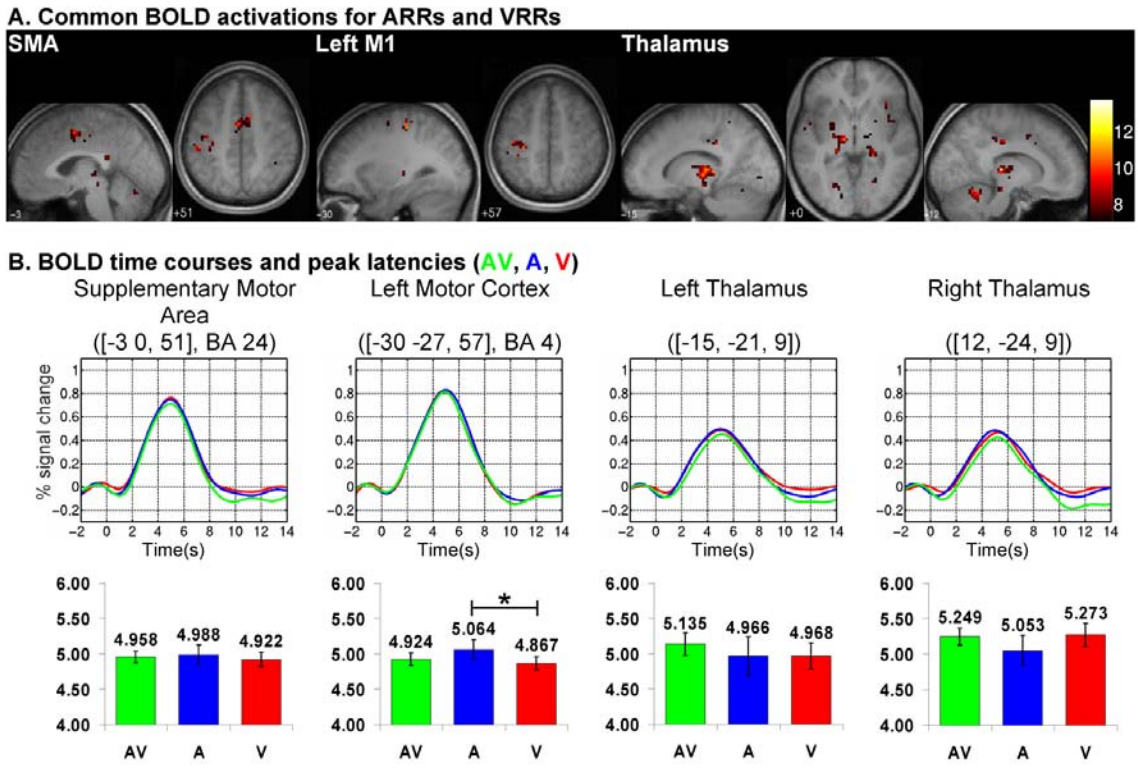

Figure 4.4: a. Conjunction of BOLD activations for ARRs and VRRs (paired t-test, 1-tailed, t-value indicated). b. BOLD time series in left primary motor cortex, supplementary motor area (SMA), and bilateral thalamic regions. MNI coordinates and Brodmann Area (BA) of the center of the cluster are indicated. Curves in green are from the multisensory (AV) conditions, in blue are from the auditory (A) condition, and in red are from the visual (V) condition. Bar graphs show mean peak latencies (s.e.m. indicated). Asterisk indicates significant difference ($p < 0.05$, paired t-test, 2-tailed).

and ARRs included other cortical and thalamic structures, no significant effects on peak latency were observed (see Fig. 4.4). Additionally, no regions showed significantly delayed multisensory responses.

To this point, our analyses revealed both multisensory convergence as well as shifts in BOLD dynamics within primary auditory and visual cortices following simultaneous auditory-visual stimulation. This method allows us to investigate interactions throughout the entire brain, but one possible shortcoming is that it does not account for inter-subject anatomical and functional variability [1, 124]. However, to our knowledge there is no universally accepted method for inter-subject alignment of functional activations, and existing approaches minimally require the pre-selection of anatomical subdivisions for analyses [116]. More specific to our study, it is possible that superposition of activated areas across individuals was incomplete. That is, for this voxel-wise analysis it is possible that a given subject did not exhibit a robust BOLD response at a particular voxel, in which case no peak latency

	Multivariate Test	Follow-up comparisons (paired t-test, 2-tailed) AV vs A	AV vs V	V vs A
Peak Latency				
Left Auditory Area	$F_{(2,10)} = 19.705$ $p = \mathbf{5.1 \cdot 10^{-4}}$	$t_{(11)} = -5.326$ $p = \mathbf{2.4 \cdot 10^{-4}}$	$t_{(11)} = -4.199$ $p = \mathbf{0.001}$	$t_{(11)} = 1.443$ $p = 0.177$
Right Auditory Area	$F_{(2,10)} = 4.941$ $p = \mathbf{0.032}$	$t_{(11)} = -2.512$ $p = \mathbf{0.029}$	$t_{(11)} = -2.413$ $p = \mathbf{0.034}$	$t_{(11)} = 0.426$ $p = 0.678$
Left Visual Area	$F_{(2,9)} = 11.246$ $p = \mathbf{0.004}$	$t_{(10)} = -2.476$ $p = \mathbf{0.033}$	$t_{(11)} = -4.417$ $p = \mathbf{0.001}$	$t_{(10)} = -0.629$ $p = 0.544$
Right Visual Area	$F_{(2,9)} = 4.386$ $p = \mathbf{0.047}$	$t_{(10)} = -2.976$ $p = \mathbf{0.014}$	$t_{(11)} = -2.652$ $p = \mathbf{0.023}$	$t_{(10)} = -0.746$ $p = 0.473$
Peak Intensity				
Left Auditory Area	$F_{(2,10)} = 4.942$ $p = \mathbf{0.032}$	$t_{(11)} = -1.962$ $p = 0.076$	$t_{(11)} = 2.955$ $p = \mathbf{0.013}$	$t_{(11)} = -3.169$ $p = \mathbf{0.009}$
Right Auditory Area	$F_{(2,10)} = 7.317$ $p = \mathbf{0.011}$	$t_{(11)} = -0.129$ $p = 0.900$	$t_{(11)} = 3.666$ $p = \mathbf{0.004}$	$t_{(11)} = -2.212$ $p = \mathbf{0.049}$
Left Visual Area	$F_{(2,9)} = 18.064$ $p = \mathbf{0.001}$	$t_{(10)} = 5.490$ $p = \mathbf{2.7 \cdot 10^{-4}}$	$t_{(11)} = -0.806$ $p = 0.437$	$t_{(10)} = 6.172$ $p = \mathbf{1.1 \cdot 10^{-4}}$
Right Visual Area	$F_{(2,9)} = 27.195$ $p = \mathbf{1.5 \cdot 10^{-4}}$	$t_{(10)} = 5.500$ $p = \mathbf{2.6 \cdot 10^{-4}}$	$t_{(11)} = -0.330$ $p = 0.747$	$t_{(10)} = 7.766$ $p = \mathbf{1.5 \cdot 10^{-5}}$

AV = auditory-visual; A = auditory; V = visual

Table 4.1: Results of statistical analyses on peak latency and intensity. Bold typeface indicates statistically significant values ($p < 0.05$)

would be measured. The above analysis can therefore be considered conservative.

To partially overcome these issues, we identified voxels within individual subject VRRs and ARRs that were also within the regions defined by the aforementioned group-level analysis of BOLD peak latency shifts performed on each voxel (see section 4.2 for details). This yielded a subset of four regions — primary visual and auditory cortices, bilaterally. For each subject we calculated the mean BOLD response time curve in response to each condition in each of these individually-defined regions (Fig. 4.3b). In other words, the cluster-wise analysis used the contiguous regions defined in the above voxel-wise analyses to screen for contiguous voxels at the individual subject level. That is, we determined which voxels showed a robust BOLD response for each subject and then took the average across them before measuring the peak response latency. Importantly, this cluster-level analysis differs from the above voxel-level analysis in that each subject contributes a value to each test, thereby maintaining the degrees of freedom while also partially allowing for variation in functional anatomy. Peak latencies and intensities were statistically compared

	Mean slope (% signal change per second)			Multivariate Test	Follow-up comparisons (paired t-test, 1-tailed)	
	AV	A	V		AV vs A	AV vs V
Left Auditory Area	0.474	0.397	0.282	$F_{(2,10)} = 14.301$ $p = \mathbf{0.001}$	$t_{(11)} = 2.350$ $p = \mathbf{0.019}$	$t_{(11)} = 5.602$ $p = \mathbf{0.001}$
Right Auditory Area	0.480	0.393	0.282	$F_{(2,10)} = 5.665$ $p = \mathbf{0.023}$	$t_{(11)} = 2.004$ $p = \mathbf{0.035}$	$t_{(11)} = 3.525$ $p = \mathbf{0.002}$
Left Visual Area	0.346	0.171	0.314	$F_{(2,9)} = 9.278$ $p = \mathbf{0.007}$	$t_{(10)} = 4.529$ $p = \mathbf{5 \cdot 10^{-4}}$	$t_{(11)} = 1.676$ $p = 0.062$
Right Visual Area	0.411	0.189	0.357	$F_{(2,9)} = 36.803$ $p = \mathbf{5 \cdot 10^{-5}}$	$t_{(10)} = 6.356$ $p = \mathbf{1 \cdot 10^{-4}}$	$t_{(11)} = 1.875$ $p = \mathbf{0.045}$

AV = auditory-visual; A = auditory; V = visual

Table 4.2: Results of statistical analyses on the slope of the BOLD response over the 20-90% peak intensity interval. Bold typeface indicates statistically significant values ($p < 0.05$). Note that 1-tailed t-tests were conducted since our analysis of peak latency would suggest that slopes would be steeper for the AV condition.

using experimental condition as the within-subjects factor. Each region showed a significant main effect of experimental condition on peak latencies that was explained by earlier peak latencies for the multisensory than either unisensory condition (Fig. 4.3b and upper portion of Table 4.1). It is important to note that the differences in peak latencies were larger than our 200 ms temporal sampling frequency, excluding the cubic fitting procedure as an explanation for the present results. A significant main effect of condition on peak intensity was also shown in each region, which was due to significantly smaller auditory responses within visual areas and smaller visual responses within auditory cortices (Fig. 4.3b and lower portion of Table 4.1). Conversely, no significant differences were obtained either between multisensory and auditory intensities within auditory areas or between multisensory and visual intensities within visual areas. Thus, the present effects on peak latency cannot follow from a simple trade-off between lower response intensity and earlier peak latencies, since responses with significantly earlier peak latencies could also have significantly larger intensities (see Table 4.1). To further exclude such a possibility, we also assessed whether the slope of the response to the AV condition was steeper than that of either unisensory condition (see section 4.2 for details). The results of these analyses can be found in Table 4.2. In agreement with our analyses of peak latency, each region showed a significant main effect of experimental condition that was explained by a steeper slope for the multisensory than either unisensory condition (Fig. 4.3b and Table 4.2).

As a final step, we investigated whether or not the observed shifts in BOLD peak latency correlated with the observed reaction time facilitation. To do this, we first calculated the peak latency difference between the V and AV conditions and between the A and AV conditions for each region exhibiting a significant facilitation in BOLD peak latency for

the AV condition (i.e. bilateral primary auditory and visual cortices). We also calculated the reaction time difference between the V and AV conditions and between the A and AV conditions. In no case was a significant correlation observed (all p-values > 0.05), providing no evidence for a direct correspondence between effects on BOLD peak latency and performance (see also [40]).

4.4 Discussion

This is the first demonstration of multisensory interactions in primary visual and auditory cortices, which manifested as dynamic shifts in BOLD response latencies. No other regions showed significant effects on peak BOLD latency. Conjointly, we observed robust responses, in terms of BOLD amplitude, to both senses within low-level cortices. Simple visual stimuli lead to responses within auditory cortices and vice versa. These findings raise the question of their underlying neurophysiologic bases. Given the emerging anatomical and electrophysiological evidence for auditory-visual multisensory interactions within the earliest processing stages (e.g. [140]), our results on peak latency are most parsimoniously interpreted as consistent with direct interactions, rather than mediation by other brain regions.

A principal finding of the present study is that primary cortices responded to stimuli of other sensory systems. This is indicative of multisensory convergence, according to the criteria defined by Stein and Meredith [147]. In primary auditory cortex bilaterally, there were robust responses to visual stimuli that were nonetheless significantly smaller than the response to either auditory or multisensory stimuli (see Fig. 4.3 and Table 4.1). Similarly, in primary visual cortices bilaterally, there were responses to auditory stimuli that, were significantly smaller (i.e. approximately half the magnitude) than the responses to either visual or multisensory stimuli (Fig. 4.3 and Table 4.1). Several recent studies have also documented auditory-visual convergence within primary or near-primary cortices [21, 116, 149]. Others, using a block design, have shown deactivation in auditory cortices in response to visual stimuli and vice versa (e.g. [80], see also [60, 72]). However, these modulations were not present on multisensory blocks [80], and the other studies were limited to examinations of selective attention to specific visual features. Thus, selective attention to one sensory modality might hinder the observation of multisensory effects such that positive multisensory convergence (i.e. stimuli of both senses leading to positive-going activations) may depend on paradigms that include a multisensory context and attention to multiple sensory modalities (see [13, 80, 149]). In the present paradigm attention was continuously allocated to both the auditory and visual modalities, since there was equal likelihood that either sense would be stimulated on a given trial.

Even if attention could account for multisensory convergence (i.e. frank responses to both sensory modalities), it cannot readily account for either the interaction effects on reaction times or the facilitation of BOLD response peak latencies for multisensory relative to both unisensory conditions in the present study (i.e. significantly faster reaction times and BOLD peak latencies to the AV condition). This is corroborated by the fact that the facilitation

of reaction times (i.e. the redundant signals effect) exceeded probability summation. That is, likelihood of a fast reaction time following a multisensory stimulus was greater than the summed likelihoods of an equally fast reaction time following either unisensory stimulus (see Fig. 4.1). This is indicative of facilitative integrative processing exceeding any contribution of selective attention. Similarly, selective attention cannot account for the fact that BOLD peak latency was facilitated for the AV condition. If such were the case, one would expect that BOLD peak latency for the AV condition would be equivalent to the faster of the two unisensory conditions. Our results, however, indicate that the peak latency in response to the AV condition was earlier than either unisensory condition and that the peak latencies in response to the two unisensory conditions did not significantly differ from each other (see Table 4.1).

Task demands, by contrast, do not appear to be a determining factor for observing multisensory convergence or interactions. For example, auditory-somatosensory multisensory convergence and supra-additive interactions have been shown using passive paradigms where subjects were nonetheless aware that stimuli would be presented in either or both sensory modalities [42, 43]. Whether or not such applies to effects on BOLD dynamics will be a topic for future experiments. However, electrophysiological studies in non-human primates provide one line of evidence that multisensory convergence and interactions occur under passive conditions and even under anesthesia. Frank responses to both visual and somatosensory stimuli have been recorded within primary and belt auditory cortices (e.g. [46, 48, 142] see also [73] for recent fMRI results in macaques); though, to our knowledge, similar experiments within visual cortices have not yet been conducted. This collective pattern of results suggests that unisensory stimulation in a paradigm lacking a multisensory context can indeed elicit multisensory effects (in particular convergence). To date, such effects have been most consistently observed using intracranial electrophysiological methods in animals. Our results nonetheless support the future use of event-related designs in combination with high-field fMRI in non-invasively identifying multisensory phenomena under unisensory conditions.

Analyses of BOLD dynamics represent a methodological advancement for identifying multisensory brain regions with fMRI. Here, multisensory interactions led to changes in BOLD latency, but not amplitude (see Fig. 4.3). Importantly, these latency effects did not follow from a simple amplitude/latency trade-off. In auditory cortices, responses to the multisensory condition peaked earlier than either unisensory condition, even though its amplitude was equal to that following auditory stimulation and larger than that following visual stimulation. Likewise, in visual cortices, responses to the multisensory condition peaked earlier than either unisensory condition, even though its amplitude was equal to that following visual stimulation and larger than that following auditory stimulation (see Table 4.1 for detailed statistics).

Several laboratories have recently been examining the validity of different analyses for identifying multisensory interactions [4, 21, 81]. As noted by one laboratory, these approaches inherently assume that signals within a given voxel emanate from a singular, homogenous neural population in terms of its responsiveness [81]. When this is not the case,

canonical criteria of convergence and enhancement can be overly liberal and yield falsely positive results. Supra-additivity as an analysis criterion has also been subject to criticism. Laurienti et al. [81] contended, based largely on the frequency of observing supra- and sub-additive interaction profiles at the individual neuron level, that at the level of fMRI voxels such populations would not be separable and that a supra-additive criterion would be prone to falsely negative results. Beauchamp [4] also suggests that this criterion is overly strict. Instead, Beauchamp supports first restricting analyses to those voxels showing activation to any experimental condition and then applying a threshold wherein the multisensory response must exceed the mean of the unisensory responses. In accord with this proposal, we first spatially restricted our analyses to voxels responsive to both audition and vision. This was done to ensure that peak latency shifts occurred in locations active under unisensory conditions, and that a peak latency shift was apparent in voxels showing a robust, positive BOLD response. More importantly, we would contend that analyses of BOLD response latency bypass the aforementioned interpretational concerns associated with analyses of BOLD response amplitude and provide a clear metric of multisensory interactions. Our methods highlight that the full range of effects may go undetected by typical analysis approaches of BOLD amplitude. One proposition is that an earlier peak reflects facilitated neural processing time [63]. While appealing, it will be important for future investigations to detail more fully the bases for latency shifts in the BOLD signal.

The present data do not allow us to differentiate feedforward from feedback activity within a cortical region. Still, the anatomical studies that first identified direct projections between primary cortices noted that axon terminals were situated predominantly within layers 1 and 6, consistent with a functionally feedback profile [129]. This interpretation is likewise supported by electrophysiological recordings in the case of visual inputs into auditory cortices, which were distributed across the cortical laminae [143]. One speculative possibility is that the magnitude of the observed BOLD responses in the present study might be representative of the distribution of inputs into the region. In the case of visual inputs into auditory cortices, this distribution may be diffuse, whereas auditory inputs into visual cortices may be rather limited or focused. One level of support for this possibility stems from the work of Logothetis and colleagues demonstrating a higher level of coupling between local field potentials, considered to be a measure of input activity within a region, and the BOLD response than between multi-unit activity, considered to be a measure of the output activity within a region, and the BOLD response (e.g. [85]). Substantiating the above speculation will require further experimentation in animal models that specify the laminar origin of signals, though some work has begun in this direction (e.g. [50, 141]). A further speculation is that direct interactions between primary auditory and visual cortices are the basis for the observed latency shifts. As mentioned above, several laboratories have now independently identified monosynaptic projections between these cortices in non-human primates [22, 36, 129]. While such information in humans would be of immense importance, it is presently not feasible with existing staining methods. An alternative viewpoint would be that the present effects are instead mediated by another region. While we cannot unequivocally exclude such a possibility, it is surprising that such a region did

not itself show a BOLD latency shift or amplitude modulation. In addition one might also have expected that latency shifts in primary cortices would be mirrored by effects in motor-related cortices that would in turn underlie the observed facilitation in reaction times. The present study provides no evidence that such is occurring. For one, no effects on peak latency were observed in M1, the SMA, or sub-cortical regions that were nonetheless identified as active under all stimulation conditions (see Fig. 4.4). Second, there was no evidence of a significant correlation between shifts in BOLD peak latency and behavioral facilitation. Finally, as discussed above, the evidence for multisensory interactions during both passive and active conditions suggests task performance is not directly linked with interactions within low-level cortices. We therefore contend that the most parsimonious interpretation of the present results is that there are direct, but not forcibly feedforward, interactions between primary auditory and visual cortices of humans.

Multisensory interactions within primary cortices and between rudimentary stimuli require that longstanding notions of cortical organization be revised to include multisensory interactions as a fundamental component of neural organization (e.g. [159]). Here, we show how investigation of BOLD dynamics can address the current gap in knowledge regarding the neurophysiological bases of and brain regions contributing to multisensory interactions.

4.5 Summary

In this chapter we analyzed the dynamics of the BOLD signal in response to a visual, auditory, or auditory-visual multisensory stimulus. Results show BOLD peak facilitation in response to multisensory stimuli within both visual and auditory primary cortices, indicative that multisensory interactions occur in primary areas. Such interactions modulate solely the temporal parameters of the BOLD signal, but not the amplitude, and cannot be detected with the traditional methods of fMRI analysis. These results revealed how the analysis of BOLD time courses can contribute to understanding human brain function and organization and can also link these results with previous findings from electrophysiological and animal studies.

Part II

The coupling of EEG and fMRI signals

5 The EEG signal

Part II deals with the comparison of the results of fMRI and electro-encephalography (EEG) data analyses. It is widely accepted that, due to their complementary characteristics, the combination of EEG and fMRI data can drastically improve the understandings of spatio-temporal brain dynamics. Unfortunately, some caveats hinder such combination. First, the nature of neurovascular coupling is still poorly understood. Second, analytical methods for combining EEG and fMRI are largely in their infancy. In addition, an improved knowledge of the link between electrophysiology and fMRI would give an important contribution in interpreting changes in BOLD time course, as pointed out in Chapters 3 and 4. The aims of this part are to introduce a new method to study the relationship between fMRI and EEG and to evaluate how this relationship varies across frequencies and brain regions.

In this chapter we first briefly describe the origin of the scalp-recorded EEG and of the inverse model used to estimate the intracranial generators of the potential acquired at the scalp. Than, we introduce a novel method to analyze EEG data as well as the results of the inverse solution, which allows for evaluating the contribution of high-frequency oscillations. Finally, we developed new metric to compare the statistical results of this analysis with the results of fMRI data analysis, and to evaluate how this correspondence of the results vary across frequency and anatomical regions.

5.1 Physiological bases of the EEG signal

EEG measures the electrical activity of neurons, either intracranially or on the surface of the scalp, and the electrical response time-locked to an external stimulus is the so-called *event-related potential* or ERP (see also [158]).

Neuronal activity is associated with two different types of electrical signals: *action potentials* and *postsynaptic potentials*. When a neuron fires, it generates a voltage spike starting from the axon hillock and traveling along the axon to its terminal where neurotransmitters

are released. These all-or-none responses constitute the action potentials and follow from a change in membrane potential beyond threshold levels (typically around 60 mV). When the neurotransmitters released by the action potential bind to the postsynaptic receptors the ion channels on the postsynaptic cell open, allowing for ions to flow and change the potential across the membrane of that cell (the postsynaptic potential).

Action potentials and postsynaptic potentials can both be measured by inserting micro-electrodes into the intracellular space nearby the neuron. The *single-unit* activity, that is the *in vivo* recordings of a single neuron, is a measure of the action potentials rather than the postsynaptic potentials. In addition to the single-unit activity, there are two distinct intracranial measures of the mean activity of a large population of neurons: the *multi-unit* activity, which reflects action potentials, and the *local field potential* (LFP), which is believed to predominantly reflect postsynaptic activity.

During an action potential, at a specific point of the axon, a current flows rapidly into and immediately afterward out from the axon. This flow of inward and outward currents moves toward the axon terminal. If two neurons with parallel and adjacent axons fire simultaneously (i.e. within a millisecond time scale), the net current flow is doubled, and consequently also the potential recorded in the nearby extracellular space is doubled. Conversely, if the two neurons do not fire synchronously the waves of current flow can cancel each other, and the net voltage acquired nearby will be much smaller. Neurons seldom fire with such a precise temporal synchrony and action potentials arising from contiguous axons typically tend to cancel out each other. Therefore, multi-unit activity is typically recorded by placing an intracranial microelectrode near the cell body.

Action potentials are a traveling wave of spikes having a duration of about a millisecond, postsynaptic potentials occur mainly at the dendrites and cell body, without generating moving waves of potential, and last for tens or hundreds of milliseconds. Due to these temporal and spatial characteristics, it is much easier to create the experimental conditions under which the postsynaptic potentials summate instead of cancel, allowing for these being recorded even at great distances from their origin. These characteristics also explain why the EEG recorded at the scalp mainly reflects postsynaptic potentials, though a contribution of action potentials to the scalp-recorded EEG cannot be entirely ruled out.

In conjunction with a change in the potential field, the neuronal activation creates two different current flows. Action potentials and local field potentials induce a large flow of positive and negative ions between the intra- and the extra- cellular space, hence creating a current flowing across the cell membrane. This current, named *impressed* or *active current*, creates an imbalance in charge accumulation at different sites, that is passively compensated by the so-called *return* or *volume current*. At the macroscopic level observable by LFPs and EEG, only volume currents give rise to a significant (measurable) effect*.

*These statements refer in particular to pyramidal cells and to measurement sites infinitely distant from the center of the dipole when compared its size. They still hold for non-pyramidal cells (interneuron cells) but the effects are not yet quantified.

5.1.1 Summation of postsynaptic activity

When excitatory neurotransmitters are released, a net current flows from the extracellular space into the cell near the dendrites and at the same time a current flows from the cell body towards the extracellular space. These two currents create a negative-charged region around the dendrites and a positive-charged region around the cell body. These two regions taken together can be modeled as a unique electrical dipole, oriented from the dendrites toward the cell body. In case of the release of an inhibitory neurotransmitter, the two currents flow in the opposite direction, yielding to a dipole oriented from the cell body toward the dendrites (see Fig. 5.1 for a schematic representation of this effect in case of an excitatory neurotransmitter).

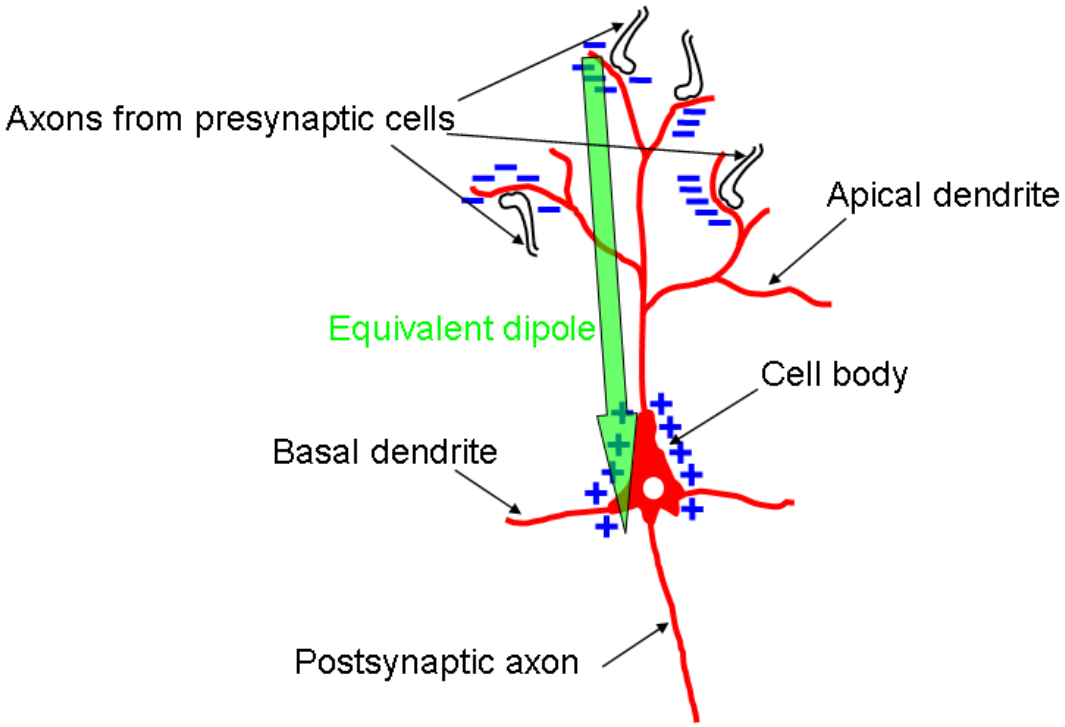

Figure 5.1: Schematic representation of the effects of the release of an excitatory neurotransmitter to a pyramidal cell. The green arrow represents the equivalent dipole modeling the positive and negative charge accumulation

If only one neuron is active, the potential generated is tiny and undetectable from a distant electrode (e.g. placed on the scalp). When thousands or millions of adjacent neurons fire more or less synchronously, the electric fields generated by each neuron (each modeled as a tiny local dipole) superimpose. If all these neurons receive the same type of stimulus, and if they are spatially aligned, the post-synaptic potentials summate and can be measured at the scalp. If the neurons are not aligned but are randomly oriented with respect to their neighbors, the positive end of one local equivalent dipole may be adjacent to the negative

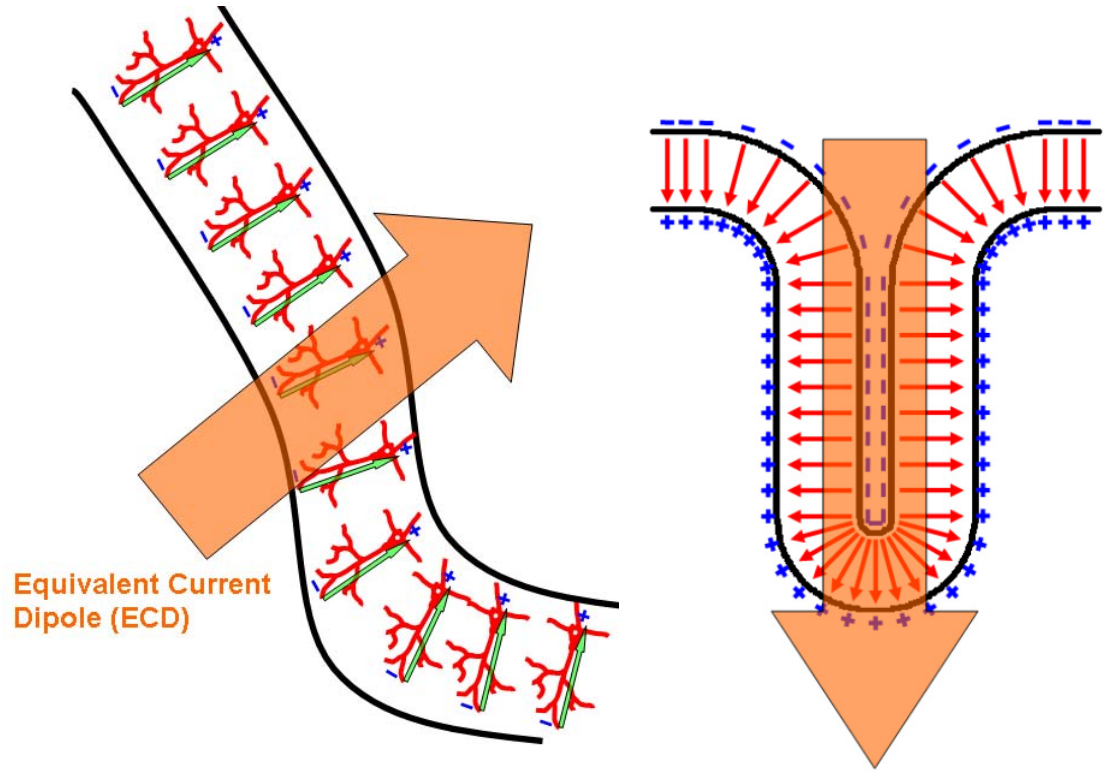

(a) The contribution of adjacent neurons summate to form the equivalent current dipole

(b) Within a sulcus, the contribution of neurons lying in the opposite faces is dramatically reduced

Figure 5.2: Schematic representation of the superposition of the effects of each neuron creating the equivalent current dipoles (represented by the orange arrow).

end of another, canceling their effects. Similarly, if in a group of neurons half of them receive an excitatory transmitter and the other half an inhibitory one, their equivalent dipoles are oriented in opposite directions and will cancel. Therefore, to be detected at the scalp the electrical activity has to be generated by a group of neurons receiving the same type of stimulation, showing a similar orientation, and firing synchronously. The potential obtained by this group of neurons is often modeled as a local average dipole, called the *equivalent current dipole* (ECD), as schematically shown in Figure 5.2a.

Cortical pyramidal neurons are aligned perpendicularly to the pial surface, and their activity is most likely to be measured by an electrode placed on the scalp. The measurement of postsynaptic activity at the scalp is also challenged by the fact the cortex is folded and these folds can partially reduce the amplitude of the equivalent current dipole. For example, imagine a group of activated neurons that show a dipole oriented towards the cortical surface, as depicted in Figure 5.2b. If these neurons lie on opposite faces of a sulcus, half of them have the equivalent dipole oriented in one direction and half oriented in the opposite direction and the intensity of the net electric field generated is dramatically reduced. One

clear example of this problem is the cerebellar cortical surface that is so highly folded to make almost impossible to measure cerebellar activity at the scalp.

The distribution of potentials generated by one or more ECDs and measured at the surface depends on their position, orientation, and intensity as well as on the shape and electrical characteristics of the head itself (in particular the gray and white matter, the cerebrospinal fluid, the skull, and the scalp). In particular, the skull has a resistance much higher than that of the other surrounding tissues. Potentials tend to spread laterally when encountering its high resistance rather than propagating directly to the scalp surface. The skull thus acts as a spatial low-pass filter, blurring the topographical map of potential across the entire surface. Consequently, activity within a given brain region can nonetheless produce a significant potential over a wide region of the scalp.

Another important point is that the impedance of brain, skull, and scalp is essentially purely resistive in the frequency band associated to scalp recorded electromagnetic responses (typically less than 1 kHz [119]). This means that for all practical purposes, the scalp-recorded EEG is an instantaneous measure of the collective postsynaptic activity occurring in the brain and linearly summating at the scalp.

5.2 The inverse solution

The main challenge in EEG analysis is to estimate the neuronal activity that generated the potential map acquired at the scalp. Those methods that estimate this neuronal activity are known as *inverse solutions*.

The estimation of the neuronal activity from the scalp recorded EEG requires the solution of an *inverse problem*. Mathematically, the inverse problem is *underdetermined* (i.e. there is no unique solution) and requires the introduction of some *a priori* constraints to be solved. A large part of past and ongoing research is studying which *a priori* knowledge should be introduced to best solve this problem.

The interest in having a reliable three-dimensional inverse solution resides in the fact that electromagnetic measures have the temporal resolution required for studying noninvasively the temporal dynamics of brain processes.

Given a certain map of potential, there are two main families of methods for estimating its generators. The first (and older) family, assumes that only a limited number of generators (usually modeled as ECDs) are active over a time period (e.g. [105, 108, 137, 145]). The maximum number of dipoles that can be simultaneously active is limited by the number of independent measures (i.e. the number of electrodes). A second family of methods does not constrain the number of simultaneous generators, but uses the general linear theory developed to solve underdeterminated inverse problems in conjunction with mathematical (see e.g. [54] for several examples) or physiological (e.g. [2, 33, 47, 56, 59, 84, 118]) *a priori* constraints. A review of these methods can be found in [99].

To compare EEG inverse solution and fMRI we use a distributed source model instead of a dipolar model, and among those we employed the ELECTRA (electrical analysis) source model [55] in conjunction with the LAURA (local auto-regressive averages) regular-

ization strategy for the inverse solution, as developed by Grave de Peralta Menendez and colleagues [56]. This model allows for estimating the LFPs that, according to Logothetis' study [86] are the signals that show the best correlation with fMRI.

5.2.1 ELECTRA source model

ELECTRA is not an inverse solution but a restricted formulation of the source model, based on neurophysiological constraints. It can be seen as a non-invasive estimator of the intracranial LFPs.

The ELECTRA source model is based on the observation that at the macroscopic level observable by LFPs and EEG, neurophysiological microscopic currents derive from the volume currents. These currents follow Ohm's law, which means their magnitude is linearly proportional to the local potential field and to the electrical characteristics of the tissue. In mathematical terms, these currents can be modeled as irrotational [55] and can be expressed as gradients of a potential field. In practical terms, estimating a scalar field rather than vectors reduces the number of free parameters (i.e. unknowns) by a factor of 3 which in turn effectively increases the spatial resolution. While the other typical distributed inverse source models estimate the modulus of the current density vector which is a positive value, ELECTRA estimates a scalar field (i.e. potentials) with both positive and negative values. Polarity information is useful to compare the solution of the inverse solution with intracranial recordings in animals as well as in humans.

Even if the constraints imposed by the ELECTRA source model reduce the number of free parameters, the solution is still non-unique. Any numerical method to solve underdetermined system can be used in conjunction with ELECTRA. In this work the regularization technique named LAURA has been chosen, as described in [56]. According to this method, the activity at one point is related to that of all other solution points by autoregressive estimators whose weights depend upon the distance with a given law, In our case, this law follows the physical model of propagation of the estimated field (i.e. the inverse of the square distance when computing potentials).

5.3 Single-trial analysis

One of the most widely used techniques in the analysis of EEG data is the study of ERPs, that is the study of the responses time-locked with stimulus onset. EEG data are often noisy and an increase in the SNR is typically obtained by averaging all the responses to the same type of stimulus. Under the hypothesis that the electrical response to the same stimulus remain constant throughout the entire experiment, the averaging technique allows for reducing all the components that are not time-locked to the stimulus, and that are considered as noise (e.g. electrical noise, physiological electrical activity unrelated to the stimulus). Unfortunately, this technique does not reduce only the noise, but also all phase-varying signals. At higher frequencies, the period of the oscillations is relatively short, such that even a small jitter in the phase of the signal across repetitions can dephase the

signal [148]. Practically, frequencies over 30-40 Hz hardly survive to the averaging, unless tightly locked to stimulus onset.

To preserve the information of the high frequencies of the signals, we developed a new method of analysis that relies on the statistical comparison of the spectral power between the pre- and post- stimulus onset periods computed for each single trial. Since this method does not compute the average of the ERPs, the information carried by the high frequency components of the EEG can be evaluated. The method is based on the spectral analysis of the pre- and post- stimulus onset periods and hence it requires the signal to be stationary during both periods. This constraint, that comes from the constraints of the spectral analysis, implies that the spectral features of the signal do not change during the time window analyzed. This method, therefore, is not suitable in case of event-related designs, where the signal generated by a response to a brief stimulus typically denotes time-varying spectral characteristics. Conversely, this method can be applied to block-design experiments, where the signal in response to a long and steady stimulation period typically show time-invariant spectral features.

The processing steps of the single trial analysis are schematically shown in Figure 5.3. After artifact rejection and interpolation of bad channels, each single trial is isolated including the same number of samples in the pre- and in the post- stimulus onset periods, and the inverse solution for each single trial separately* is estimated. For each of those inverse estimates, we compute the power spectrum in the pre- and in the post- stimulus onset periods. Since these two periods had the same number of samples (i.e. the same duration), the spectral resolution of the two power spectrum densities have the same frequency resolution. Contrasting the pre- versus post- stimulus spectral power, we can statistically test at which position in the brain and at which frequency a change in the spectral power in response to the stimulus is observable. Therefore, we obtain one statistical map per spectral line indicating whether the estimated signal of the inverse solution shows a change in spectral power following the stimulus. Statistical significance is non-parametrically tested using the sign test.

The single-trial analysis tests the differences in the spectral power between the pre- and the post- stimulus onset periods. Noise is assumed to be equally distributed across both periods, which means that there should be no statistical difference in the noise level between the pre- and post- stimulus onset periods and hence the noise does not contribute to the estimation of the power changes elicited by the stimulus. Therefore, this method can detect power changes driven by the stimulus even at very high frequencies, where typically the noise is much higher than the signal.

Inference on the population is obtained using a second level of statistics. For each subject we can estimate the median of the power spectral difference between the pre- and post- stimulus periods and these estimates are then submitted to the non-parametric sign test to test whether these estimates come from a population with zero median.

*In this work the ELECTRA inverse solution (see section 5.2.1) has been adopted, but the choice of the inverse solution is irrelevant for the single trial analysis technique. This method can be applied on the results of all the other inverse solution algorithms as well as on the surface EEG data

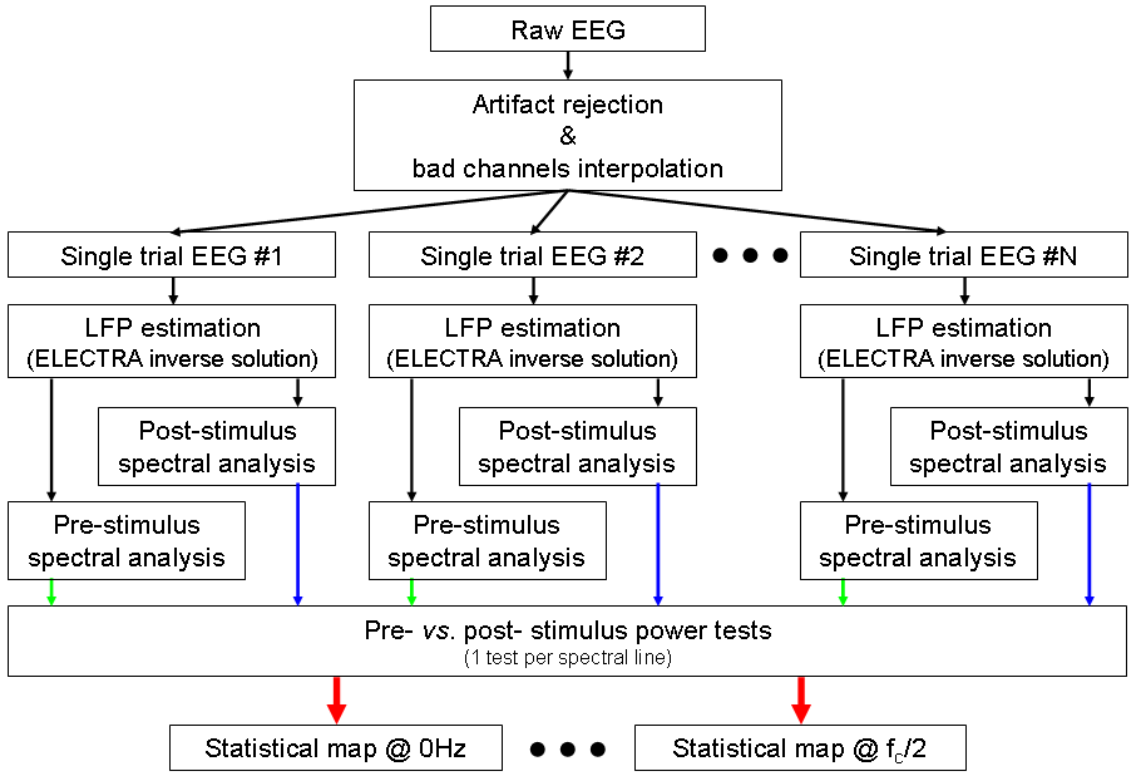

Figure 5.3: Schematic representation of the single-trial analysis for the EEG dataset

5.4 Comparison between fMRI and EEG analyses

EEG and fMRI signals reflect the same underlying phenomenon, that is the neuronal activation. Neuronal activity produces both changes in the potential field and changes in blood flow and oxygenation. The systems that link the neuronal activity to the measured EEG and BOLD signals are completely different, they have different time constants and are sensitive to different characteristics of this activity. EEG and fMRI give us an insight into the neuronal activity from two different points of view, and the information carried by these two signals overlap only partially. Hence, to have a better view on the brain processes it is important to combine these to signals. The first step in this combination is to understand which are the features in common between EEG and fMRI signals and how they correlate.

Logothetis and colleagues [86] acquired fMRI and intracranial EEG within the primary visual cortex of anesthetized monkeys and showed that LFP is the component of neural activity that better correlates with the fMRI signal. Starting from this previous finding we studied the correlation between the fMRI signal and results of the ELECTRA inverse solution that estimates the intracranial LFPs, as discussed in section 5.2.1. In addition, the frequency band used by Logothetis and colleagues to define the LFP (40-130 Hz) reside in the gamma band and those frequencies hardly survive after the averaging process. Therefore, we decided to employ the single trial analysis (see section 5.3) that preserves the information

of the high frequency components, while also preserving lower frequencies too, which were excluded by Logothetis and colleagues.

The single trial analysis method computes one statistical map per each frequency (or frequency band) analyzed and the comparison of the results of the fMRI and the EEG single trial analyses allows us for discriminating which EEG frequencies correlate more with the BOLD signal.

The solution points of the inverse problem, that is the nodes where the solution is computed, form a grid of points regularly spaced (e.g. $6\times6\times6\,\mathrm{mm}^3$) within the gray matter. To compare the fMRI signal with the estimated LFPs, we downsampled the resolution of the fMRI dataset to that of the inverse solution. In addition the comparison is carried out only in those voxels common to both the fMRI volume and inverse solution points.

When comparing the active areas as labeled by fMRI and EEG there are many details to consider. First, inverse solution estimates the intracranial LFPs, but there can be a certain error in the localization of these potentials. Similarly, fMRI results can be slightly displaced with respect the real active areas. Therefore it is not advisable to perform a voxel-wise comparison between the two statistical maps because even small misalignment of the fMRI results and of the estimated LFPs can produce high under-estimation of the correlation. This observation lead us to conduct a region-wise instead of a voxel-wise analysis. Moreover, there is no *a priori* hypothesis supporting the idea that the neuro-vascular coupling is constant across brain regions. For these two reasons we decided to separate the different Brodmann areas (BA) of the brain and to compute the comparison between EEG and fMRI within each area separately.

The metric used to compute the resemblance of the activation maps for each region r and frequency f is defined as

$$\text{resemblance}(r,f) = 1 - \frac{|m_{r,\text{LFP}}(f) - m_{r,\text{fMRI}}|}{m_{r,\text{LFP}}(f) + m_{r,\text{fMRI}}}, \tag{5.1}$$

where $m_{r,\text{LFP}}(f)$ is the number of LFP active voxels within the region r at the frequency f divided by the total number of LFP active voxels at the frequency f, and $m_{r,\text{fMRI}}$ is the number of fMRI active voxels within the region r divided by the total number of fMRI active voxels. By construction, resemblance is bounded by 0 and 1 and higher values indicate higher local resemblance of the two statistical maps within that specific region and at that specific frequency.

5.5 Summary

In this chapter we described a novel method for the analysis of EEG data. This technique can be used with both scalp-recorded EEG signals and results of the inverse solution. This method is based on the statistical evaluation of changes in spectral power between the pre- and post- stimulus onset periods for each single trial, separately. The information carried by the high frequencies is preserved, since no averaging step is included. Moreover, we defined the resemblance, which is a novel metric to compare the statistical results of the

single-trial analysis applied on the results of the inverse solution with those of fMRI. This metric, in conjunction with the single-trial analysis, allows for evaluating how changes in the relationship between EEG and fMRI vary across frequencies and anatomical regions of the brain. An example of the application of the single trial analysis and resemblance metric is presented in Chapter 6.

Frequency-dependant correlation between estimated LFPs and BOLD responses in humans

6

In this chapter we first apply the analysis methods described in sections 5.3 to the estimated intracranial LFPs generated by a passive visual paradigm. Then, we compare these results with those obtained by an fMRI experiment conducted using the same experimental protocol with the same subjects in a separate recording session. Such comparison of the results is performed by using the resemblance metric defined in section 5.4, testing how the relationship between the results of EEG and fMRI analyses varies across frequencies and across the different anatomical areas. Logothetis and colleagues [85, 86] found a correlation between BOLD signal and LFPs within the occipital lobe in anesthetized monkeys. In this chapter we apply the abovementioned methods to test if such relationship can be similarly detected in awake humans and if this relationship varies across anatomical regions.

6.1 Introduction

EEG and fMRI are two complementary non-invasive tools for investigating brain functions. While the recent development of fMRI allows for demarcating functional anatomy on a millimeter spatial scale, its temporal resolution is intrinsically limited by the rate of oxygenation and blood flow changes. Conversely, EEG is characterized by a sub-millisecond temporal resolution but has a poor spatial resolution due to the fact the estimation of intracranial generators requires the solution of an underdetermined inverse problem. Due to their complementary characteristics, there is an increasing interest in combining fMRI and EEG (so-called *multimodal imaging*). Unfortunately, a direct comparison of fMRI and EEG data

sets is hindered by the fact that the coupling between fMRI and scalp-recorded EEG signals remains poorly understood, although it is clear that neural activity underlies both signals. Many studies have already attempted to evaluate the relationship between neuronal activity and BOLD signal. Heeger et al. [61] and Rees et al. [126] compared the average spiking rate acquired in monkeys V1 and V5, respectively, with the BOLD signal acquired in humans in the same regions and found a proportional relationship between BOLD amplitude and average spiking rate. Mukamel et al. [106], found a high linear correlation between BOLD signal, high-frequency LFP and spiking activity within human auditory areas, with fMRI and intracranial recordings acquired on two different samples of the human population. Studying fMRI and intracranial recordings within visual cortex of cats, Kayser et al [74] found a good match between BOLD and LFP signals within the gamma band of LFP. In primary visual cortex of anesthetized cats, Niessing et al. [111] found a tight correlation between intracranial recordings within 52-90 Hz band and hemodynamic amplitude measured simultaneously with optical methods. More recently, Logothetis et al. [85, 86] succeeded in acquiring simultaneously fMRI and intracranial EEG within the primary visual cortex of anesthetized monkeys. They showed that the BOLD signal is correlated with both MUA and LFP, but the latter is the EEG component that better correlates with the fMRI signal. To our knowledge, the neurovascular coupling within the same sample of human subjects has yet to be investigated non-invasively. In this study we compared hemodynamic and electrical signals acquired from the same subjects during two different acquisition sessions. In order to obtain comparable statistical maps from both the EEG and fMRI data sets, without losing sensitivity to high-frequency oscillations, we applied the method described in section 5.3. We then compared the results of EEG and fMRI data analysis, applying the method described in section 5.4.

6.2 Material and Methods

6.2.1 Subjects and Paradigm

Eight subjects (mean ± SD age = 31 ± 3.8 years; 4 female) with normal or corrected-to-normal vision, and no history of neurological or psychiatric disease participated at the experiment. Experimental procedures were approved by the Ethics Committee of the Faculty of Biology and Medicine at the University of Lausanne.

Subjects participated in separate EEG and fMRI sessions involving an identical experimental protocol. Subjects passively viewed a visual stimulus (70° wedge of a black-on-gray circular checkerboard presented to the lower left visual quadrant and flickering at 8 reversals per second) for durations of 12 s followed by 18 s of rest (i.e. a blank screen with the fixation point). The experiment consisted of 42 (fMRI) or 126 (EEG) repetitions of the stimulation block.

6.2.2 Magnetic Resonance Imaging

Functional MRI data were acquired on a 3.0 T Siemens Trio system equipped with an 8-channel head coil using a single-shot gradient-echo EPI sequence (TR = 2 s, TE = 30 ms, FoV = 224 mm, flip angle = 90°, matrix size 64 × 64). Each volume comprised 32 slices (slice thickness 3 mm, gap 0.3 mm). For each subject, a sagittal T1-wighted gradient-echo sequence (MPRAGE) was also acquired (160 contiguous sagittal slices, slice thickness 1 mm, matrix size 256 × 256, TR = 1480 ms, TE = 3.42 ms, FoV = 256 mm, flip angle = 15°).

Magnetic resonance images were processed with SPM2 (Wellcome Department of Cognitive Neurology, London, UK). Structural data were normalized to the Montreal Neurological Institute (MNI) template and resampled to a resolution of $1 \times 1 \times 1\,\mathrm{mm}^3$. Functional data were first coregistered to the structural volume and spatially realigned to the first image acquired (to minimize the effect of head motion during the acquisition). Volumes were than normalized to the Montreal Neurological Institute (MNI) template, and resampled to the resolution of the inverse solution grid used in the analysis of EEG data (i.e. $6 \times 6 \times 6\,\mathrm{mm}^3$). The temporal signal at each voxel was low-passed filtered to minimize the effect of a baseline drift. Statistical analysis was conducted according to the General Linear Model (GLM) using as basis function the boxcar representing the experimental protocol convolved with the canonical hemodynamic response function, as defined in SPM2 [45].

Inference on population (group analysis) was obtained by a second-level of statistics, according to the random field theory (voxel-level threshold $p < 0.01$ uncorrected, 3 voxel cluster-size threshold).

6.2.3 EEG data

Continuous EEG data were acquired on a BioSemi Active Two 128-channel AD-box (BioSemi, Amsterdam, The Netherlands) at a sampling rate of 512 Hz.

Preprocessing procedures included single trial selection (from -500 ms prestimulus to 500 ms poststimulus onset), artifact rejection ($\pm 100\,\mu$V artifact rejection criterion in addition to the removal of EEG epochs containing eye blinks or other noise transients), interpolation of signal at artifact electrodes [117], and re-referencing to the common average. For each subject, intracranial LFPs were estimated by applying the ELECTRA inverse solution [55, 56] and a single-trial analysis (as described in section 5.3) was conducted. Since we analyzed pre- and post-stimulus onset periods of 500 ms of duration, we obtained a spectral resolution of 2 Hz. Statistical significance was non-parametrically tested using the sign test.

Inference on the population was obtained using a second level of statistics. For each subject, we estimated the median of the power spectral difference between the pre- and post- stimulus onset periods and these estimates (one per subject) were then submitted to the non-parametric sign test to assess whether these estimates come from a population with zero median (voxel-level threshold $p < 0.01$ uncorrected, 3 voxel cluster-size threshold).

6.2.4 Comparison of the results

The analyses of the fMRI and EEG data yielded two different statistical maps of the activation in the brain. To compare these two maps we employed the metric defined in section 5.4 for each Broadmann Area (BA) within the occipital lobe separately.

For each region separately, we obtained a value of resemblance and, to asses its statistical significance, we compared this value with the empirical distribution estimated for each BA separately. To compute the empirical distribution, we calculated the resemblance between the fMRI values of the region and an equal number of LFP values randomly sampled across the brain. The empirical distribution was obtained by iterating this process 100000 times. Statistics on the metric were calculated on the estimated empirical distribution and thresholded at $p < 0.05$.

6.3 Results

The results of fMRI analysis ($p < 0.01$ uncorrected, 3-voxels cluster threshold) are shown in a glass brain in Figure 6.1. In the first row of Figure 6.2 the same results are shown in slices overlaid on the mean structural volume. Active regions as defined by fMRI were mainly identified within BA 17 of the right hemisphere and BA 18 and 19 bilaterally (see Fig.6.3a for the definition of BAs), as well as in areas adjacent to the main visual cortices (BA 7, 37, and 40).

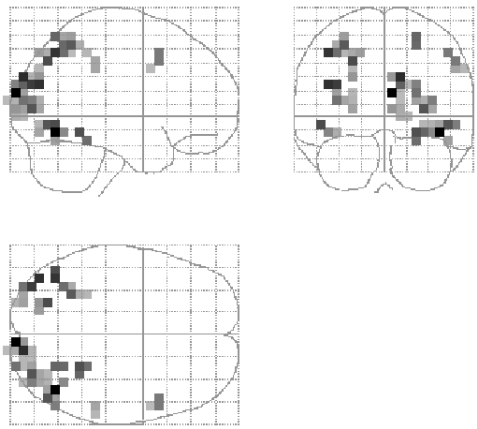

Figure 6.1: Glass brain representation of fMRI activations ($p < 0.01$ uncorrected, cluster-threshold 3 voxels)

The spatial distribution of LFP modulations differed as a function of frequency. While, for example, at 30 Hz few and relatively sparse voxels show a change in spectral power between the pre- and post- stimulus onset periods, at 52 and 216 Hz there are power changes in locations similar to those identified by the fMRI.

To better evaluate the co-localization of LFP and fMRI activity, we computed the resemblance metric (see section 5.4 for the details) across frequencies within each Brodmann

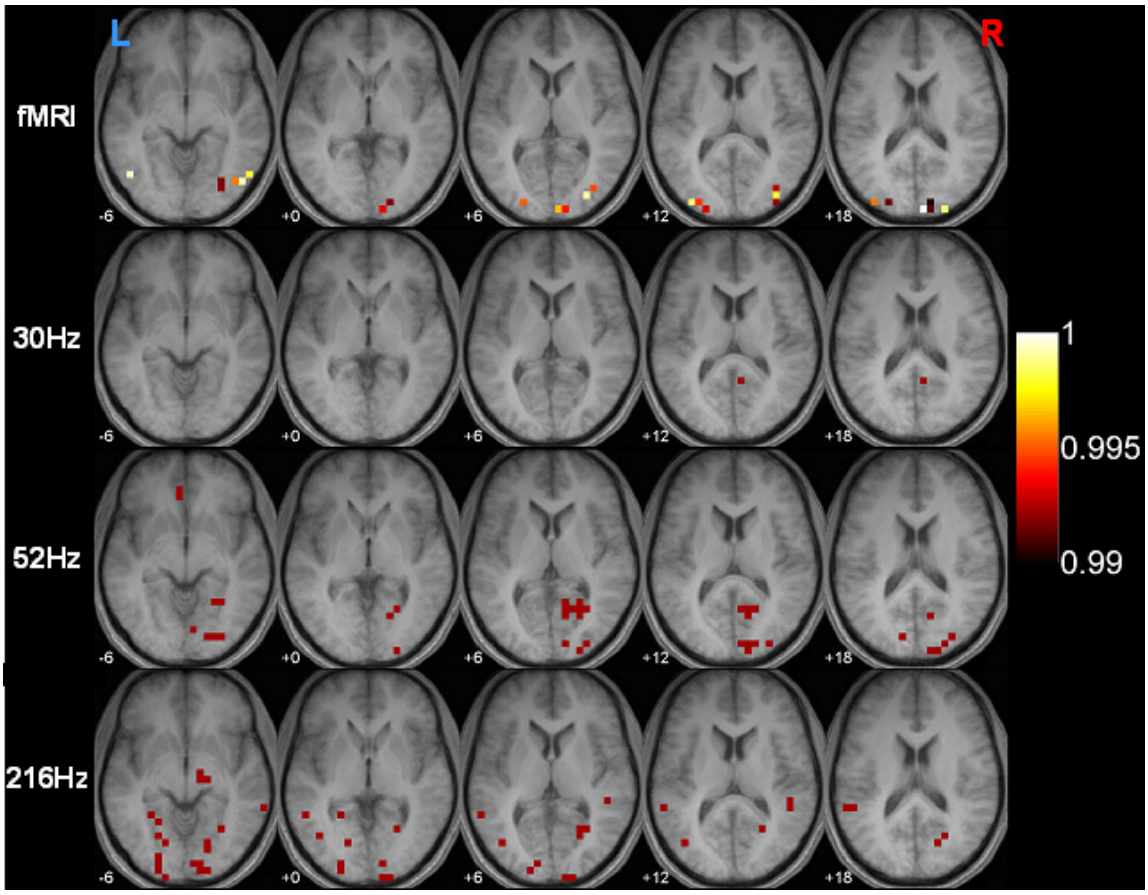

Figure 6.2: Activation areas ($p < 0.01$ uncorrected, cluster-threshold 3 voxels) for the fMRI and for the LFPs at 30, 52, and 216 Hz

area. Figure 6.3 shows the results for the areas within the occipital cortices: BAs 17, 18, and 19 bilaterally. BA 17 shows a non-zero resemblance only within the right hemisphere (contralateral to the stimulus). Here we observed one statistically significant spectral region at very high frequencies (i.e. 218 Hz), and one that approached statistical significance ($0.05 < p < 0.1$) within the gamma band, at around 50-60 Hz. Within BA 18, we qualitatively observed a more bilateral resemblance, even though statistically significant values lie within the hemisphere contralateral to the stimulus. In this region, in addition to the frequency excited within the right BA 17 we observe significant power changes at the lower frequencies as well as at 170 Hz. Within BA 19, it bilaterally shows statistically significant values. These values are in correspondence of all the frequencies already noticed within BA 18 with in addition some other frequencies, in particular at 90 and 100 Hz in the right hemisphere and at 144 Hz in the left.

Resemblance was also computed for regions adjacent to the occipital lobes that showed activation in the fMRI analysis. Results are reported in Figure 6.4. Within BA 7, only the left hemisphere showed some activations, and we found statistically significant resemblance values in the low frequency band (10 Hz), in the gamma band (58 Hz), and in the very high

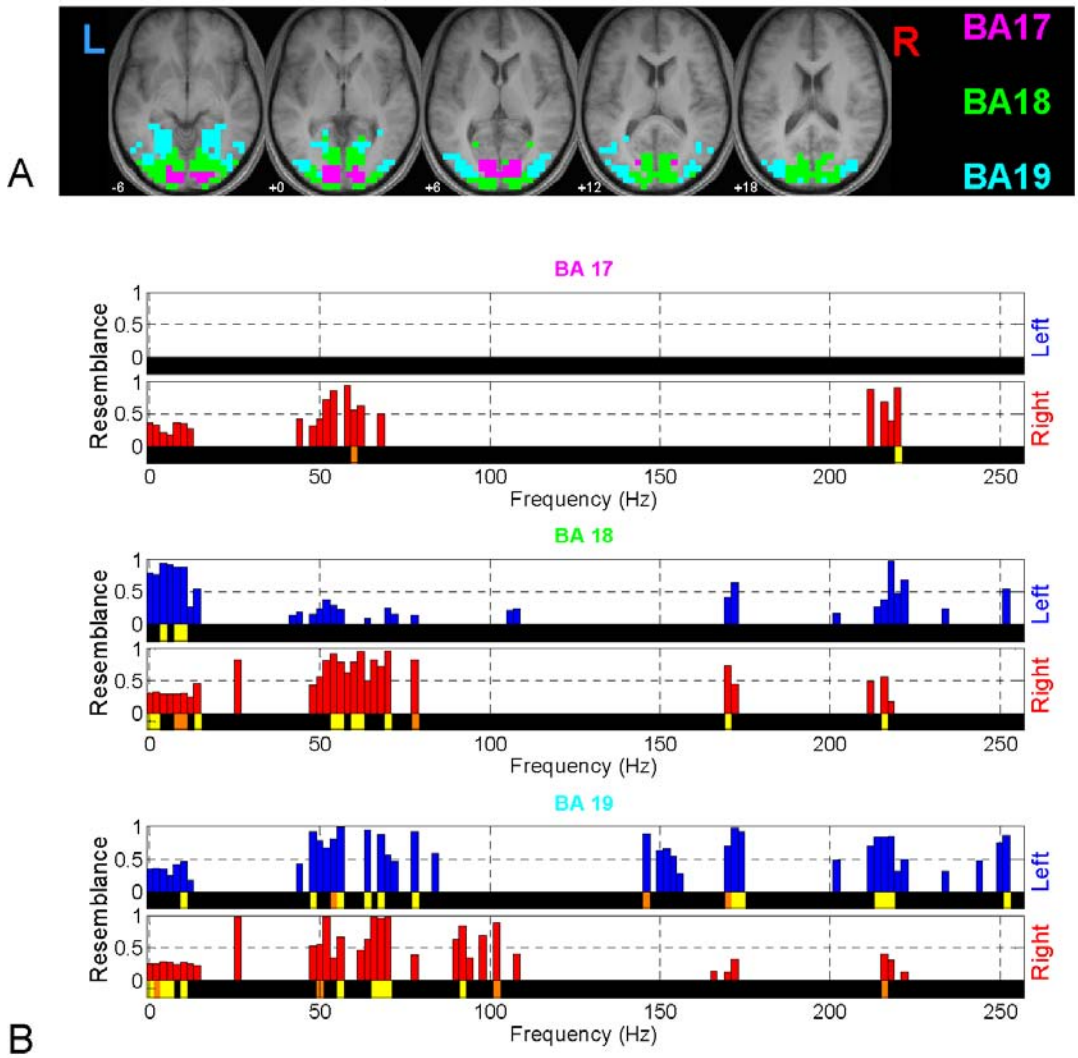

Figure 6.3: a) Definition of Brodmann Areas 17 (magenta), 18 (green), and 19 (cyan). b) Resemblance between fMRI and LFP analyses within BAs 17, 18, and 19. Below the barplots orange ($0.05 < p < 0.1$) and yellow ($p < 0.05$) lines indicate the statistical significance of the resemblance value. Blue bars represent the left hemisphere, red bars the right hemisphere.

frequency oscillation (VHFO) band (252 Hz). At around 160, 166 and 216 Hz we found resemblance values approaching the significance criterion. While BA 37 showed bilateral activations, only EEG activity at 222 Hz within the right hemisphere showed a resemblance value close to our significance criterion, and the same happened within BA 40, where the resemblance was nearly significant for the left hemisphere in the very low-frequency band (<2 Hz).

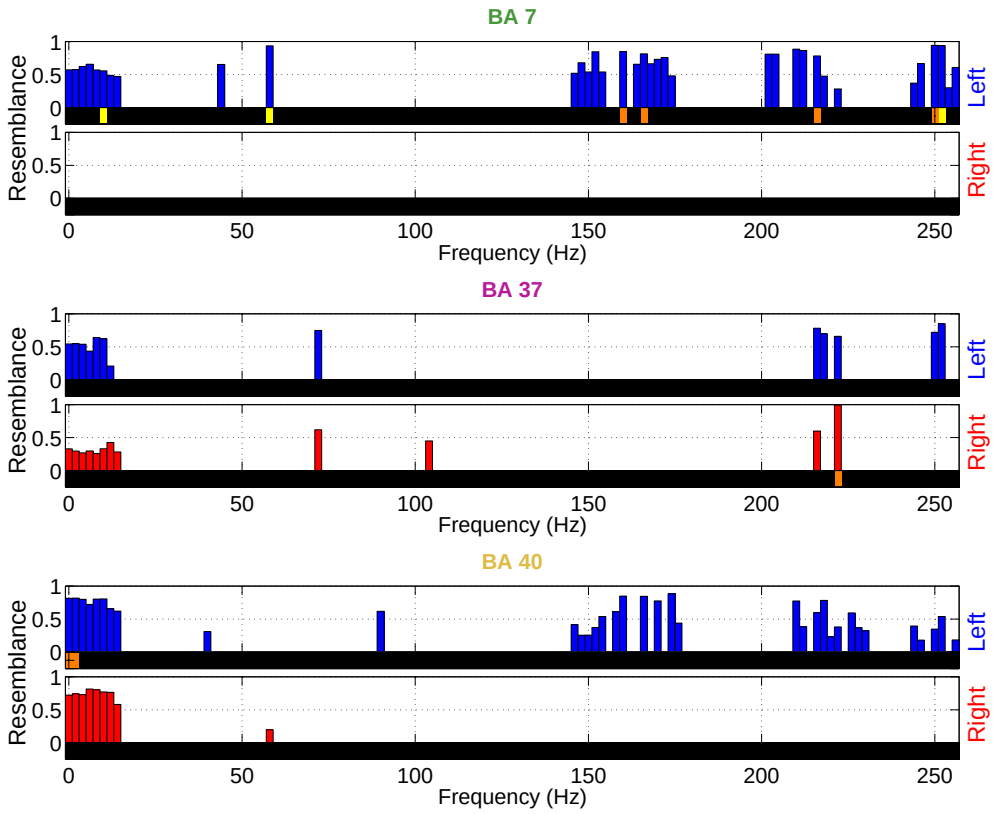

Figure 6.4: Resemblance between fMRI and LFP analyses within BAs 7, 37, and 40. Below the barplots orange ($0.05 < p < 0.1$) and yellow ($p < 0.05$) lines indicate the statistical significance of the resemblance value. Blue bars represent the left hemisphere, red bars the right hemisphere.

6.4 Discussion

This is the first study comparing in humans results of fMRI analysis with those from LFPs estimated by the scalp-recorded EEG, and therefore in a completely non-invasive manner. The comparison was conducted comparing the statistical maps obtained by the fMRI and LFP analyses for each single frequency. To preserve the contribution of high-frequency oscillations, we developed a new method for testing changes in power between the pre- and post- stimulus onset periods. A more qualitative comparison was obtained by introducing a new metric to evaluate the regional resemblance of two statistical maps. The first finding of this study is that only few frequencies show a change in their spectral power after the stimulus onset. In particular, this study points out changes within the gamma band (i.e. 30-80 Hz) and within VHFO band (i.e. from 100 to above 200 Hz). These frequencies are often discarded because their signal level is poor and traditional analytical methods do not allow for separating their contribution from noise. Contrasting the pre- versus the post-stimulus onset spectral power, the contribution of the noise (supposed to be independent from the stimulus onset) is cancelled. The method we developed allows the evaluation

of the contribution of all the frequencies, even those that are below the noise level, and demonstrates the importance of single-trial analysis in the study of brain electrical activity, as already pointed out by Gonzalez et al. [51–53]. Even if it is not completely clear their origin and their functional role, there is increasing evidence of the importance of VHFOs in brain processes in rats and cats [25, 57, 146] as well as in humans [51]. The non-invasive study of VHFOs has always been limited by their small amplitude on the scalp, typically below the noise level. The method we developed, therefore, can give an important contribution to the study of the functional role played by VHFOs in humans. Consistent with previous studies (e.g. [74, 85, 86, 111]), we found a high and significant resemblance between LFPs and BOLD statistical images in the gamma band within V1. In particular, like Kayser et al. [74] and Niessing et al. [111], we found high correlation within the gamma band of the LFP. In addition to the gamma band, we found a significant resemblance also in correspondence of VHFOs. While Logothetis et al. [86] and Niessing et al. [111] were surely impeded in detecting such high-frequency components by their definition of LFPs (obtained by filtering the signal in the 40-130 Hz range), our results seem in contrast with Kayser et al. [74]. This difference may derive from the inter-species variability (cats versus humans). It may also be directly related to the temporal window we analyzed. In this paper we focused our attention to the first 500 ms after stimulus onset, which is much shorter than the period analyzed by Kayser and colleagues. In our study, therefore, transient effects related to stimulus onset play a much more important role than in Kayser's study, which is dominated by the sustained effects of the stimulation.

Another important results of the present study is the regional variability of the resemblance between BOLD and LFP analyses. When passing from the lower to the higher order visual areas (i.e. from BA 17 to BA 18 and finally to BA 19), the pattern of the resemblance becomes more complex, involving at each step new frequencies, particularly within the side ipsilateral to the visual stimulus. To this point we can not ascertain if this result is due to the involvement of new frequencies at each step of the visual processing, or to a regional change in the neurovascular coupling, meaning that the frequencies that correlate with the BOLD signal are specific of a certain region.

In conclusion, in this work we first set up a new method for the analysis of single trials that allowed for showing how VHFOs are involved in the processing of a rudimentary visual stimulus within visual areas. Comparing the statistical maps obtained by the LFP analysis with fMRI results, we showed that fMRI is tightly linked with gamma band and VHFOs, and that this link is regionally specific.

6.5 Summary

In this chapter we studied the electrical and hemodynamic responses during passive visual stimulation. The use of the single-trial analysis (see section 5.3) and resemblance metric (see section 5.4), in conjunction with the ELECTRA inverse solution [55, 56], permitted the evaluation of the relationship between fMRI and estimated intracranial LFPs in a completely non-invasive manner. Fully understanding the relationship between LFPs and fMRI

is a crucial step for correctly relating changes in BOLD signal to the underlying neuronal activity, and for the development of a non-invasive method that allows for extensively investigating such relationships in human populations.

Single-trial analysis revealed that the estimated intracranial LFPs show a response to a passive visual stimulus that varies across frequency. In particular we were able to show reliable responses even at very high frequencies, that are difficult to study with the traditional methods of analysis.

The comparison between results of LFP and fMRI analyses revealed that the relationship varies across frequencies and anatomical regions. Passing from lower to higher cortical levels of processing the pattern of resemblance becomes more complex, involving new frequencies at each step.

7 Conclusions

7.1 Achievements

The work of this thesis addressed two main topics. First, we investigated the temporal dynamics of the BOLD signal, which is the hemodynamic response of the brain to an external stimulus (Part I, which includes Chapters 2, 3, and 4). Throughout these chapters we defined a novel method of jittering stimulus delivery and image acquisition that allows for estimating the BOLD signal with a temporal resolution much finer that the TR (i.e. the image acquisition rate). While the basic idea of this method had already been developed and used in functional neuroimaging, this is the first time that this technique was used to achieve a temporal resolution of a few hundred milliseconds. The estimation of the BOLD response with such a fine temporal resolution allowed for studying how the temporal characteristics of the signal are modulated by experimental conditions within the same brain regions. In particular, we focused our attention on shifts in peak latency and response slope. We point out how the analysis of BOLD temporal dynamics can reveal effects and interactions that are not otherwise detectable with typical fMRI analysis strategies, while also circumventing interpretational caveats of analyses of BOLD response amplitude.

The second part of this thesis investigated the correlation between fMRI and EEG (Part II, which includes Chapters 5 and 6). In this part, we first defined a new method for analyzing EEG data and applied it to the result of the ELECTRA inverse solution. This method is based on the contrast of the spectral power of each single trial between the pre- and post- stimulus periods. Since no averaging step is included in this method, the contribution of very high frequencies oscillations (VHFOs) can be evaluated. The output of the single-trial analysis is one statistical map per frequency studied. As a next step, we compared these statistical maps with those obtained with fMRI (under the same experimental conditions). To do this, we defined a novel metric, termed resemblance. We applied this resemblance metric in the case of a passive visual paradigm. We found that

the correlation between EEG and fMRI signals varies across frequencies and anatomical regions, and that VHFO activation maps have a statistically significant correlation with fMRI.

7.2 Perspectives

The investigation of BOLD dynamics with high temporal resolution opens new possibilities for investigating how the hemodynamic response is modulated by stimulus conditions. This analytical method can be conducted in parallel with the traditional fMRI analysis, because its measures (i.e. changes in the temporal features) are orthogonal to those of traditional fMRI methods (i.e. changes in the amplitude of the signal). Many questions still remain unresolved. First, it will be necessary to evaluate the sensitivity of this method in the context of successive activations/stimulations where linear summation is believed to apply. For example, when stimuli are not widely spaced in time, so that the hemodynamic responses overlap, is this method still able to detect changes in the temporal features of the BOLD signal? Is the approximation of linear summation sufficient for resolving small modulations of the temporal characteristics? Which are the least sensitive features of this approximation? Answering these questions is important for employing the temporal analysis with experimental protocols that require a short inter-stimulus interval.

Another noteworthy point is the fact that the detection of a change in BOLD dynamics reveals that a phenomenon occurred in the underlying neuronal activation, but fails to explain the nature of this change. Further investigations are required to better understand the neuro-vascular coupling, and in particular to understand how changes of the different features of the BOLD dynamics reflect changes in the underlying neuronal activity.

Technical improvements in MR technology will help in addressing these issues. The use of higher magnetic fields produces fMRI acquisitions with better signal-to-noise ratio. The analysis of BOLD dynamics can receive an important improvement by the use of high-field magnets, because dealing with a less noisy signal allows for a more precise and more reliable estimation of its parameters. The use of high-field scanners is therefore advisable for investigating the changes in the temporal features of the BOLD signal.

The method developed for the comparison of fMRI and EEG statistical maps represents a first step for combining the results of these two non-invasive techniques. The obvious continuation of this study is the comparison of the statistical maps obtained under different stimulus conditions. Is the frequency-dependant and/or regional-dependant relationship consistent across sensory modalities? Another natural extension of the present study is the use of the developed analytical methods with EEG and fMRI data sets that have been simultaneously (rather than separately) acquired. Simultaneous acquisition allows also for a correlation analysis between the BOLD signal time course and the estimated LFPs, or one filtered version of estimated LFPs, which in turn allows for evaluating frequency-dependant correlations.

While the method described in sections 5.3 and 5.4 is useful for understanding the correlation between EEG and fMRI in case of block-design experiments, the estimation of

the BOLD signal with high temporal resolution is useful in the case of event-related studies, where one can imagine correlating a certain set of features of the BOLD signal with a potentially different set of features of the estimated LFPs. In this case, an estimation of the BOLD signal with high temporal resolution can lead to a more precise evaluation of the BOLD parameters and, hence, to a potentially better sensitivity of the analysis correlation.

Bibliography

[1] K. Amunts et al. (2000). Brodmann's areas 17 and 18 brought into stereotaxic space-where and how variable? *Neuroimage* **11**(1):66–84.

[2] F. Babiloni et al. (2003). Multimodal integration of high-resolution eeg and functional magnetic resonance imaging data: a simulation study. *Neuroimage* **19**(1):1–15.

[3] P. A. Bandettini et al. (1992). Time course EPI of human brain function during task activation. *Magn Reson Med* **25**(2):390–397.

[4] M. S. Beauchamp (2005). Statistical criteria in fMRI studies of multisensory integration. *Neuroinformatics* **3**(2):93–113.

[5] M. S. Beauchamp et al. (2004). Unraveling multisensory integration: patchy organization within human STS multisensory cortex. *Nat Neurosci* **7**(11):1190–1192.

[6] P. S. Bellgowan, Z. S. Saad, P. A. Bandettini (2003). Understanding neural system dynamics through task modulation and measurement of functional MRI amplitude, latency, and width. *Proc Natl Acad Sci USA* **100**(3):1415–1419.

[7] O. Blanke et al. (1999). Visual activity in the human frontal eye field. *Neuroreport* **10**(5):925–930.

[8] J. Bodurka, P. A. Bandettini (2002). Toward direct mapping of neuronal activity: MRI detection of ultraweak, transient magnetic field changes. *Magn Reson Med* **47**(6):1052–1058.

[9] G. M. Boynton, S. A. Engel, G. H. Glover, D. J. Heeger (1996). Linear system analysis of functional magnetic resonance imaging in human V1. *J Neusosci* **16**(13):4207–4221.

[10] T. Brandt et al. (2000). Hemifield visual motion stimulation: an example of interhemispheric crosstalk. *Neuroreport* **11**(12):2803–2809.

[11] C. M. J. Braun (1992). Estimation of interhemispheric dynamics from simple unimanual reaction time to extrafoveal stimuli. *Neuropsychol Rev* **3**(4):321–365.

[12] C. M. J. Braun, A. Achim, L. Villeneuve (1999). Topography of averaged electrical activity relating to interhemispheric dynamics in normal humans: where does the critical relay take place? *Int J Psychophysiol* **1**(32):1–14.

[13] M. Brosch, E. Selezneva, H. Scheich (2005). Nonauditory events of a behavioral procedure activate auditory cortex of highly trained monkeys. *J Neurosci* **25**(29):6797–6806.

[14] W. S. Brown, E. B. Larson, M. A. Jeeves (1994). Directional asymmetries in interhemispheric transmission time: evidence from visual evoked potentials. *Neuropsychologia* **32**(4):439–448.

[15] M. Brysbaert (1994). Interhemispheric transfer and the processing of foveally presented stimuli. *Behav Brain Res* **64**(1–2):151–161.

[16] H. Buchner et al. (1997). Fast visual evoked potential input into human area V5. *Neuroreport* **8**(11):2419–2422.

[17] R. L. Buckner et al. (1996). Detection of cortical activation during averaged single trials of a cognitive task using functional magnetic resonance imaging. *Proc Natl Acad Sci USA* **93**(25):14878–14883.

[18] J. Bullier (2001). Integrated model of visual processing. *Brain Res Brain Res Rev* **36**(2–3):96–107.

[19] A. Burkhalter, K. L. Bernardo (1989). Organization of corticocortical connections in human visual cortex. *Proc Natl Acad Sci USA* **86**(3):1071–1075.

[20] V. Calhoun, T. Adali, M. Kraut, G. Pearlson (2000). A weighted leastsquares algorithm for estimation and visualization of relative latencies in event-related functional MRI. *Magn Reson Med* **44**(6):947–954.

[21] G. A. Calvert (2001). Crossmodal processing in the human brain: insights from functional neuroimaging studies. *Cereb Cortex* **11**(12):1110–1123.

[22] C. Cappe, P. Barone (2005). Heteromodal connections supporting multisensory integration at low levels of cortical processing in the monkey. *Eur J Neurosci* **22**(11):2886–2902.

[23] M. Catani, D. K. Jones, R. Donato, D. H. ffytche (2003). Occipito-temporal connections in the human brain. *Brain* **126**(Pt 9):2093–2107.

[24] C. Cavina-Pratesi, E. Bricolo, B. Pellegrini, C. A. Marzi (2004). At what stage of manual visual reaction time does interhemispheric transmission occur: controlled or ballistic? *Exp Brain Res* **155**(2):220–230.

[25] J. J. Chrobak, G. Buzsaki (1996). High-frequency oscillations in the output networks of the hippocampal-entorhinal axis of the freely behaving rat. *J Neurosci* **16**(9):3056–3066.

[26] V. P. Clark, S. Fan, S. A. Hillyard (1995). Identification of early visual evoked potential generators by retinotopic and topographic analyses. *Hum Brain Mapp* **2**:170–187.

[27] J. M. Clarke, E. Zaidel (1989). Simple reaction times to lateralized flashed: Varieties of interhemispheric communication routes. *Brain* **112**(Pt 4):849–870.

[28] S. Clarke (1994). Association and intrinsic connections of human extrastriate visual cortex. *Proc R Soc Lond B Biol Sci* **257**(1348):87–92.

[29] S. Clarke (2003). The role of homotopic and heterotopic callosal connections in humans. In E. Zaidel, M. Iacoboni (eds.), *The Parallel Brain*, pp. MIT Press, Cambridge, MA, 461–472.

[30] S. Clarke, J. Miklossy (1990). Occipital cortex in man: organization of callosal connections, related myelo- and cyto- architecture, and putative boundaries of functional visual areas. *J Comp Neurol* **298**(2):188–214.

[31] S. Clavagnier, A. Falchier, H. Kennedy (2004). Long-distance feedback projections to area V1: implications for multisensory integration, spatial awareness, and visual consciousness. *Cogn Affect Behav Neurosci* **4**(2):117–126.

[32] M. C. Corballis, P. M. Corballis, M. Fabri (2003). Redundancy gain in simple reaction time following partial and complete callosotomy. *Neuropsychologia* **42**(1):71–81.

[33] A. M. Dale, M. I. Sereno (1993). Improved localization of cortical activity by combining EEG and MEG with MRI cortical surface reconstruction: A linear approach. *J Cogn Neurosci* **5**:162–176.

[34] G. Di Virgilio, S. Clarke (1997). Direct interhemispheric visual input to human speech areas. *Hum Brain Mapp* **5**(5):347–354.

[35] J. R. Duann et al. (2002). Single-trial variability in event-related BOLD signals. *NeuroImage* **15**(4):823–835.

[36] A. Falchier, S. Clavagnier, P. Barone, H. Kennedy (2002). Anatomical evidence of multimodal integration in primate striate cortex. *J Neurosci* **22**(13):5749–5759.

[37] D. J. Felleman, D. C. Van Essen (1991). Distributed hierarchical processing in the primate cerebral cortex. *Cereb Cortex* **1**(1):1–47.

[38] D. H. ffytche et al. (2000). Human area V5 and motion in the ipsilateral visual field. *Eur J Neurosci* **12**(8):3015–3025.

[39] E. Formisano, R. Goebel (2003). Tracking cognitive processes with functional MRI mental chronometry. *Curr Opin Neurobiol* **13**(2):174–181.

[40] E. Formisano et al. (2002). Tracking the mind's image in the brain: time-resolved fMRI during visuo-spatial mental imagery. *Neuron* **35**(1):185–194.

[41] J. J. Foxe, G. V. Simpson (2002). Flow from V1 to frontal cortex in humans: a framework for defining "early" visual processing. *Exp Brain Res* **142**(1):139–150.

[42] J. J. Foxe et al. (2000). Multisensory auditory-somatosensory interactions in early cortical processing revealed by high-density electrical mapping. *Brain Res Cogn Brain Res* **10**(1–2):77–83.

[43] J. J. Foxe et al. (2002). Auditory-somatosensory multisensory processing in auditory association cortex: an fmri study. *J Neurophysiol* **88**(1):540–543.

[44] K. J. Friston, P. Jezzard, R. G. Turner (1994). Analysis of functional MRI time-series. *Hum Brain Mapp* **1**(2):153–171.

[45] K. J. Friston et al. (1998). Event-related fMRI: characterizing differential responses. *Neuroimage* **7**(1):30–40.

[46] K. M. Fu et al. (2003). Auditory cortical neurons respond to somatosensory stimulation. *J Neurosci* **23**(20):7510–7515.

[47] M. Fuchs, M. Wagner, T. Kohler, H. A. Wischmann (1999). Linear and nonlinear current density reconstructions. *J Clin Neurophysiol* **16**(3):267–295.

[48] A. A. Ghazanfar, J. X. Maier, K. L. Hoffman, N. K. Logothetis (2005). Multisensory integration of dynamic faces and voices in rhesus monkey auditory cortex. *J Neurosci* **25**(20):5004–5012.

[49] M. H. Giard, F. Peronnet (1999). Auditory-visual integration during multimodal object recognition in humans: a behavioral and electrophysiological study. *J Cogn Neurosci* **11**(5):473–490.

[50] J. B. Goense, N. K. Logothetis (2006). Laminar specificity in monkey V1 using high-resolution SE-fMRI. *Magn Reson Imaging* **24**(4):381–392.

[51] S. L. Gonzalez et al. (2006). Very high frequency oscillations (VHFO) as a predictor of movement intentions. *Neuroimage* **32**(1):170–179.

[52] S. L. Gonzalez Andino, M. M. Murray, J. J. Foxe, R. G. de Peralta Menendez (2005). How single-trial electrical neuroimaging contributes to multisensory research. *Exp Brain Res* **166**(3–4):298–304.

[53] S. L. Gonzalez Andino et al. (2005). Prediction of response speed by anticipatory high frequency oscillations in the human brain. *Hum Brain Mapp* **24**(1):50–58.

[54] R. Grave de Peralta Menendez, S. L. Gonzalez Andino (1999). Distributed source models: standard solutions and new developments. In C. Uhl (ed.), *Analysis of Neurophysiological Brain Functioning*, pp. 176–201, Springer-Verlag, Berlin.

[55] R. Grave de Peralta Menendez et al. (2000). Imaging the electrical activity of the brain: ELECTRA. *Hum Brain Mapp* **91**(1):1–12.

[56] R. Grave de Peralta Menendez et al. (2004). Electrical neuroimaging based on biophysical constraints. *Neuroimage* **21**(2):527–539.

[57] F. Grenier, I. Timofeev, M. Steriade (2001). Focal synchronization of ripples (80-200 Hz) in neocortex and their neuronal correlates. *J Neurophysiol* **86**(4):1884–1898.

[58] D. A. Handwerker, J. M. Ollinger, M. D'Esposito (2004). Variation of bold hemodynamic responses across subjects and brain regions and their effects on statistical analyses. *Neuroimage* **21**(4):1639–1651.

[59] O. Hauk, A. Keil, T. Elbert, M. M. Muller (2002). Comparison of data transformation procedures to enhance topographical accuracy in time-series analysis of the human EEG. *J Neurosci Methods* **113**(2):111–122.

[60] J. V. Haxby et al. (1994). The functional organization of human extrastriate cortex: a PET-rCBF study of selective attention to faces and locations. *J Neurosci* **14**(3 Pt 2):6336–6353.

[61] D. J. Heeger, A. C. Huk, W. S. Geisler, D. G. Albrecht (2000). Spikes versus BOLD: what does neuroimaging tell us about neuronal activity? *Nat Neurosci* **3**(7):631–633.

[62] D. J. Heeger, D. Ress (2002). What does fMRI tell us about neuronal activity? *Nat Rev Neurosci* **3**(2):142–151.

[63] R. N. Henson et al. (2002). Detecting latency differences in event-related BOLD responses: application to words versus nonwords and initial versus repeated face presentations. *Neuroimage* **15**(3):83–97.

[64] M. Hollander, D. A. Wolfe (1973). *Nonparametric Statistical Methods*, pp. 147–148. John Wiley & Sons, Inc., New York.

[65] A. P. Holmes, K. J. Frston (1998). Generalisability, random effects, and population inference. *Neuroimage* **7**:S754.

[66] B. Horwitz, K. J. Friston, J. G. Taylor (2000). Neural modelling and functional brain imaging: An overview. *Neural Netw* **13**(8–9):829–846.

[67] M. Iacoboni, E. Zaidel (2000). Crossed-uncrossed difference in simple reaction times to lateralized flashes: between- and within-subjects variability. *Neuropsychologia* **38**(5):535–541.

[68] M. Iacoboni, E. Zaidel (2003). Interhemispheric visuo-motor integration in humans: the effect of redundant targets. *Eur J Neurosci* **17**(9):1981–1986.

[69] M. Iacoboni, E. Zaidel (2004). Interhemispheric visuo-motor integration in humans: the role of the superior parietal cortex. *Neuropsychologia* **42**(4):419–425.

[70] A. Ipata, M. Girelli, C. Miniussi, C. A. Marzi (1997). Interhemispheric transfer of visual information in humans: the role of different callosal channels. *Arch Ital Biol* **135**(2):169–182.

[71] O. Josephs, R. Turner, K. Friston (1997). Event-related fMRI. *Hum Brain Mapp* **5**(4):243–248.

[72] R. Kawashima, B. T. O'Sullivan, P. E. Roland (1995). Positron-emission tomography studies of cross-modality inhibition in selective attentional tasks: closing the "mind's eye". *Proc Natl Acad Sci USA* **92**(13):5969–5972.

[73] C. Kayser, C. I. Petkov, M. Augath, N. K. Logothetis (2006). Integration of touch and sound in auditory cortex. *Neuron* **48**(2):373–384.

[74] C. Kayser et al. (2004). A comparison of hemodynamic and neural responses in cat visual cortex using complex stimuli. *Cerb Cortex* **14**(8):881–891.

[75] F. Kruggel, D. Y. von Cramon (1999). Modeling the hemodynamic response in single-trial functional MRI experiments. *Magn Reson Med* **42**(4):787–797.

[76] F. Kruggel, D. Y. von Cramon (1999). Temporal properties of the hemodynamic response in functional MRI. *Hum Brain Mapp* **8**(4):259–271.

[77] K. K. Kwong et al. (1992). Dynamic magnetic resonance imaging of human brain activity during primary sensory stimulation. *Proc Natl Acad Sci USA* **89**(12):5675–8679.

[78] S. Lai, G. H. Glover, E. M. Haacke (2000). Spatial selectivity of BOLD contrast: Effects in and around draining veins. In C. T. W. Moonen, P. A. Bandettini (eds.), *Functional MRI*, pp. 221–231, Springer-Verlag, Berlin.

[79] J. L. Lancaster et al. (2000). Automated Talairach atlas labels for functional brain mapping. *Hum Brain Mapp* **10**(3):120–131.

[80] P. J. Laurienti et al. (2002). Deactivation of sensory-specific cortex by cross-modal stimuli. *J Cogn Neurosci* **14**(3):420–429.

[81] P. J. Laurienti et al. (2005). On the use of superadditivity as a metric for characterizing multisensory integration in functional neuroimaging studies. *Exp Brain Res* **166**(3–4):289–297.

[82] A. Ledlow, J. M. Swanson, M. Kinsbourne (1978). Differences in reaction times and averaged evoked potentials as a function of direct and indirect neural pathways. *Ann Neurol* **3**(6):525–530.

[83] C. H. Liao et al. (2002). Estimating the delay of the fMRI response. *Neuroimage* **16**(3):593–606.

[84] A. K. Liu, A. M. Dale, J. W. Belliveau (2002). Monte Carlo simulation studies of EEG and MEG localization accuracy. *Hum Brain Mapp* **16**(1):47–62.

[85] N. K. Logothetis (2003). The underpinnings of the BOLD functional magnetic resonance imaging signal. *J Neurosci* **23**(10):3963–3971.

[86] N. K. Logothetis et al. (2001). Neurophysiological investigation of the basis of the fMRI signal. *Nature* **412**(6843):150–157.

[87] A. Martinez et al. (1999). Involvement of striate and extrastriate visual cortical areas in spatial attention. *Nat Neurosci* **2**(4):364–369.

[88] R. Martuzzi et al. (2006). Multisensory interactions within human primary cortices revealed by BOLD dynamics. *Cereb Cortex* DOI:10.1093/cercor/bhl077.

[89] R. Martuzzi et al. (2006). Visuo-motor pathways in humans revealed by event-related fMRI. *Exp Brain Res* **170**(4):472–487.

[90] C. A. Marzi, P. Bisiacchi, R. Nicoletti (1991). Is interhemispheric transfer of visuomotor information asymmetric? Evidence from a meta-analysis. *Neuropsychologia* **29**(12):1163–1177.

[91] C. A. Marzi et al. (1999). Pathways of interhemispheric transfer in normals and in a split-brain subject. A positron emission tomography study. *Exp Brain Res* **126**(4):451–458.

[92] Matlab (2000). *Signal Processing Toolbox User's Guide, Third reprinting*, pp. 20–21. The MathWorks Inc, Natick, MA.

[93] P. M. Matthews (2001). An introduction to functional magnetic resonance imaging of the brain. In P. Jezzard, P. M. Matthews, S. M. Smith (eds.), *Functional MRI: an introduction to methods*, pp. 3–34, Oxford University Press, New York.

[94] M. J. McKeown et al. (1998). Analysis of fMRI data by blind separation into independent spatial components. *Hum Brain Mapp* **6**(3):160–188.

[95] R. S. Menon, B. G. Goodyear (2001). Spatial and temporal resolution in fMRI. In P. Jezzard, P. M. Matthews, S. M. Smith (eds.), *Functional MRI: an introduction to methods*, pp. 145–158, Oxford University Press, New York.

[96] R. S. Menon, S. G. Kim (1999). Spatial and temporal limits in cognitive neuroimaging with fMRI. *Trends Cogn Sci* **3**(6):207–216.

[97] R. S. Menon, D. C. Luknowsky, J. S. Gati (1998). Mental chronometry using latency-resolved functional MRI. *Proc Natl Acad Sci USA* **95**(18):10902–10907.

[98] C. M. Michel, M. Seeck, M. M. Murray (2004). The speed of visual cognition. In M. Hallett, L. Phillips, D. Schomer, J. Massey (eds.), *Advances in Clinical Neurophysiology, Supplements to Clinical Neurophysiology*, Elsevier, Amsterdam.

[99] C. M. Michel et al. (2004). EEG source imaging. *Clin Neurophysiol* **115**(10):2195–2222.

[100] F. M. Miezin et al. (2000). Characterizing the hemodynamic response: effects of presentation rate, sampling procedure, and the possibility of ordering brain activity based on relative timing. *Neuroimage* **11**(6):735–759.

[101] J. Miller (1982). Divided attention: evidence for coactivation with redundant signals. *Cognit Psychol* **14**(2):247–279.

[102] S. Molholm et al. (2002). Multisensory auditory-visual interactions during early sensory processing in humans: a high-density electrical mapping study. *Brain Res Cogn Brain Res* **14**(1):115–128.

[103] S. Morand et al. (2000). Electrophysiological Evidence for Fast Visual Processing through the human koniocellular pathway when stimuli move. *Cereb Cortex* **10**(8):817–825.

[104] J. T. Mordkoff, J. Miller, A. C. Roch (1996). Absence of coactivation in the motor component: evidence from psychophysiological measures of target detection. *J Exp Psychol Hum Percept Perform* **22**(1):25–41.

[105] J. C. Mosher, P. S. Lewis, R. M. Leahy (1992). Multiple dipole modeling and localization from spatio-temporal MEG data. *IEEE Trans Biomed Eng* **39**(6):541–557.

[106] R. Mukamel et al. (2005). Coupling between neuronal firing, field potentials, and FMRI in human auditory cortex. *Science* **309**(5736):951–954.

[107] M. M. Murray et al. (2001). Visuo-spatial neural response interactions in early visual cortical processing during a simple reaction time task: a high-density electrical mapping study. *Neuropsychologia* **39**(8):828–844.

[108] M. M. Murray et al. (2002). The spatiotemporal dynamics of illusory contour processing: combined high-density electrical mapping, source analysis, and functional magnetic resonance imaging. *J Neurosci* **22**(12):5055–5073.

[109] M. M. Murray et al. (2004). Rapid discrimination of visual and multisensory memories revealed by electrical neuroimaging. *Neuroimage* **21**(1):125–135.

[110] M. M. Murray et al. (2005). Grabbing your ear: rapid auditory-somatosensory multisensory interactions in low-level sensory cortices are not constrained by stimulus alignment. *Cereb Cortex* **15**(7):963–974.

[111] J. Niessing et al. (2005). Hemodynamic signals correlate tightly with synchronized gamma oscillations. *Science* **309**(5736):948–951.

[112] L. Nowak, J. Bullier (1997). The timing of information transfer in the visual system. In J. H. Kass, K. Rockland, A. Peters (eds.), *Cerebral Cortex*, pp. 204–241, Plenum Press, New York.

[113] S. Ogawa et al. (1992). Intrinsic signal changes accompanying sensory stimulation: functional brain mapping with magnetic resonance imaging. *Proc Natl Acad Sci USA* **89**(13):5951–5955.

[114] R. C. Oldfield (1971). The assessment and analysis of handedness: the Edinburgh Inventory. *Neuropsychologia* **9**(1):97–113.

[115] K. Omura et al. (2004). Different mechanisms involved in interhemispheric transfer of visuomotor information. *Neuroreport* **15**(18):2707–2711.

[116] J. Pekkola et al. (2005). Primary auditory cortex activation by visual speech: an fMRI study at 3 t. *Neuroreport* **16**(2):125–128.

[117] F. Perrin et al. (1987). Mapping of scalp potentials by surface spline interpolation. *Electroencephalogr Clin Neurophysiol* **66**(1):75–81.

[118] C. Phillips, K. J. Rugg, M D nd Friston (2002). Anatomically informed basis functions for EEG source localization: combining functional and anatomical constraints. *Neuroimage* **16**(3 Pt 1):678–695.

[119] R. Plonsey, D. B. Heppner (1967). Considerations of quasi-stationarity in electrophysiological systems. *Bull Math Biophys* **29**(4):657–664.

[120] A. T. Poffenberger (1912). Reaction time to retinal stimulation with special reference to the time lost in conduction through nervous centers. *Arch Psychol* **23**:1–73.

[121] C. Preibisch, H. A (2001). Perfusion imaging using spin-labeling methods: contrast-to-noise comparison in functional MRI applications. *Magn Reson Med* **46**(1):172–82.

[122] P. L. Purdon, V. Solo, R. M. Weisskoff, E. N. Brown (2001). Locally regularized spatiotemporal modeling and model comparison for functional MRI. *Neuroimage* **14**(4):912–923.

[123] D. Raab (1962). Statistical facilitation of simple reaction times. *Trans N Y Acad Sci* **24**:574–590.

[124] J. Rademacher et al. (2001). Probabilistic mapping and volume measurement of human primary auditory cortex. *Neuroimage* **13**(4):669–683.

[125] J. C. Rajapakse, F. Kruggel, J. M. Maisog, D. Y. von Cramon (1998). Modeling hemodynamic response for analysis of functional MRI time-series. *Hum Brain Mapp* **6**(4):283–300.

[126] G. Rees, K. Friston, C. Koch (2000). A direct quantitative relationship between the functional properties of human and macaque V5. *Nat Neurosci* **3**(7):716–723.

[127] W. Richter et al. (2000). Motor area activity during mental rotation studied by time-resolved single-trial fMRI. *J Cogn Neurosci* **12**(2):310–320.

[128] A. Ritzl et al. (2003). Functional anatomy and differential time courses of neural processing for explicit, inferred, and illusory contours. an event-related fMRI study. *Neuroimage* **19**(4):1567–77.

[129] K. S. Rockland, H. Ojima (2003). Multisensory convergence in calcarine visual areas in macaque monkey. *Int J Psychophysiol* **50**(1–2):19–26.

[130] M. D. Rugg, C. R. Lines, A. D. Milner (1985). Further investigation of evoked potentials elicited by lateralized stimuli: Effects of stimulus eccentricity and reference site. *Electroencephalogr Clin Neurophysiol* **62**(2):81–87.

[131] Z. S. Saad, E. A. DeYoe, K. M. Ropella (2003). Estimation of FMRI response delays. *Neuroimage* **18**(2):494–504.

[132] Z. S. Saad, K. M. Ropella, R. W. Cox, E. A. DeYoe (2001). Analysis and use of FMRI response delays. *Hum Brain Mapp* **13**(2):74–93.

[133] C. D. Saron, J. J. Foxe, C. E. Schroeder, H. G. J. Vaughan (2003). Complexities of interhemispheric interaction in sensory-motor tasks revealed by high-density event-related potential mapping. In K. Hugdahl, R. J. Davidson (eds.), *The Asymmetrical Brain*, pp. 341–408, MIT press, Cambridge, MA.

[134] C. D. Saron, J. J. Foxe, G. V. Simpson, H. G. J. Vaughan (2003). Interhemispheric visuomotor activation: Spatiotemporal electrophysiology related to reaction time. In E. Zaidel, M. Iacoboni (eds.), *The Parallel Brain*, pp. MIT Press, Cambridge, MA, 171–219.

[135] C. D. Saron, D. R. J (1989). Visual evoked potential measures of interhemispheric transfer time in humans. *Behav Neurosci* **103**(5):1115–1138.

[136] C. D. Saron, C. E. Schroeder, J. J. Foxe, H. G. J. Vaughan (2001). Visual activation of frontal cortex: segregation from occipital activity. *Brain Res Cogn Brain Res* **12**(1):75–88.

[137] M. Scherg (1990). Fundamentals of dipole source potential analysis. In F. Grandori, M. Hoke, G. Romani (eds.), *Auditory Evoked Magnetic Fields and Electric Potentials*, pp. 40–69, Karger, Basel.

[138] M. T. Schmolesky et al. (1998). Signal timing across the macaque visual system. *J Neurophysiol* **79**(6):3272–3278.

[139] E. Schröger, A. Widmann (1998). Speeded responses to audiovisual signal changes result from bimodal integration. *Psychophysiology* **35**(6):755–759.

[140] C. E. Schroeder, J. J. Foxe (2005). Multisensory contributions to low-level, 'unisensory' processing. *Curr Opin Neurobiol* **15**(4):454–458.

[141] C. E. Schroeder, A. D. Mehta, S. J. Givre (1998). A spatiotemporal profile of visual system activation revealed by current source density analysis in the awake macaque. *Cereb Cortex* **8**(7):575–592.

[142] C. E. Schroeder et al. (2001). Somatosensory input to auditory association cortex in the macaque monkey. *J Neurophysiol* **85**(3):1322–1327.

[143] C. E. Schroeder et al. (2003). Anatomical mechanisms and functional implications of multisensory convergence in early cortical processing. *Int J Psychophysiol* **50**(1–2):5–18.

[144] E. Seifritz et al. (2002). Spatiotemporal pattern of neural processing in the human auditory cortex. *Science* **297**(5587):1706–1708.

[145] K. Sekihara et al. (1999). Application of an MEG eigenspace beamformer to reconstructing spatio-temporal activities of neural sources. *Hum Brain Mapp* **15**(4):199–215.

[146] M. Siegel, P. Konig (2003). A functional gamma-band defined by stimulus dependent synchronization in area 18 of awake behaving cats. *J Neurosci* **23**(10):4251–4260.

[147] B. E. Stein, M. A. Meredith (1993). *The Merging of the Senses.* MIT Press, Cambridge, MA.

[148] C. Tallon-Baudry, O. Bertrand (1999). Oscillatory gamma activity in humans and its role in object representation. *Trends Cogn Sci* **3**(4):151–162.

[149] H. C. Tanabe, M. Honda, T. Sadato (2005). Functionally segregated neural substrates for arbitrary audiovisual paired-association learning. *J Neurosci* **25**(27):6409–6418.

[150] M. Tettamanti et al. (2002). Interhemispheric transmission of visuomotor information in humans: fMRI evidence. *J Neurophysiol* **88**(2):1051–1058.

[151] G. Thut et al. (1999). Evidence for interhemispheric motor-level transfer in a simple reaction time task: an EEG study. *Exp Brain Res* **128**(1–2):256–261.

[152] G. Thut et al. (2000). Internally driven vs. externally cued movement selection: a study on the timing of brain activity. *Brain Res Cogn Brain Res* **9**(3):261–269.

[153] G. Thut et al. (2000). Visually induced activity in human frontal motor areas during simple visuomotor performance. *Neuroreport* **11**(13):2843–2348.

[154] R. B. H. Tootell et al. (1998). The representation of the ipsilateral visual field in human cerebral cortex. *Proc Natl Acad Sci USA* **95**(3):818–824.

[155] K. Ugurbil, L. Toth, D. S. Kim (2003). How accurate is magnetic resonance imaging of brain function? *Trends in Neurosci* **26**(2):108–114.

[156] L. G. Ungerleider, M. Mishkin (1982). Two Cortical Visual Systems. In D. J. Ingle, M. A. Goodale, R. J. W. Mansfield (eds.), *Analysis of Visual Behavior*, pp. 549–586, MIT Press, Cambridge, MA.

[157] N. van Atteveldt, E. Formisano, R. Goebel, L. Blomert (2004). Integration of letters and speech sounds in the human brain. *Neuron* **43**(2):271–282.

[158] H. G. J. Vaughan (1996). Two relationship of brain activity to scalp recordings of event-related potentials. In E. Donchin, D. B. Lindsley (eds.), *Average evoked potentials. Methods, results and evaluations*, pp. 45–75, National Aeronautics and Space Administration Washington, DC.

[159] M. T. Wallace, R. Ramachandran, B. E. Stein (2004). A revised view of sensory cortical parcellation. *Proc Natl Acad Sci USA* **101**(7):2167–2172.

[160] B. Weber et al. (2005). Attention and interhemispheric transfer: a behavioral and fMRI study. *J Cogn Neurosci* **17**(1):113–123.

[161] J. H. Xiong, P. T. Fox, J. H. Gao (2003). Directly mapping magnetic field effects of neuronal activity by magnetic resonance imaging. *Hum Brain Mapp* **20**(1):41–49.

[162] T. A. Yousry et al. (1997). Localization of the motor hand area to a knob on the precentral gyrus. A new landmark. *Brain* **120**(Pt 1):141–157.

[163] S. Zeki (1993). *A Vision of the Brain*. Blackwell Scientific Publications, Oxford, UK.

[164] K. Zilles, S. Clarke (1997). Architecture, connectivity, and transmitter receptors of human extrastriate visual cortex. In K. Rockland, J. H. Kaas, A. Peters (eds.), *Cerebral Cortex*, pp. 673–742, Plenum Press, New York.

Curriculum Vitæ

Name:	Roberto Martuzzi
Degrees:	Master of Science in Electronical Engineering at the Turin University of Technology (Politecnico di Torino)
Date of birth:	August 12$^{\text{th}}$, 1973 in Turin (Italy)
Citizenship:	Italian
Marital status:	Single
Contact Address:	CHUV, Service de Radiodiagnostic et Radiologie Interventionnelle Rue du Bugnon, 46 1011 Lausanne Switzerland
Phone:	+41 21 314 44 53
Email:	Roberto.Martuzzi@chuv.ch

Currently

- ***Ph.D. student*** at Signal Processing Institute at the EPFL (École Polytechnique Fédérale de Lausanne)

Educational and Professional History

- ***From June 2003***: Ph.D. Student at the Signal Processing Institute at the EPFL, under the supervision of Prof. J.P. Thiran and Prof. R. Meuli

- ***From March 2001***: Research assistant at the Department of Radiology at the Lausanne University Hospital in the domain of functional Magnetic Resonance Imaging (fMRI)

- ***July 2000***: M.Sc. degree in Electronical Engineering at the Turin University of Technology (Politecnico di Torino), with the thesis entitled *Functional magnetic resonance*

imaging data analysis tools – A new method to compute SPMs and its comparison with the existing ones

- ***September 1999 – June 2000***: Development of the Master's Thesis at the Helsinki University of Technology as Erasmus student
- ***June 1992***: Scientific diploma at the "Liceo Scientifico Umberto I°", in Turin

Skills

Languages

Italian:	mother tongue
French:	fluent oral and written
English:	fluent oral and written

Computing

Operating systems:	Linux, Unix, Windows
Programming languages:	Matlab

Awards

- 2006 Best Poster Award at the 2nd Lemanic Neuroscience Meeting for the work entitled, *Auditory-visual multisensory interactions modulate the dynamics of BOLD responses in primary cortices*
- 2005 Graduate Student Award at the 6th International Multisensory Research Forum for the work entitled *Auditory-visual multisensory interactions modulate the dynamics of BOLD responses in unisensory cortices*

Publications

Journal papers

- Martuzzi R., Murray M.M., Michel C.M., Maeder P.P., Thiran J.P., Clarke S., Meuli R.A. (2006). Multisensory interactions within human primary cortices revealed by BOLD dynamics. *Cereb Cortex* DOI:10.1093/cercor/bhl077.
- Hagmann P., Cammoun L., Martuzzi R., Maeder P., Clarke S., Thiran J.P., Meuli R. (2006). Hand preference and sex shape the architecture of language networks. *Hum Brain Mapp* **27**(10):828-835.
- Martuzzi R., Murray M.M., Maeder P.P., Fornari E., Thiran J.P., Clarke S., Michel C.M., Meuli R.A. (2006). Visuo-motor pathways in humans revealed by event-related fMRI. *Exp Brain Res* **170**(4):472-487.

- Grave de Peralta Menendez R., Murray M.M., Michel C.M., Martuzzi R., Gonzalez Andino S.L. (2004). Electrical neuroimaging based on biophysical constraints. *Neuroimage* **21**(2):527-539.

Oral presentations

- Martuzzi R., Murray M.M., Michel C.M., Maeder P., Thiran J.P., Clarke S., Meuli R. Auditory-visual multisensory interactions modulate the dynamics of BOLD responses in primary cortices. Presented at the HBM 2005 - 11th International Conference on Functional Mapping of the Human Brain, Toronto, Canada.

- Martuzzi R., Murray M.M., Michel C.M., Maeder P., Thiran J.P., Clarke S., Meuli R. Auditory-visual multisensory interactions modulate the dynamics of BOLD responses in unisensory cortices Presented at the 6th International Multisensory Research Forum, Rovereto, Italy.

Posters

- Martuzzi R., Murray M.M., Meuli R., Thiran J.P., Maeder P.P., Michel C.M., Gonzalez Andino S.L., Grave de Peralta Menendez R. Frequency-dependent correlation between estimated LFPs and BOLD responses in human. Presented at the HBM 2006 - 12th International Conference on Functional Mapping of the Human Brain, Florence, Italy.

- Martuzzi R., Murray M.M., Michel C., Maeder P., Thiran J.P., Clarke S., Meuli R. Auditory-visual multisensory interactions modulate the dynamics of BOLD responses in primary cortices. Presented at the HBM 2005 - 11th International Conference on Functional Mapping of the Human Brain, Toronto, Canada.

- Martuzzi R., Cammoun L., Hagmann P., Maeder P., Clarke S., Thiran J.P., Meuli R., 2004. Language-related asymmetries of the arcuate fasciculus in right- and left-handers: a DT-MRI and fMRI combined study. HBM 2004 - 10th International Conference on Functional Mapping of the Human Brain. Budapest, Hungary.

- Martuzzi R., Maeder P., Fornari E., Thiran J.P., Meuli R., 2003. Simultaneous acquisition of BOLD, perfusion, and diffusion brain activation maps. HBM 2003 - 9th International Conference on Functional Mapping of the Human Brain. New York, NY, USA.

- Martuzzi R., Fornari E., Maeder P., Thiran J.P., Clarke S., Michel C.M., Meuli R., 2002. Delays of the BOLD signals in different brain regions during visuo-motor task. HBM 2002 - 8th International Conference on Functional Mapping of the Human Brain. Sendai, Japan.

- Martuzzi R., Fornari E., Maeder P., Thiran J.P., Clarke S., Michel C.M., Meuli R., 2002 Functional connectivity between visual and motor areas: an ER-fMRI study.

HBM 2002 - 8th International Conference on Functional Mapping of the Human Brain. Sendai, Japan.